Development and Optimization of Planar Potentiometric Sensors for Point-of-Care Use

A DISSERTATION

SUBMITTED TO THE FACULTY OF THE

UNIVESITY OF MINNESOTA

BY

Eliza Jane Herrero

IN PARTIAL FULFILLMENT OF THE REQUIREMENTS

FOR THE DEGREE OF

DOCTOR OF PHILOSOPHY

Dr. Philippe Bühlmann, Advisor

October 2023

Acknowledgments

I would like to thank the following individuals for their help and support throughout my Ph.D.:

Dr. Philippe Bühlmann, my PhD advisor, for his continued support and guidance throughout my entire time at the University of Minnesota. From teaching me how to write a scientific manuscript and design electrochemical experiments to encouraging me to participate in conferences and explore many career options, he has been an endless source of knowledge and advice.

Previous group members: Dr. Blair Troudt for her mentorship starting in the summer before I began coursework, for teaching me how to fabricate and use capillary reference electrodes, and constant support, and Dr. Celeste Rousseau for help in troubleshooting my research and always being willing to explain a new concept or method to me.

Former and present members of the Chemistry Department Women in Science and Engineering (WISE) group and faculty advisors Dr. Kyle Bantz and Dr. Letitia Yao for sharing their passion, energy, and time to improve the climate for women in our department and beyond.

All the Bühlmann group members for support and collaboration including Dr. Kwangrok Choi, Vilma Brandao, Xin Chen, Brian Spindler, Emily Robinson, Madeline Honig, Ali Arshad, Kuzi Madungwe, and Zubaer Zaman.

In terms of specific contributions, I would like to thank Blair Troudt for

making the capillary reference electrode I used to study chloride leaching from conductive inks and Takumi Goto for his help on screening and identifying potential complexes for use as redox buffer project.

My family and friends for their endless support over the many years of my scientific career. I was truly blessed to have so many people encourage me to go after my dreams and help me in countless ways throughout this long journey.

Dedication

This thesis is dedicated to:

My husband, Connor: thank you for never letting me doubt myself, picking me up when I fall, and always putting a smile on my face

And to my parents: thank you for always supporting me no matter what challenge I decide to face.

Abstract

The monitoring of electrolytes and charged biomolecules in body fluids is a crucial step in both the diagnosis and management of many diseases, including chronic kidney disease and cardiovascular disease. Ion-selective electrodes (ISEs) are considered the gold standard in analyzing these analytes in clinical settings due to their high selectivity, near instant response time, and linear response. These ISEs are generally incorporated into a mainframe clinical blood analyzer which, due to the high cost, fragility, and need for trained staff to operate, are in centralized hospitals or laboratories. As a result, patients living in remote, or resource-limited areas often do not have access to such clinical diagnostics. There is, therefore, a need for point-of-care based ISEs, characterized by low-cost, high ease of use, and portability. Despite recent interest in the development of point-of-care based ISEs, there remain fundamental issues in the design and performance of these sensors, which I address in my research. This thesis presents work that supports the advancement of point-of-care based ISEs in several key areas.

While paper has been proposed as a substrate for point-of-care sensors, it has impurities from manufacturing and being natural in origin. Moreover, its structure and surface composition are highly heterogeneous, which are disadvantageous when designing sensors for high reproducibility. In this work, I propose the use of a novel synthetic textile with higher purity and a more controlled structure to serve as a supporting substrate for miniaturized, membrane-free ISEs. To expand the versatility of these devices, I embedded both ion-sensing and reference membranes into the polyester fabric and successfully measured the activity of chloride (a highly relevant clinical biomarker) in aqueous solutions and 100% blood serum. This is the first example of an ISE that both

embeds membranes into a fabric and uses the fabric to wick samples into contact with those membranes. I also determined the effect of pore structure on device performance, a finding applicable not only to textile-based ISEs, but also to other porous materials such as paper. I showed that devices fabricated on the textile had an order of magnitude improvement in the lower limit of detection (LOD) of chloride as compared to analogous paper-based devices.

I also further the understanding of the sources of non-ideal performance in paper-based ISEs through a systematic study of both sensor materials and interactions between materials and aqueous samples. While it has been suggested by many that these limitations are due to interactions of paper with sample or sensing components, to date this has not been thoroughly investigated. To this end, I studied interactions of target ions with paper by using a range of analytical techniques. My data shows two main reasons that explain the sub-optimal performance of paper-based devices for chloride sensing, which I explain and propose novel fabrication techniques to overcome.

A key performance parameter in ISEs designed to be used outside of central laboratories is that of reproducibility, with the goal of calibration-free devices. Our group has previously improved sensor-to-sensor reproducibility with the use of redox buffers, which buffer redox-active impurities in the system. I propose the use of a novel cobalt(III/II)bis(terpyridine) as a hydrophilic redox buffer to be incorporated into the inner filling solution of ISEs for anion sensing. Conventional ISEs with a plasticized poly(vinyl)chloride ion-exchange membrane for Cl^- and the redox buffer incorporated into the inner filling solution resulted in a E^0 SD of 0.3 mV–one of the lowest reported SD thus far in the literature. The redox buffer was also found to be compatible with reference

membranes as well as textile-based sensing setups.

As the purpose for these devices is to be used in clinical diagnostics, it is also crucial to increase the number of analytes measured to include clinically relevant ions such as K^+, Ca^{2+}, and pH. I therefore also show the use of textile-based devices with ionophore-containing membranes that selectively complex target ions. While a textile-based Ca^{2+} ISE was fabricated and successfully detected Ca^{2+} in aqueous samples, performance limitations arose in the detection of K^+, H^+, Ag^+, and CO_3^{2-}. A study of the effects of textile coating techniques and considerations of material-membrane interactions seek to address these shortcomings.

Table of Contents

List of Abbreviations

AgCl/Ag	silver chloride-silver
BME-44	2-Dodecyl-2-methyl-1,3-propanediyl bis[*N*-[5′-nitro(benzo-15-crown-5)-4′-yl]carbamate]
CNT	carbon nanotubes
DOS	bis(2-ethylhexyl) sebacate
DSC	differential scanning calorimetry
EMF	electro-motive force
ETH 500	tetradodecylammonium tetrakis(4-chlorophenyl)borate.
ETH 5234	N,N-Dicyclohexyl-N′,N′-dioctadecyl-3-oxapentanediamide
ETH 6010	1-heptyloxycarbonyl-4-trifluoroacetylbenzene
ICP-OES	inductiviley coupled plasma-optical emission spectroscopy
IE	indicator electrode
IFS	inner filling solution
ISE	ion-selective electrode
ISM	ion-selective membrane
KTpClPB	potassium tetrakis(4-chlorophenyl)borate
LiTPFPB	lithium tetrakis(pentafluorophenyl)borate ethyl etherate
LOD	limit of detection
NH_4T3ClPB	ammonium tetrakis(3-chlorophenyl)borate
o-NPOE	o-nitrophenyl octyl ether
PEDOT	poly(3,4-ethylenedioxythiophene)
PET	polytheylene terephthalate
PSS	polystyrene sulfonate
PVC	poly(vinyl chloride)
RE	reference electrode
RM	reference membrane
SD	standard deviation
SEM	scanning electron microscopy
SI	supporting Information
SWCNT	single walled carbon nanotubes
T_{99}, T_{95}	temperature at 1 and 5 % mass loss, respectively
TDA	tridodecylamine
TDDMACl	tridodecylmethylammonium chloride
TGA	thermogravimetric analysis
THF	tetrahydrofuran
[C8mim+][C1C1N−]	1-methyl-3-octylimidazolium bis(trifluoromethylsulfonyl)imide
^{1}H NMR	proton nuclear magnetic resonance spectroscopy

Chapter 1. Challenges in the Miniaturization of Potentiometric Sensors for Point-of-Care Analysis

PREFACE

Despite decades of interest in the development of electrochemical point-of-care sensors, there are still many unfulfilled needs for commercial applications. For potentiometric sensors, such research has focused on a variety of aspects, including using an underlying substrate to support the sensors, increasing the degree to which sensing components are integrated into the substrate, and incorporating solid-contact materials to improve performance and testing in real-life applications. This review analyzes recent work in the field of miniaturized potentiometric devices, with a focus on evaluating how device design and materials affect relevant performance characteristics. Our goal is to highlight challenges in the design and performance of potentiometric point-of-care sensors that are still preventing their wider use for real life applications. Differences in the design of strip-type, sandwich-type, fully integrated, and fiber- and yarn-based sensors are briefly introduced. The focus of the discussion lies, however, in the effects of materials and substrates on response slopes, potential reproducibility, and limits of detection.

INTRODUCTION

Despite decades of interest in and numerous publications on the development of point-of-care based electrochemical sensors, there have been limited advancements in commercially available sensors. The ASSURED criteria (Affordable, Sensitive, Specific, User-Friendly, Rapid, Robust, Equipment-Free and Deliverable to end user) for point-of-care diagnostics as put forth by the World Health Organization (WHO) presents a framework to guide and evaluate novel devices. Only devices that meet most of these criteria can truly function as point-of-care devices and thereby have the potential to make it to market.[1,2]

Affordability of a device in production is often difficult to estimate from academic settings but worth consideration nonetheless.[3] Performance related criteria–sensitive, specific and rapid–depend upon the particular sensing mechanism chosen as well as any performance issues that arise in miniaturization of the test. Meeting the “user-friendly” criteria means minimal steps for an untrained user and includes calibration-free designs, a difficult feat with heavy commentary.[4,5] In addition to testing device performance in lab, field testing allows further optimization in realistic use settings with non-trained personal, as a recent report of a case study for a colorimetric test development outlines.[6]

Ion-selective electrodes (ISEs) are already the method of choice in clinics in the measurement of ions and charged biomolecules due to excellent speed, sensitivity, and specificity.[7] Therefore, many efforts have been made to develop ISEs for point-of-care usage.[8–14] The earliest commercially available clinical blood analyzers designed to be used outside of centralized laboratories, including the Kodak Ektachem benchtop

analyzer of the early 1980s[15] and the i-Stat portable clinical blood analyzer introduced into hospitals in the early 1990s,[16] brought clinical chemistry testing to patient bedsides by replacing the conventional rod- or tube-shaped electrodes with slides or cartridges with low dimensionality. In contrast to traditional ISEs, ISEs designed for point-of-care usage must incorporate an underlying support substrate to support the electrochemical cell. The design of an ISE that complies with the ASSURED criteria is difficult, as there are often tradeoffs in device design and analytical performance.

This review discusses relevant research on the design, fabrication, and performance of ISEs for point-of-care usage. We begin by explaining common sensor designs, categorized based off the degree of miniaturization of the sample holder, reference electrode, and ion-sensing electrode. Miniaturized potentiostats, displays integrated into ISEs devices, and chemically sensitive field-effect transistors are out of scope of the current review. We then introduce common materials that have been used as the underlying support substrate upon which miniaturized ISEs are fabricated, with an emphasis on relevant the physiochemical characteristics of the materials. In the following sections, we examine how the sensor design and/or identity of the supporting substrate affects deviations of the sensor performance from ideal behavior. In particular, we compare the slope, reproducibility, and limit of detection of miniaturized ISEs to those of analogous conventional ISEs. In critically analyzing the performance limitations correlated with design and material choice, this review will serve as a guide in future miniaturized potentiometric device design.

DESIGNS OF MINIATURIZED POTENTIOMETRIC SENSORS FOR POINT-OF-CARE USAGE

Substrate-Based Sampling

In substrate-based sampling a sample is wicked across a single-use, hydrophilic substrate into contact with traditional rod-shaped sensing and reference electrodes (see Fig. 1-1A). Such substrates include various types of papers, textiles, and sponges and are discussed in Section 3. This design was originally introduced as a dot-blot model assay with two vertically oriented electrodes–one upside down and another right side up–with filter paper sandwiched between them and sample dropped onto the paper to wick into contact with electrodes.[17] An analogous design was also reported with two horizontally oriented electrodes with the upper part of a piece of filter paper sandwiched between them and the lower part dipped into sample below.[18]

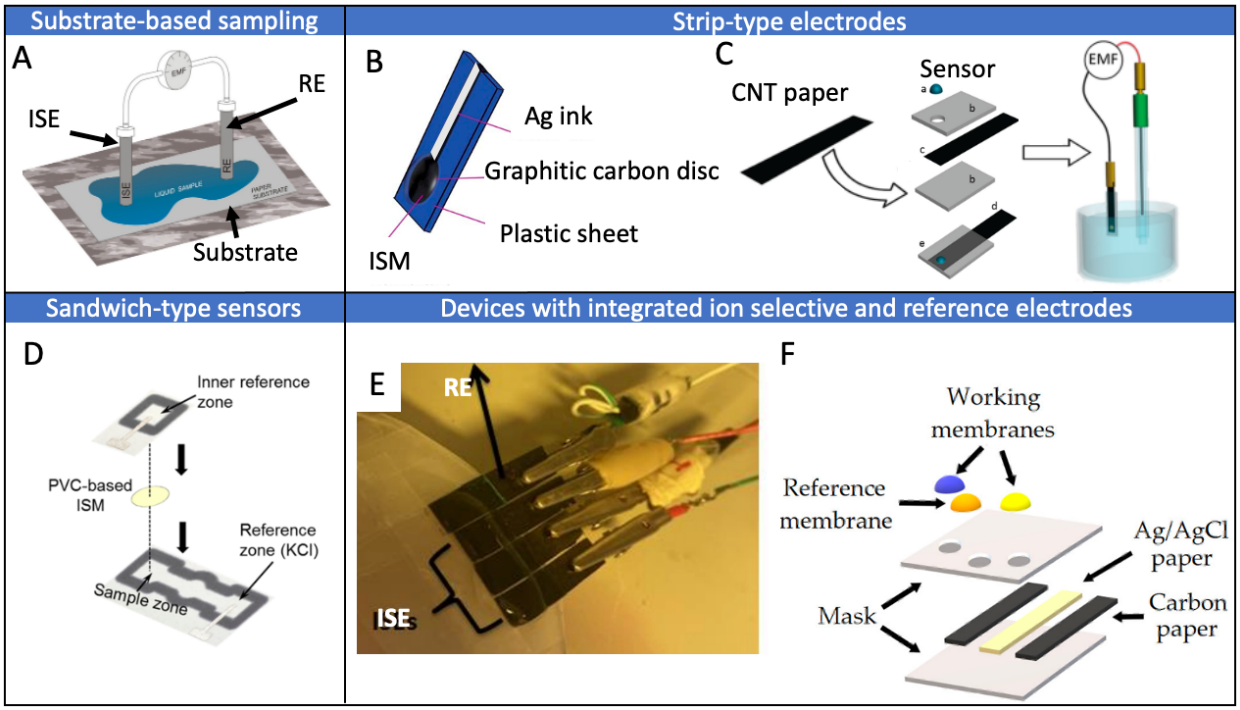

Figure 1-1. Design of ISEs for point-of-care analysis: (A) substrate-based sampling, (B) strip-type electrodes with the solid-contact restricted to the lower portion of the strip, (C) strip-type electrodes with the solid-contact entirely covering the entire substrate, (D) sandwich-type devices, as well as (E),(F), and (G) devices with both an ISE and RE. Adapted from references 19–25.

The next generation of substrate-based sampling included two vertically oriented electrodes clamped into place and.[19,26–33] Further, the conventional single junction reference electrode (RE) was replaced by a reusable Ag/AgCl rod and a disposable salt bridge. For the latter, a separate piece of filter paper was coated with dry KCl and placed between the Ag/AgCl rod and the filter paper containing the sample. This further isolates the electrode from contact with and thereby fouling by sample.[34] In addition to greatly

reducing the required sample volume to 200 µL, substrate-based sampling also filters particulates from samples such as soil and sludge which harm electrodes in traditional sampling methodology.[19,29–31] However, the use of a conventional ISE necessitates a trained user to re-calibrate the ISE, limiting the use of such designs.

Strip-Type Electrodes

Strip-type electrodes use the underlying substrate as a physical support but not for sample holding. Electrodes are built vertically on top of a substrate, which is often, but not always, filter paper, through application of a conductive lead, solid contact, polymeric membranes, and an insulating mask which prevents contact between sample and the conductive leads (Fig. 1-1B). The sensor is connected to a potentiostat through the conductive lead and submerged into a sample, typically in conjunction with a conventional reference electrode.[8,10,20,21,35–38] While these sensors can be referred to as disposable, they are reusable and can be rinsed between samples.

The earliest strip-type ISEs used a coated-film design in which a film of the polymeric sensing membrane was deposited on top of Ag-coated filter paper.[8] However, the interface between an ISM and conducting metal is blocked and the phase boundary potential is not clearly defined, resulting in poor stability and reproducibility.[35] Therefore, subsequent devices of this type were designed with solid contacts such as conducting polymers.[35]

For devices in which the solid contact is restricted to the area just below the ion-selective membrane (ISM), separate paths of electron conducting materials that are not also ion-to-electron transducers such as Ag, connect it to a potentiometer (see Fig. 1-1B).

These conductive paths are commonly applied by screen printing,[39] or drawn with a 3D pen,[40] as first shown with ion-sensing pencils.[40] Such strip sensors have been used in many settings, including as a real-time alternative to off-line HPLC testing when monitoring the rate of drug release from solid-dose pharmaceuticals in vitro.[20]

While in the previous designs the solid contact only covers a small section of the device, designs in which filter paper is fully-coated with carbon nanotubes (CNTs) have also been used in strip sensors for the detection of various ions (see Fig. 1-1C).[21,36,37] This inherently uses more material but does not require the use of a stencil or detailed deposition of ink. With any strip-type sensor used by dipping into sample, an insulating layer such as a plastic mask must also be deposited to prevent contact between conductive leads and the sample solution.

While analysis is commonly done in a beaker with large sample volumes, this could be done in smaller volumes so long as the liquid junction of the RE is covered with solution. Although strip-type sensors are smaller and more robust than conventional ISEs, the need for a conventional RE, an insulating layer, and enough sample solution to dip electrodes into are all hurdles to use in true point-of-care settings. Therefore, strip-type sensors are best seen as a steppingstone towards fully integrated devices.

Devices with Integrated Ion-Sensing and Reference Electrodes

Moving towards more integrated devices, many groups have fabricated both reference and sensing electrodes onto the same unit. As in strip-type sensors, these devices use the underlying substrate solely as a physical support and the sample is not contained in any part of the device. These require manual application of sample to

sensing elements or submersion of the device into a sample. As with strip-type sensors, they are reusable and can be rinsed between samples.

A crucial step is the fabrication of planar reference electrodes. Common solid-contact reference electrodes include CNT coated paper with an ionic liquid containing reference membrane,[24,41,42] graphene/multi-walled CNT coated substrate in contact with a reference membrane containing AgCl and a hydrophilic electrolyte, such as KCl or NaCl,[43–45] as well as AgCl/Ag coated filter paper in contact with poly(vinyl butyral) membrane containing NaCl, and $AgNO_3$.[46]

One method to include reference and sensing electrodes in a single unit is to couple separately prepared strip-type ion-selective and reference electrodes.[24,41,46] This has been done by taping a rubber spacer between strip electrodes to form a cavity for sample introduction,[41,46] as well as by taping strip electrodes side by side to form a flat array (see Fig. 1-1F).[24,42] In a more efficient design, three separate strips of conductive material were sandwiched between plastic masks and then membranes were deposited onto pre-cut holes to form an array of sensing and reference electrodes (see Fig. 1-1E).[23] While these combinations of strip-type reference and sensing electrodes overcome the need for a conventional RE, the fabrication process still comprises multiple steps. Fabrication is simplified by using a single piece of supporting substrate as a base for both sensing and reference electrodes.

Screen-printing or spray-coating conductive leads and/or solid contacts, and then drop casting membranes by hand is used by many to quickly fabricate integrated sensors,

as previously mentioned for strip-type sensors. A poly(ethylene terephthalate) (PET) substrate was coated with single walled carbon nanotubes (SWCNTs) solid contact using a screen-printing method for both ion-selective and reference electrodes (see Fig. 1-1G).[25] An ISE array for analysis of urine samples was fabricated via a screen printing process, with devices dipped into samples for analysis.[43] Similarly, graphene was deposited on a paper substrate using spray coating with a stencil for an ISE array and used as a patch for sweat sensing.[44] Another fabrication method is the use of a Chinese brush pen to "write" on all components of a sensor array–including graphene leads and polymeric membranes – onto the substrate.[45]

While these arrays include both reference and sensing electrodes, they still require connection to an external unit for converting and reading data. Therefore, screen-printed ISEs have also been coupled with miniaturized integrated circuit boards in microsensors used for on-body detection of glucose, lactate, Na^+ and K^+ in sweat.[47,48] These designs are used as patches directly on skin sweat, but it is unclear how old sweat wicks away from the sensor and new sweat comes in.

While these designs show a step towards integration, they are limited for use in real samples by the lack of a wicking component. Electrodes must either be dipped into samples, as typical for strip-type electrodes, or samples must be deposited onto the sensing membrane. However, the lack of figures and clear explanations of the experimental setup makes this distinction in use difficult for certain reports.

Sandwich-Type Sensors

Sandwich-type designs, in which a free-standing sensing membrane is placed between two pieces of filter paper, combine both the reference and sensing elements into the device and have inherent wicking capabilities in the underlying support substrate (see Fig. 1-1D). In this design, the free-standing membrane may be reused for multiple measurements, but the filter paper onto which the sample and reference solutions are deposited need to be replaced for each measurement.

The reference element in these types of sensors is based off a paper-based design introduced originally in the context of voltammetric sensing.[49] The design consists of wax barriers in a dumbbell shape to define reference, sample and central contact zones, with a strip of Ag/AgCl ink in the reference and sample zones, These designs were produced with ink-jet printing of wax barriers and heated to ensure full penetration, as is common for fabricating hydrophobic barriers on filter paper.[50,51] By maintaining a constant KCl concentration on one side of the dumbbell shape, the design can be used as a coated wire type Cl^- ISE.[49]

Incorporation of an ISM was achieved by clipping a free-standing membrane between a filter paper reference piece and a piece of filter paper onto which sample was deposited below.[22] These are analogous to a RE with an inner filling solution. This was shown to work for ion-exchange membranes [22,52] as well as ionophore-containing ISMs.[22] Fabrication of sandwich-type designs was then simplified by the use of a single piece of filter paper folded onto itself–instead of 3 distinct pieces–and incorporation of a 3D printed ISM.[53] While these devices contain both sensing and reference electrodes, as well as a

component to wick samples into contact with electrodes, they still require multiple pieces, which require a trained end user.

Devices Containing both Electrodes and Wicking Components

Combining both sensing components and wicking abilities into a single piece of supporting substrate is a promising approach that minimizes both fabrication steps and user-setup. This is achieved by using a hydrophilic support material that has inherent wicking capabilities and by integrating the membranes into the material itself.

By hand spotting both sensing and reference membranes into the filter paper and using Ag/AgCl ink in contact with a KCl solution as a reference electrode, the number of pieces in Cl^- and K^+ ISEs was reduced from three[22] to one (see Fig. 1-2A).[54] This design was also then applied to textile.[55] Use of these devices requires deposition of one droplet of reference solution to each of the two reference zones, and one droplet of sample to sample zone. While these devices use a single piece of material to contain electrodes, sample, and reference solution, they still require the application of an inner filling solution, which limits use.

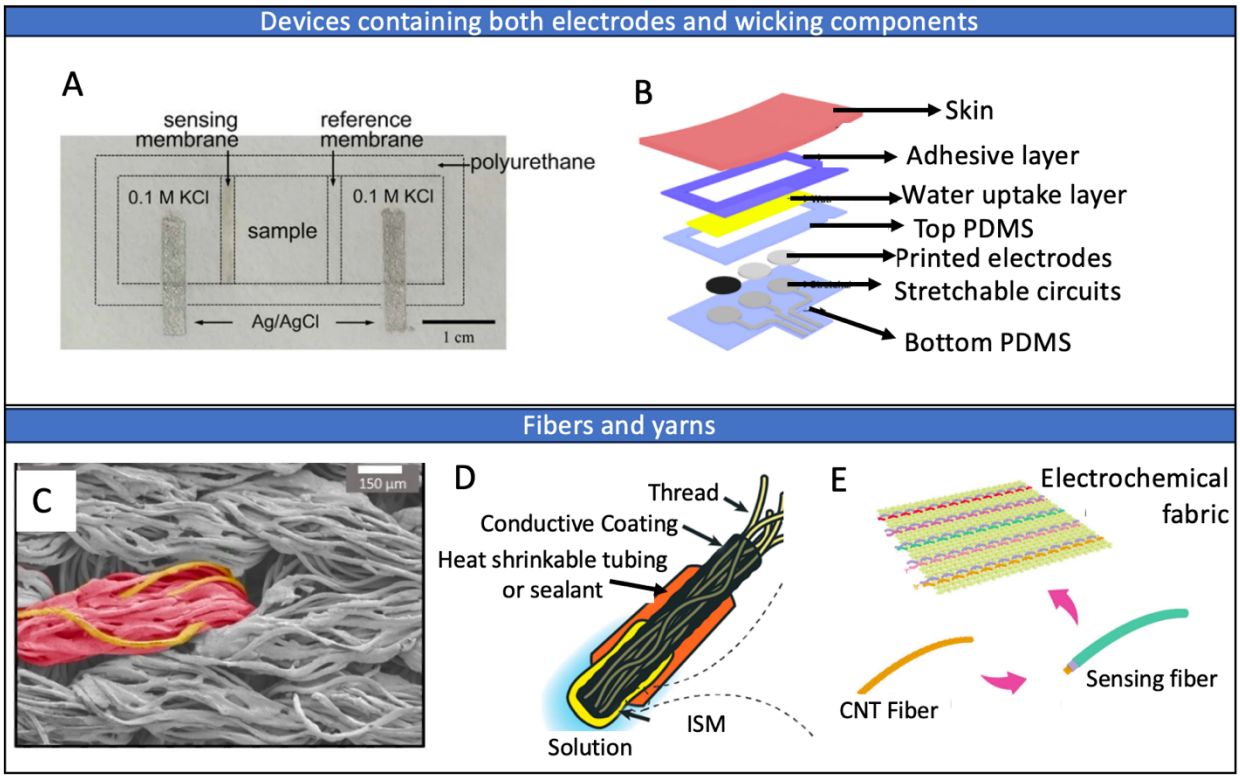

Figure 1-2. Examples of (A) miniaturized ISEs containing both electrodes and sample-wicking components integrated into the support substrate, and (B) devices containing integrated reference and sensing electrodes with a separate sample wicking component. (C) Scanning electron microscopy image of a fabric, with a single yarn highlighted in red and individual fibers in yellow. (D) Thread-based ISE and (E) thread-based ISEs woven into a piece of fabric. Adapted from references 54–58.

This can be further optimized through replacement of the inner filling solution with a solid contact, as used in many screen-printed ISEs reviewed above. A proof-of-concept fully integrated solid-contact RE was introduced through the application of colloid-imprinted mesoporous carbon doped with a hydrophobic redox couple in contact with the

previously used ionic-liquid-based reference membrane and Ag/AgCl ink for Cl^- sensing.[59] Further work showed the compatibility of this paper-based RE with a hydrophilic high-capacity anion-exchange membrane for Cl^- detection.[60] While in this design all components were applied by hand, automated fabrication is still preferable and inkjet printing has also been used for fully integrated devices consisting of a Ag/AgCl/KCl/reference membrane reference electrode and graphene/poly(3,4-ethylenedioxythiophene)(PEDOT) doped with polystyrene sulfonate (PSS)/ISM based ISE.[61] In both of these fully-integrated solid-contact designs, each single use device only requires application of sample solution–10 or 20 µL, respectively–and connection to a potentiostat a stable signal is reached within 30 sec.

While these examples are targeted for external analysis, such an integrated design can also be incorporated into wearable devices. For example, a microfluidic sensor was fabricated on a cotton T-shirt by infusing the shirt with acrylonitrile butadiene styrene to form hydrophobic barriers and screen-printing both ion-selective and reference membranes for Ca^{2+} detection and then coupling to a wearable potentiometer for on-body readout.[62] In addition to introducing novel, scalable approach to creating hydrophobic barriers on textiles, this report also demonstrated the need for microfluidics to refresh sweat in detection zones by comparing errors in devices with and without the patch.

In some devices without integrated sample containing capabilities, another element can be added to enable fluid to flow across electrodes. In one fully reusable device, a piece of filter paper was incorporated into a thermoplastic unit containing an ISE and RE to move sample from the inlet well into contact with sensors.[63] Another way to do

this is to 3D print a separate microfluidic cell and couple it with a screen printed electrode to ensure old sweat moves away from sensors and new sweat enters, as in a reusable sweat patch for on-body measurements.[64] On-body patches for measuring concentrations in sweat have also coupled sponges[56] and filter paper[65] into devices containing reference and sensing electrodes (see Fig. 1-2B). Sweat was also wicked into contact with ion-selective and reference electrodes printed onto a single piece of polyethylene terephthalate (PET) coupled into a custom built smart watch for immediate and local reading of results.[66]

Fibers and Yarns

Within the field of textile-based sensors, there is limited consensus on the use of the terms thread, yarn, and fiber. For clarity, we define the terms here for use throughout this review. Fiber is the smallest base unit for textiles; thread is a thin strand of fibers normally used in sewing and embroidery; and yarn is a thick strand of fibers used in knitting and crocheting (see Fig. 1-2C). Electrodes have been made from all three.

Threads are coated with conductive inks and membrane cocktails by either dip-coating[67] or application with swabs[57] or brushes and have a diameter of 1 mm or less (see Fig. 1-2D). Cross-sectional images confirm a coating of external threads but no penetration into internal fibers.[57,67] As with strip-type ISEs mentioned previously, thread-based ISEs have also been used by immersion into a sample, with small sample volumes as a major benefit. For example, several thread based ISEs with diameters of 600 μm were coupled together for multiplex sensing in sample volumes as low as 200 μL.[57] However, this multiplexed sensor was measured against a conventional reference

electrode and authors acknowledged the need to develop a thread-based RE for a fully integrated device. Another thread-based sensor used by sample immersion was improved by replacing the initial conventional RE with a thread-based RE to obtain a more integrated thread-based device.[67,68]

Thread-based ISEs have also been incorporated into setups that contain a wicking component, expanding the applications of these sensors to uses without a separate sample holder. For example, a cotton yarn based ISE coupled with a commercial mini-RE was attached with heat shrinking tape to a band-aid for continuous sensing of wound pH.[69] Thread-based ion-selective and reference electrodes were also glued into an on body patch that contained a cotton strip to wick sample into contact with threads.[70]

Threads have also been reported to maintain high flexibility and mechanical strength when used for ISEs, which allows them to be sewn/woven into textiles (see Fig. 1-2E).[58,71,72] For example, thread based ISEs and RE were sewn into a bandage, held in place by a hydrophobic adhesive film and coupled with a strip of gauze for wound monitoring.[72] The removal of all glues and adhesives in contact with ISEs is also desirable, to both simplify design and remove any potential source of contamination. For example, sensing and reference fibers were directly woven into a fabric without any additional materials.[58] The sensing fabric maintained structural integrity despite bending, twisting and rinsing, while screen printed electrochemical textiles often suffer delamination under similar conditions.[58]

Fiber-based electrodes are much smaller and often require a 2-step integration to be incorporated into textiles. For example, ISM or reference membrane coated Au

nanowires with final diameters of 500 μm were wound around a length of spandex that was then integrated into a headband.[71] Additionally, a reduced graphene oxide microfibers-based electrodes were woven into a fiber and then into a textile.[73]

MATERIALS AND SUBSTRATES USED

Guiding principles

To comply with the demands for a point-of-care device, the materials to be used as supporting substrates must meet certain minimum criteria, namely, high mechanical strength, compatibility with mass production methods, high availability, low cost, and lack of interference with sample analytes. High mechanical strength is necessary if devices are to be transported to, and used in, field settings but the material does not need to be as robust as that for wearable devices. For devices to be produced on a large scale, all fabrication steps must shift from handmade to mass-production methods. Additionally, the material must be inert towards both sample and sensing components and not affect analytical performance. An acceptable alternative is a material whose surface chemistry can be easily altered to meet these criteria. Finally, high availability and low cost are also important to prevent sourcing or cost issues.[1,74] For a fully integrated device that moves sample from a sample introduction zone into contact with sensing components, the material must also have wicking abilities, and sample uptake, evaporation speed and wicking rate should all be considered. Compatibility with wax printing, or the ability to form hydrophobic barriers to control fluidic flow is desired to fabricate devices with sample containment. However, the latter can also be achieved through laser cutting, which then

evidently does not require compatibility with wax printing.

Characterization of substrates chosen is important for identification of possible interactions, contaminants, and more information necessary to understand the performance issues that will be discussed in the Sections 4-6. When using materials purchased from companies that have online databases and materials sheets, authors often include little characterization information as they assume that readers can look up additional information online. However, such information may not reflect changes to commercial products over the years, is not guaranteed to be available to future readers, and is often limited due to proprietary reasons. Therefore, we recommend that authors list in their publications as much information from materials safety data sheets as well as other supplier information as available. In addition, in many articles, supporting substrates were reported to come from “local stores,” providing readers no opportunity to obtain additional information. In such cases, it is particularly important for authors to report a full physiochemical characterization of all materials used.

Polymeric Supports

One broad category of supports are non-porous synthetic polymeric materials which serve only as a physical backing and support. PET, an economical thermoplastic polymer of high tensile strength that can be spun into textiles or extruded as a hard plastic,[75,76] is one of the most common synthetic polymers used. It has been used in the preparation of ISEs as sheets[10,25,45,65,66,77] and films[47,48] of various thicknesses (see Fig 1-3A). Other nonporous polymeric substrates used as supports of ISE devices include polyimide,[78] a flexible polyurethane support (in this case full details on in-house

preparation and characterization provided),[64] 200 µm thick polydimethylsiloxane,[56] a 3D drawn polylactide,[38] and polypropylene synthetic paper.[43]

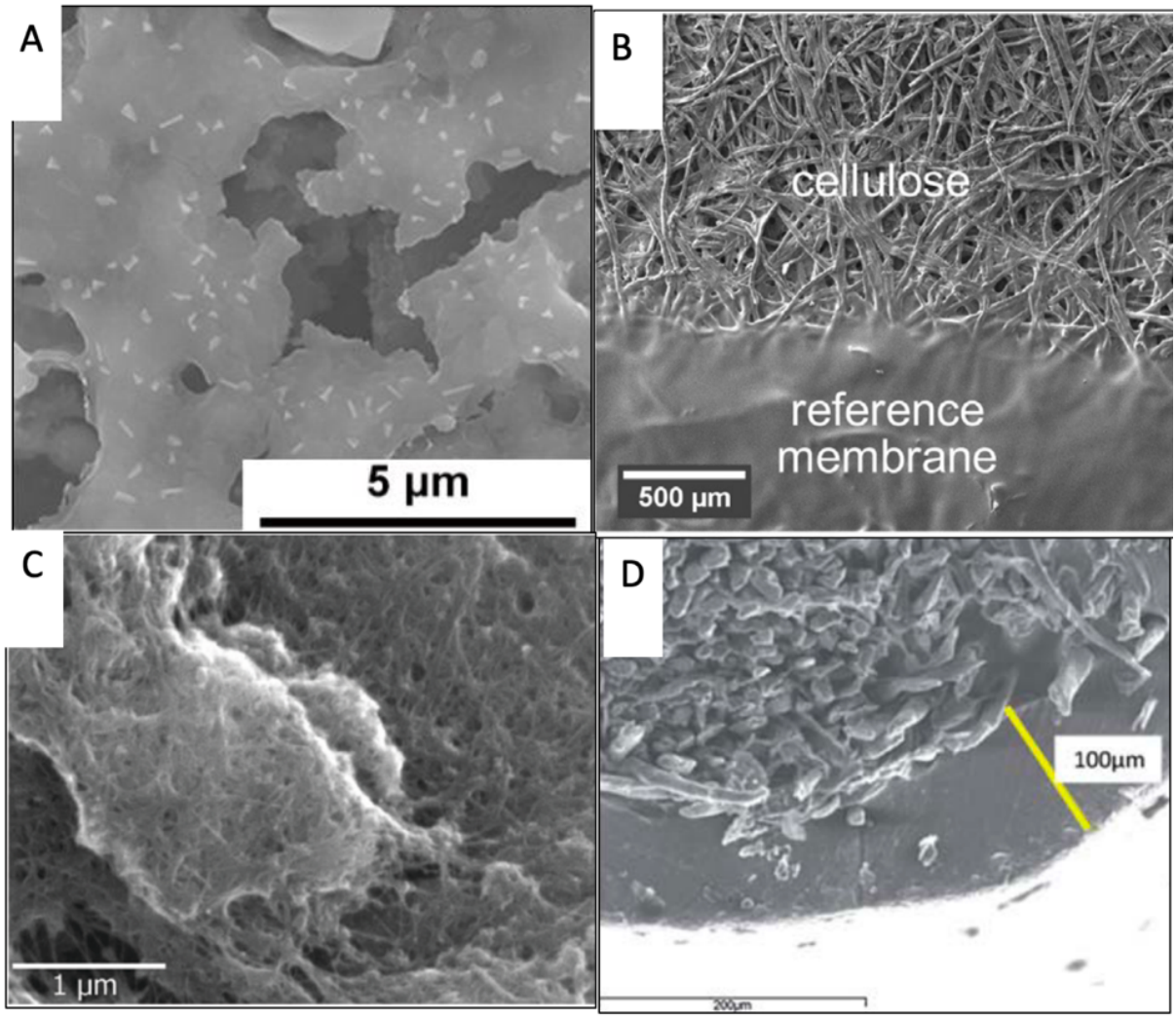

Figure 1-3. Scanning electron microscopy images of coated substrates: (A) NaCl doped poly(vinyl butyral) reference membrane deposited on top of a sheet of PET, (B) ashless filter paper coated with a PVC reference membrane, (C) CNT coated filter paper, and (D) cross sectional view of a membrane coated yarn. Adapted from references 21,48,54,79.

Paper

Filter paper, composed of randomly oriented alpha cellulose fibers, is another very common material used in point-of-care devices due to its high mechanical stability, wicking abilities, bio-degradability, and low-cost when purchased in bulk quantities.[8,13,15,80–82] The use of wax-printing to quickly print hydrophobic barriers to control fluid flow, as first shown in 2009,[50,51] has greatly increased paper's popularity.

As filter papers are traditionally used in separations and purifications, they are available in many pore sizes and ash contents. Devices have been made with qualitative filter paper of 11 µm pore size (Whatman 1, ash 0.01%),[22,52] and ashless quantitative filter papers of 12-25 µm (Whatman 589/1, Black-Ribbon),[18,19] 4-12 µm (Whatman 589/2, White Ribbon),[18,54,59,60] and 2 µm (Whatman 589/3, Blue Ribbon)[19] pore size (see Fig. 3B). Nitrocellulose paper with a pore size of 0.2 µm was also used.[17] While filter paper is the most common form used in potentiometric devices, other cellulose-based materials such as tissues and delicate task wipes have also been tested in substrate-based sampling.[19]

Filter paper has also been modified in a variety of ways to minimize interactions with analytes, enhance ease-of-use, or create highly conductive surfaces. The negatively charged cellulose structure may interact with samples (discussed in Sections 4-6), therefore, modifications to reduce interactions of filter paper and sample through acidification[30] and soaking in inorganic salts,[27] heavy metals,[30] and ISM components[28] have been reported. Modifications to improve sensors' ease-of-use, such as protamine-

doping to enable ionic-strength independent measurements[33] and Au modified filter paper to reduce biofouling of conventional sensors by blood,[26] have also been reported. Paper has also been saturated with KCl to serve as a pseudo-RE[34,61] and fully coated with conductive inks such as CNT (see Fig. 3C), [21,36,37,41,42] carbon and AgCl/Ag[23]. Finally, paper has also been fully functionalized with trichloro(1*H*,1*H*,2*H*,2*H*-perfluorooctyl)silane and then coated with graphene to create a highly hydrophobic, conductive substrate upon which to print electrodes.[44] While modification may enhance device overall performance, many modifications result in a loss of hydrophilicity, add significant costs and fabrication steps, and complicate final disposal of devices, in which case one wonders whether "paper-based" is really all that attractive anymore.

Textiles

While textile-based sensors are commonly known for use in wearable devices, many of the characteristics that make them well suite in wearable devices also make them well-suited for miniaturized sensors for point-of-care usage.[14,83] These include including high flexibility, robustness, and ease of control of physical dimensions.

A variety of non-conductive textiles are used as supports for miniaturized sensors, with cotton and polyester as the two most common. As a naturally derived material, cotton is generally seen as more sustainable and able to be disposed of easier than synthetic materials. Cotton has been used in the form of thread (see Fig. 3D),[57,67,79] a 0.3 mm thick shirt,[62] purchased from local clothing stores (without further description),[31,84] and as a blend with 5 % elastane.[31] Polyester is the most commonly used synthetic material for textile-based sensors and has been used as threads,[72] a cleanroom wipe,[55] purchased

from local clothing stores (without further description),[31,84] as well as blended with 5% elastane,[31] and coated with polyurethane.[84] While PET is the most common form of polyester used in fiber production,[85] it cannot be assumed that all commercially available polyesters do not contain alternative monomers. If purity cannot be guaranteed from a vendor, a simple basic hydrolysis of the material can be performed to obtain monomeric units for analysis.[55] Polyimide, as well as polyimide-elastane blends have also been used in substrate-based sampling.[31]

Threads composed of conductive fibers offer the same physical advantages of fibers while removing the need to apply a conductive coating and are therefore gaining popularity. Lab-made conductive fibers synthesized and incorporated into potentiometric sensors include lab-spun CNT fibers,[58] Au nanowires and styrene-ethylene/butylene-styrene fibers,[71,86] and reduced graphene oxide fibers.[73] While in-house fabrication offers control over fiber properties, high availability is another key property when evaluating possible supporting substrates. In an effort to address this concern, commercially available conductive threads of carbon (1 mm ∅ with 6 μm ∅ fibers[70] and 0.27 mm ∅ with 0.08 mm ∅ fibers[67]) and stainless-steel fibers[72] have also been used. While commercially available conductive threads simplify fabrication of sensors, the cost is still significantly higher than non-conductive materials and is a significant drawback.

Thus far, no supporting material reviewed meets all the demands of a point-of-care device. Rather, each material offers distinct advantages and disadvantages which must be evaluated in the context of the specific setting and of the device to be designed. The final factor that must be considered is the potential interaction of the material with sample

or sensing components. Such interferences can alter device performance and are examined in the following sections on slope, reproducibility, and lower limits of detection.

SLOPE

Overview of Slopes in Potentiometry

The electromotive force (EMF), as measured with an ISE, is as a function of the activity of the target ion in the sample. It is predicted by the Nernst equation, $EMF = E^0 + (2.303RT)/(z_iF)\log a_i$, where R, T, z_i, F, and a_i represent the universal gas constant, temperature, ion valency, Faraday's constant, and activity of target ion i with charge z_i, respectively.[87] For a cation at 20 °C, this results for the plot of EMF versus log a_i in a linear response with a slope of 58.2 mV z^{-1} / decade, referred to as a Nernstian response.

The response slope of an ISE should be referred to as non-Nernstian when the value of the Nernstian slope falls outside of the confidence interval determined from a fit of the experimental data. However, the literature often only reports slope values, even though standard deviations or confidence intervals would be readily available from such fits. Therefore, we refer here to distinctly sub- or super-Nernstian response slopes when a reported response slope deviates by $6\ \mathrm{mV}\ z^{-1}$ / decade or more from the theoretical response slope. In the absence of a widely accepted criterion for when a response slope deviates significantly from theory, we chose this value because it corresponds to >10% deviation from the theoretically predicted Nernstian slope. While a sensor with a linear but non-Nernstian response slope can still be used to make accurate determinations of target ion activities, it is important to understand the source of non-theoretical responses

to assess the robustness of a device. Too often, a non-theoretical response slope also comes along with limited reproducibility.

Common Sources of Non-Theoretical Slopes

In reviewing response slopes for miniaturized devices as reported in the literature, we noticed three common origins for non-ideal performance: improper calculation of slopes, slopes computed using data outside of the Nernstian range, and interactions between target ions and underlying support substrates.

When two electrolyte solutions contact each other, as at the interface of a sample and a bridge electrolyte that separates the sample from a RE, a liquid junction potential arises. If this liquid junction potential varies over the range of the calibration curve, the response slope deviates from the expected theoretical (Nernstian) value. This can be avoided by correcting for the liquid junction potential using the Henderson equation.[87] Similarly, if activity coefficients vary with the sample composition, plots of the EMF versus the logarithm of the sample concentration will give nonlinear response slopes. This can avoided by converting the concentration of the target ions to activities, which can be done, e.g., using a two-parameter Debye–Hückel approximation.[88] This will appear obvious to many readers, but we note that there are quite a number of literature examples that do not account for either liquid junction potentials or activity coefficients.[27,28,30,34,43,48,56,57,61,78]

The effect of such improper calculations of slopes depends on the composition of both the reference electrode and the sample solution. When using a 3 M KCl based reference electrode in a sample of 1-100 mM KCl, the slope would decrease by 0.4, 3.6, and 3.9 mV/decade Cl^- when failing to account for liquid junction potentials, activity, and

liquid junction potentials and activity, respectively. For the same reference electrode in a sample of 1-100 mM $CaCl_2$, the slope would increase by 1.0, 2.1 and 3.0 mV/decade Ca^{2+} when failing to account for liquid junction potentials, activity, and liquid junction potentials and activity, respectively. While most of these deviations are less than the $6\,\mathrm{mV}\,z^{-1}$/ decade tolerance defined above, they are still an important factor to consider when evaluating any deviations from Nernstian behavior.

The second pattern observed in the reporting of non-ideal slopes for miniaturized potentiometric devices is that of poorly chosen linear fits. If a linear fit is chosen past either the upper or lower LOD, it will be skewed by data points that are not in the linear sensing region of the ISE and result in an artificially high or low slope. While some papers provide the linear fit both with and without these additional data points, it is often the case that visual observation of a calibration curve reveals an improper fit and the reader must make an educated guess at the proper slope with only points in the linear region.[47,48,72]

The third source of non-ideal slopes in the miniaturized ISEs reviewed here is the occurrence of interactions between target analytes and the underlying support substrate. The most common of these being the complexation of divalent cations and filter paper, which results in super-Nernstian response slopes for the detection of the divalent cations, and whose impact correlates with the strength of interaction between ions and wood fibers.[19,34] A super-Nernstian jump at lower concentrations was also found,[27] similar to that seen in either unconditioned membranes or samples with ion-flux towards the inner filling solution.[89] Comparisons of sensor performance as a function of the supporting material show the interaction depends on the physiochemical structure of the support.[29,31]

While pore structure in particular has also been shown to correlate with performance, it is not generally taken into consideration.[29,72]

Slopes in substrate-based sampling

When using substrate-based sampling, super-Nernstian responses have been reported in both the full linear range and isolated to the lower end of linear ranges. When using a solid-contact RE and a solid-contact K^+ ISE with filter paper-based sampling, pore size was shown to correlate inversely with slope. A slope of 63.1 ± 5.8 mV/decade was found for paper with 2 µm pores in contrast to 54.7 ± 2.1 mV/decade for paper with 12-25 µm pores. Additionally, when varying the shape of the sampling substrate the response slope of the paper with larger pores was less sensitive to changes compared to paper with smaller pores. While one might think this observation to be caused by evaporation differences due to pore size, the authors found drift to vary minimally between paper substrates, disproving that hypothesis.[18] The effect of an alternative RE design has also been tested. With solid-contact ISEs and a RE of a disposable 3 M KCl loaded paper in contact with a reusable Ag/AgCl element, Cl^- responses remained unchanged while K^+ responses increased by 3 mV/decade and Na^+ by 4 mV/decade.[34]

In additional testing of paper-based sampling, several ions exhibited increases in slope compared to analogous beaker-based setups.[19,34] When using crystalline solid-state ISEs, Cl^- responses increased by 3 mV/decade and Cd^{2+} by 6 mV/decade, resulting in a super-Nernstian response, and Pb^{2+} exhibited a super-Nernstian response from 10^{-3}-10^{-4} M (see Fig. 4A). The shift to a super-Nernstian response is more pronounced at lower concentrations, seen as a super-Nernstian jump.[27] In contrast, textile-based

sampling has been shown to shift responses slopes towards both sub- and super-Nernstian responses. For Cl^- sensing with a crystalline solid-state sensor there was no change in response slope from beaker to textile-based sensing but when using a conducting polymer containing solid-contact Cl^- ISE, response slopes were sub-Nernstian for all synthetic textiles but still Nernstian for cotton textiles.[31] The material-dependent shift in response slopes is attributed to the high redox sensitivity of the conducting polymers in the solid-contact electrode.[31] However, these same textiles exhibited Nernstian responses when used with solid-contact ISEs for Na^+ and K^+, indicating that redox sensitivity of the PEDOT contact is also dependent upon target ion. When measuring Cd^{2+} and Pb^{2+} with crystalline solid-state ISEs, a shift from Nernstian to super-Nernstian slopes at lower concentrations was observed for all textiles, again explained in terms of strengths of binding of the divalent cation to the cellulose or polyester blends used.

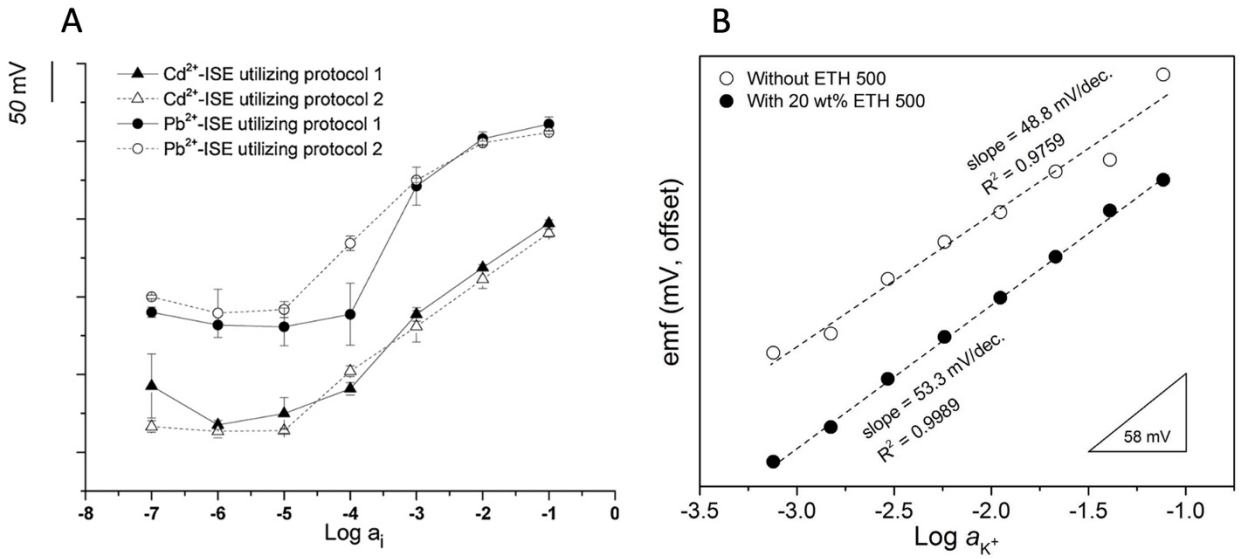

Figure 1-4. Potentiometric responses of Cd^{2+} and Pb^{2+} ISEs in filter paper-based sampling with pristine (Protocol 1) and inorganic salt-soaked filter paper (Protocol 2), (B) Potentiometric response of paper-based K^+ ISEs with and without tetradodecylammonium tetrakis(4-chlorophenyl)borate (ETH 500) in the ISM. Adapted from references 27,54.

By understanding these systems, successful efforts have been made to mediate non-ideal slopes. For example, in sponge-based sampling, adsorption of Cd^{2+} and Pb^{2+} by commercially produced polyurethane and cellulose sponges as well as natural sea sponges was quantified and used as a screening criterion to choose the ideal sponge for sampling. In this system, sponges were cut into pieces $3 \times 2 \times 0.5$ cm^3 and had macro-sized pores, in contrast to the previously used filter paper and textiles that were thinner than 1 mm and had smaller pores. Polyurethane was chosen due to its low sorption and Nernstian responses were achieved for both Cd^{2+} and Pb^{2+} in addition to K^+, Na^+, and Cl^-.[29] Again, the physical structure of the material was not studied, and it would have been

interesting to see data for a cellulose-based sponge to confirm responses deviations were due to the chemical nature of materials rather than the pore structure.

Super-Nernstian responses in filter-paper based sampling were overcome by soaking paper in an inorganic salt with the cation the same as the target ion (see Fig. 3A),[27] various ISM components,[28] and acidification with HCl.[30] Interestingly, when examining the effect of ISM modified filter paper, the authors also found a super-Nernstian response when the modified filter paper was kept in contact with electrodes but placed into a beaker of sample solution, showing that sample volume does not affect performance.[28]

Interferences depend upon chemical characteristics of the substrate as well as the identity of the target ion and can be overcome through modifications. It is interesting to note that the only anion measured in the setups reviewed is Cl^-, with ionophore-free membranes while all cations were measured in ionophore-containing membranes. It can therefore not be concluded that the interferences are also due to the presence of an ionophore.

Slopes in Strip-Type Sensors

Similar to with substrate-based sampling, Nernstian responses for Na^+ and K^+ ISEs were found with strip-type sensors in which PET[24] or paper[37] was coated with a SWCNT/poly(3-octylthiophene) suspension. In contrast to substrate-based sampling, here the underlying substrate is fully coated with SWCNT, and there is no substrate/sample or substrate/ISM interface. However, slight sub-Nernstian responses were found for Cd^{2+} (27.4 ± 0.4 mV/decade), Ag^+ (54.2 ± 0.6 mV/decade), and K^+ (56.7 ±

0.8 mV/decade)[36] when SWCNT coated filter paper was then coated with Au and finally poly(3-octylthiophene).[36]

A super-Nernstian response (exact value not reported) was also found in the low concentration region (below 10^{-5}) for strip-type sensors of CNT-coated filter paper coated with a K^+ ISM. This was attributed to Na^+ interfering ions at the backside of the ISM, present in the CNT suspension. It is interesting to note that the interference was observed in paper and not in conventional setups because of the different amounts of CNT suspension used.[90] This scaling consideration is very important to keep in mind; it was also shown that trace level contamination from conductive inks used for Cl^- sensing effect the performance with volumes of 20 µL sized samples but not 100 mL samples.[91]

When using a strip-type sensor of ISMs drop cast on a 3D-drawn support of polylactide and carbon black composite, sub-Nernstian responses were observed for all ions measured (Ca^{2+}: 24.6 ± 1.2, K^+: 55.5 ±0.6, and Cl^-: -52.2 ± 0.3 mV/decade).[38] In contrast to devices mentioned earlier in this section, where the underlying support was coated with CNT, here the solid contact consisted of a thermoprocessable carbon black/polylactide composite drawn onto the underlying polylactide.

Slopes in Sensors Built on Top of a Substrate

A K^+ ISE integrated with a RE was built on a PET substrate with conductive strips of carbon ink, a layer of SWCNT functionalized with octadecylamine groups and either a K^+ ISM or reference membrane. In this device both membranes were made of a photo-cured poly(*n*-butylacrylate) and the K^+ ISM contained, in addition to standard ionophore and ionic site, 1 wt % ETH 500. Nernstian responses were observed both upon immersion in

a beaker (volume not specified) versus a conventional RE and with the integrated RE.[25]

In one report, a silver ink was screen printed on a homemade polyurethane substrate followed by drop casting of a multi-walled carbon nanotube suspension and then either an ISM or an ionic-liquid-based reference membrane. Nernstian responses were reported for Cl^- and K^+ sensing but sub-Nernstian responses for Na^+ (53.5 ± 0.9). While the authors did not address these low response slopes, conventional all-solid-state ISEs of analogous designs also gave sub-Nernstian responses when used with beaker-based sampling (54.4 ± 2.2 mV/decade), suggesting that the low slope was not due to miniaturization but rather electrode design or ISM composition.[64] This highlights the importance of reporting control experiments for proper comparisons and analysis of sub-optimal performance.

When using a screen-printed ISE of a plasticized, ionophore-doped ISM on graphene/PEDOT:PSS coated filter paper, with 20 µL droplets, Nernstian response slopes of 62.5 and 62.9 mV/decade were observed for Na^+ and K^+, respectively. Interestingly, the authors also noted that sub-Nernstian responses (Na^+: 43.6, K^+ 46.1 mV/decade) were observed when graphene was not also doped into the PEDOT:PSS, which they attribute to PEDOT:PSS's tendency to form a water layer.[61]

An array of Na^+ and K^+ ISEs and a RE of membrane drop cast on Au screen printed onto PI substrate gave a sub-Nernstian response for Na^+ (43.76 mV/decade) but Nernstian for K^+. Here calibration conditions are unclear: the volume of solution used and whether a pure salt solution or a PBS solution was used. Such information would guide interpretation of the use of concentration instead of activity, and comparison with devices

reported by other groups.[78]

An array of ionophore-doped poly(vinyl) chloride (PVC) ISM/reduced graphene oxide/Au nanoparticle/carbon ink/Ag nano wire sensors for Ca^{2+}, AgCl/Ag ink for Cl^- detection and a RE, all on top of PDMS material, gave a Nernstian response for Ca^{2+} (28.53 mV/decade) but sub-Nernstian for Cl^- (-51.5 mV/decade). There are several possible factors that could explain the low slope including the previously listed analysis of data and possible interference from the sponge of unspecified material used for sample uptake.[56] Again, lack of experimental detail or running of controls makes it difficult to generalize from this data.

Another array included ionophore-doped nanocomposites containing both polystyrene and Au nanoparticles for Na^+ and K^+ sensing. In addition, nanocomposites doped with Ag^+ ionophore were used for a calibration channel, which accounts for background signal as the urine samples used have a constant and negligible Ag^+ concentration. When tested in simulated urine samples, the sensor gave sub-Nernstian responses of 50.3 ± 1.3 and 53.5 ± 1.2 mV/decade in Na^+ and K^+, respectively.[43] As neither control experiments with the nanocomposites and a Ag^+ calibration channel, nor calibrations of the array in pure salt solution were reported, it is unclear whether the sub-Nernstian response was due to the novel ISE design, miniaturization, or interference from the urine matrix. In another system for epidermal sweat sensing bis(2-ethylhexyl) sebacate (DOS) plasticized PVC ISMs was drop cast on screen-printed carbon on PET.[48] Here a sub-Nernstian slope of 48.5 mV/decade was reported for K^+ sensing, however a poorly chosen selection of the range for the linear fit and the use of a Na^+ counter salt of

the ionic site without conditioning may explain some of the low response slope. Interestingly, the K^+ ISE gave a slightly super-Nernstian response of 63.1 mV/decade while the pH ISE had a response of 55.50 ± 6.31 mV/pH, within error of Nernstian.

Slopes in Sandwich-Type Sensors

Sub-Nernstian responses have been observed in sandwich-type setups with filter paper and either ionophore-containing or ionophore-free sensing membranes. In ionophore-containing membranes, a sub-Nernstian slope of 22.9 ± 0.8 mV/decade was observed for Ca^{2+} while Nernstian responses of 54.9 ± 0.6 and 54.8 ± 1 mV/decade were observed for K^+ and Na^+ respectively.[22] In contrast, a membrane-free Cl^- sensing system using the same filter paper gave a Nernstian response (61.8 ± 1.0 mV/decade). Another sandwich-type setup was developed for ionophore-free bilirubin sensing (ISM of PVC, DOS, tridodecylmethylammonium chloride), a divalent anion, and again a sub-Nernstian response (-22 mV/decade) was observed.[52]

All the membranes mentioned in this section thus far have been PVC based. However, the same sandwich-type setup was used with a 3D-printed ion exchange membrane composed of a photocurable acrylate monomer, DOS as plasticizer and tetrakis(*p*-chlorophenyl)borate as ion exchanger, and gave a slope of 58.4 mV/decade. In is interesting to note however, that the slope still differs from the same ISM in an analogous setup with a beaker-based measurement and inner filling solution containing ISE (52.5 mV/decade).

Slopes in Sensors with Wicking and Membranes Incorporated into One Piece

Sub-Nernstian slopes have also been reported in setups with membranes

integrated into the underlying substrate. Using a polyether ether ketone-based hydrophilic high-capacity anion exchange membrane for Cl^- sensing and an ionic-liquid-based PVC reference membrane and a filter paper support, a Nernstian response was achieved with both an inner filling setup (-57.3 mV/decade)[54] and a redox-buffer doped colloid-imprinted mesoporous carbon solid-contact design (-60.6 mV/decade).[60] When switching to an ionophore-doped PVC membrane for K^+ sensing, a sub-Nernstian response of 48.8 mV/decade was observed, but it was improved to 53.3 mV/decade by the addition into the ISM of 20 wt % ETH 500, an inert electrolyte (see Fig. 3B).[54] While resistance may have played some role affecting this slope, it must be noted that ETH 500 decreased the resistance by less than an order of magnitude, and the 10.9 ± 1.2 MΩ initial resistance was significantly lower than the 10 TΩ input impedance of the potentiometer.

A PET textile embedded with a PVC Cl^- ion exchange membrane with the same setup as the previous paper-based devices also gave a slightly sub-Nernstian response (55.5 ± 1.7 mV/decade). A hydrophilic high-capacity anion-exchange membrane was also incorporated into the polyester textile, but results were reported for serum samples only and not for aqueous KCl solution, as all the other data here, so a comparison is difficult.[55]

Slopes in Textile-Based Sensors

In a cotton thread-based ISE with a conventional double-junction RE, sub-Nernstian responses were observed for Ca^{2+} (26.3 ± 0.5 mV/decade), and Cl^- (–52 mV/decade; as estimated from a figure), while a Nernstian response was observed for K^+ (53.6 ± 0.7 mV/decade) and Na^+ (59.1 ± 1.1 mV/decade). These authors also explored different support materials for K^+ sensing with the same graphite ink. Devices with a Nylon

support had slopes of –60.4 ± 4.0 mV/decade while those with a cotton support had slopes of 55.2 ± 1.4 mV/decade but were not pursued due to poor E^0 reproducibility (± 26.8 mV compared to ± 11.2 mV). While the ISM was not in contact with support, it is clear that contact between the solid contact and support material may result in interactions.[57]

Deviations in slope are also reported for other textile-based setups with integrated REs. For CNT fibers coated with either an ISM or a Ag/AgCl ink and NaCl doped reference membrane, sub-Nernstian responses were observed for Na^+, K^+ and pH (45.8, 35.9, and 42 mV/decade estimated from graph) while a super-Nernstian response was observed for Ca^{2+} (52.3 mV/decade).[58] In each of these membranes the Na^+ salt of the ionic site was used and membranes were not conditioned, which would explain a slight sub-Nernstian response for K^+ but none of the other deviations. It is also interesting to note that a single design here gives both super- and sub-Nernstian responses for different cations; one would expect a similar deviation for similarly charged species.

Overall, substrate-based sampling generally results in increases in slope compared to conventional sensing, while setups with the ISE and/or RE built into the underlying material generally result in sub-Nernstian responses, ultimately suggesting interactions between substrates and samples cause these problems. A more complete understanding of the nature of possible interactions is made difficult to reach with data reporting that may not account for liquid junction potentials and activity coefficients or provide comparison to beaker-based measurements for analogous electrodes.

REPRODUCIBILITY

Overview of reproducibility in potentiometry

The term “calibration-free” has been used to refer to sensors with a low standard deviation in the standard electrochemical potential (E^0) of various electrodes of the same design.[4] If the standard deviation of E^0 between devices is sufficiently low, a single calibration curve may be performed on one electrode and used for all subsequent electrodes. However, there is no universal acceptable value for the SD of E^0. Instead, each application dictates the tolerable limits. For example, for diagnostic tests the U.S. Food and Drug Administration mandates a maximum acceptable error for Na^+ of ± 4 mM within the range of 80-200 mM, which translates to a 0.7 mV acceptable standard deviation for an ISE,[92] while manufacturers of clinical mainframe analyzers, which are recalibrated very frequently, strive for substantially narrower confidence intervals.

Unfortunately, reproducibility is often not reported for miniaturized sensors. Parameters such as % RSD of several electrodes of the same batch,[67,70,93] day-to-day reproducibility of the same sensor,[94] SD of EMF at a single concentration,[41,52] average of the SDs for various electrodes in the same solution within the linear range,[21,24] error calculated from student’s t-test,[79] and unclear statements of SD[38,53,62,73] are reported instead, which makes direct comparisons often difficult. Relative errors of E^0 are not a helpful parameter to report, as E^0 values vary by orders of magnitude and therefore are not comparable across designs. Some literature reports include the %RSD as well as the average E^0, in which case the reader can calculate the SD of E^0, however, this is not an ideal practice. It is important to report the reproducibility of data to compare various

designs aimed toward calibration-free sensing. In this section, therefore, we only discuss articles in which the SD of E^0 (or % RSD along with average E^0) was reported.

Reproducibility of E^0 in non-optimized, miniaturized ISEs

Reproducibility in non-optimized, miniaturized ISEs is generally on the order of several mV and is often attributed to the handmade nature of the many components. An early report of a rectangle laser-printed on PET and then a PEDOT:PSS solid contact followed by drop cast of a Ca^{2+} ISM gave a SD of 0.7 mV.[35] In thread-based sensing, a cotton thread painted with conductive ink and dip-coated in ISMs gave SDs of 2.3, 3.4, 2.6, and 0.5 mV “or better" for K^+, Na^+, Ca^{2+}, and Cl^-, respectively.[57] However, these were both used with a double-junction RE and beaker-based sampling.

Steps towards integrated devices include a RE in an array of sensors built up on top of a substrate. For an array made of graphene paper strips dipped into *o*-NPOE plasticized PVC ISM cocktail, with tetrahydrofuran as solvent, and laid on plastic, with no underlying support for the solid contact, SDs of 18, 21, and 16 mV were reported for K^+, Ca^{2+}, and pH, respectively. It is unclear whether this data was obtained with a miniaturized RE comprising a photocured polyacrylate reference membrane doped with KCl, AgCl and ETH 500 or a conventional double-junction RE. The high SDs were hypothesized to be due to inhomogeneities in the thickness and composition of the graphene nanopaper and poor adherence between paper and the ISM.[95]

Another array with polystyrene-Au ionophore doped nanocomposites for Na^+ and K^+ sensing, polystyrene-Au ionophore doped nanocomposites for Ag^+ ISE-based calibration channel, and a NaCl doped poly(vinyl butyral) RE had an E^0 SD of 5.6 and 6.0 mV (n=10)

for Na^+ and K^+, respectively.[43] Unfortunately, in both of these arrays, the experimental details do not clearly state whether the arrays were used by dipping into beakers of solution or by dropping samples onto them and whether data is from use of a custom or a conventional RE. These details are important to include when considering the effects of miniaturization on device performance.

Integrated sensors that use a wicking material with the sample size close to clinical relevance (20-30 µL) provide reproducibility data more similar to real-world use. Textile-based devices with embedded ISM and ionic-liquid-based reference membrane showed similar SDs for Cl^- ion exchange membranes in aqueous and serum samples, and hydrophilic high-capacity anion-exchange membrane in serum (4.2, 3.5, and 3.0 mV, respectively).[55] Paper-based devices with the same reference membrane showed similar reproducibility with a hydrophilic high-capacity anion-exchange membrane in aqueous samples and serum, as well as K^+ ionophore containing ISMs (SD of 2.0, 1.6, and 1.6 mV).[54] Additionally, paper infiltrated with the hydrophilic high-capacity anion-exchange membrane was also tested in a conventional setup and gave a SD of 2.2 mV, showing that in these sensors miniaturization did not worsen the reproducibility. In another similar setup, fully-inkjet-printed sensors with a lipophilic salt containing reference membrane and ionophore containing ISMs gave a SD of 5.1 and 2.8 mV for Na^+ and K^+ sensing, respectively.

Some articles also compare the performance of miniature ISEs when used with conventional or miniaturized REs, which allows analysis of the effect of miniaturization of RE on reproducibility. Lithium sensing yarns gave a SD of 8.7 mV when tested against a

double junction RE but 13.0 mV when tested against a Ag/AgCl coated carbon fiber dip coated with a reference membrane.[67] An ion patch for Cl^-, K^+, Na^+ and pH detection was tested with respect to both a double-junction RE and a patch RE. While the SD of E^0 upon using a patch RE showed minimal change for Cl^- sensing (5.2 to 6.8 mV), it decreased significantly for Na^+ sensing (from 12.7 to 0.3 mV), and increased for pH sensing (4.6 to 12.5 mV), suggesting analyte specific effects of RE integration.[64]

Reproducibility of E^0 in sensors designed for high reproducibility

Some of the recent work on miniaturized sensors has specifically focused on improving the E^0 reproducibility. One strategy is based on the use of a molecular redox buffer that resists changes in the phase boundary at the interface between the ISM and the underlying electron conductor, much like a pH buffer resists changes in the pH of a solution. In the first example for incorporation of equimolar amounts of redox buffers into miniaturized sensors, the hydrophobic redox buffer cobalt(II/III)tris(4,4′-dinonyl-2,2′-bipyridyl) was included into both the ISM overlying and an ionic-liquid-based reference membrane, both overlying a colloid-imprinted mesoporous carbon solid contact. In this fully-integrated paper-based device, an impressive SD of 2.1 mV was obtained, compared to a SD of 2.8 for an analogous conventional setup.[59]

In the next generation of devices, the previous design was improved to include a sensing membrane and a different redox buffer; 7,7,8,8-tetracyanoquinodimethane and the corresponding anion radical. While use of this in a conventional setup redox buffer resulted in a fairly reproducible SD of 4.3 mV without conditioning, after 24 h, the SD increased to 14.0 mV and translation to a paper-based setup resulted in poor linearity

and the SD was not reported. Future work was said to be done to develop a more hydrophobic buffer that did not leach out of membranes, as posited to be the main problem in this study.[60]

Other work has also shown that non-equimolar amounts of redox species improve reproducibility as well. For example, CNT coated filter paper was coated with a cobalt(II)porphyrin and cobalt(III)corrole doped CNT layer before drop casting of a K^+ ISM in an effort to improve reproducibility. Indeed, an impressive SD of 1.7 mV was obtained on Day 1 and lowered to 0.6 mV on Day 2. Such high reproducibility and stability over time were said to be due to the ability of the porphyrinoids to limit ion-flux across the membrane.[90] However, in response, it was shown that even small impurities in redox active reagents result in redox pairs, which then control the interfacial potentials, thereby negating the claim that non-paired redox couples improve reproducibility.[96]

In other work, ferrocyanide with a 6.9:1 ratio of ferrocyanide:ferricyanide was used as a dopant in the transduction layer of miniaturized ISEs to improve reproducibility. Screen-printed electrodes with potassium ferrocyanide doped carbon layer and drop cast K^+ ISM exhibited a SD of 2.8 mV during 24-36 h of conditioning (see Figs. 5A and B). Authors suggested the use of equimolar amounts of ferrocyanide:ferricyanide in future work to further improve reproducibility.[97]

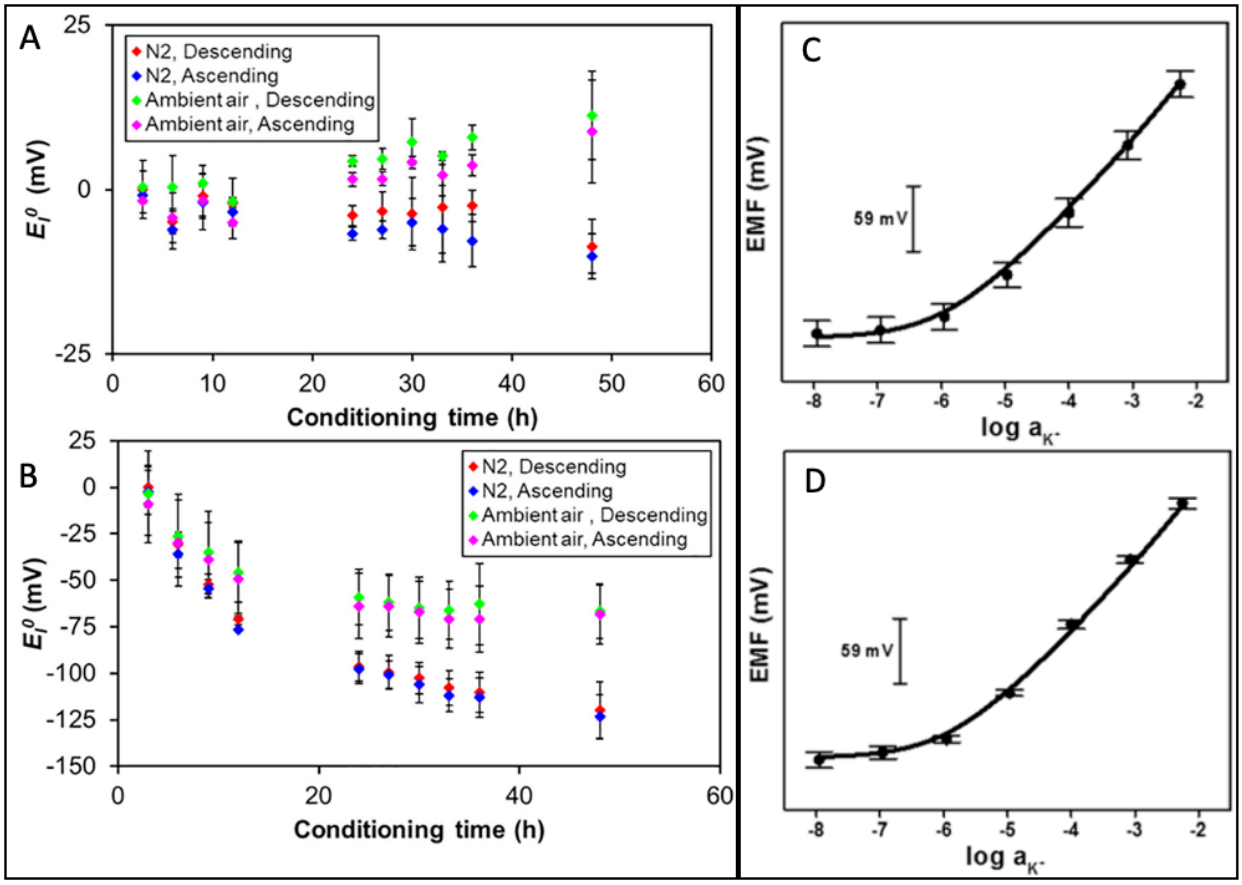

Figure 5. E^0 for screen printed ISEs in various conditioning environments (A) with and (B) without ferrocyanide in the solid-contact layer. Potentiometric response of strip-type ISEs with (C) tetrahydrofuran and (D) cyclohexanone as the solvent in the ISM. Adapted from references 37,97.

The reproducibility of strip-type ISEs with supporting substrates coated with SWCNTs, poly(3-octylthiophene) and PVC-based ISMs has been optimized through systemic study of fabrication procedures. It must be noted, however, that in these reports the SD of the EMF of 3 devices in the same solution, rather than the SD of E^0 was

reported. It was found that using cyclohexanone rather than tetrahydrofuran as the solvent for ISM improved the SD from approximately 10 mV to 5.0 mV for K^+ ISEs, due to the solvent-dependent dissolution of poly(3-octylthiophene) upon drop casting of the ISM (see Figs. 5C and D). Additionally, single-step integration of a poly(3-octylthiophene)/SWCNT solution rather than a 2-step deposition further improved the SD to 2 mV for K^+ ISEs, attributed to increased hydrophobicity.[37] These are significant improvements compared to earlier works of CNT-coated paper strip sensors with reported SDs of "as much as 30 mV"[21] and 10 mV.[36] Applying these two improvements to the fabrication of ISEs, PET based strips incorporated into an array gave a SD of 1 mV or less for Na^+ and K^+ in both aqueous and artificial sweat samples, showing that the SD does not worsen in a complex matrix.[21,24]

Short-circuiting multiple electrodes to a reference electrode is another recent strategy shown to improve reproducibility in E^0 values in conventional solid-contact K^+ ISEs.[98] This strategy was also used with carbon-fiber based Na^+ ISEs, improving the E^0 SD from 37.6 to 1.45 mV (n=4) for sampling in aqueous solution against a conventional double-junction RE.[70] While a carbon-fiber based RE was also developed and used for testing in an integrated setup with artificial sweat, repeatability was reported only for slope; visual inspection of the calibration plot suggests a worsened SD of E^0.[70] While there are some interesting and promising approaches to improve reproducibility, more standardized reporting will enable better comparison of performance across sensor designs.

LOWER LIMIT OF DETECTION (LOD)

The Lower LOD in Ion-Selective Potentiometry

By well accepted convention, the lower LOD for ISEs is determined by extrapolation of the linear EMF response to the value observed when no target ion is added to the sample.[99] Therefore, when dynamic ranges are mentioned in this section, it is because no detection limits was reported. As the failure to account for activity coefficients or liquid junction potentials impacts LOD calculations only marginally, these effects are not touched on in this section.

Lower LODs of Sensors with Substrate-Based Sampling

When coupling conventional solid-contact ISEs with substrate-based sampling the lower LOD is generally worsened by an order of magnitude or larger, compared to in conventional beaker-based sampling. Early work using nitrocellulose paper for sampling with a Ag^+ ISE as indicator and Ca^{2+} ISE as pseudo RE resulted in an LOD of 10^{-5} M compared to 10^{-8} M for beaker-based sampling. The significant worsening of the lower LOD was posited to be due to either sluggish mass transport of Ag^+ or adsorption of Ag^+ onto cellulose.[17] However, Ag^+ adsorption onto filter paper was later tested for using ICP-OES on aliquots of $AgNO_3$ solutions exposed to filter paper and revealed that adsorption occurred at only high concentrations.[91] In light of this finding, it appears most likely that sluggish mass transport of Ag^+ is responsible for the poor lower LOD.

Filter paper sampling with a solid-contact K^+-ISE and solid-contact RE also resulted in 3 orders of magnitude worsening of LOD in K^+ sensing, with the exact value depending on the shape of the paper sampling unit,[18] and slightly less than one order of magnitude

worsening for Na^+ sensing.[26] However, when using a single-junction RE with paper sampling, the lower LOD of a solid-contact Cl^--ISE was the same (10^{-5} M) in both paper and beaker-based sampling.[19] Interestingly, when replacing the RE with a paper-based reference unit coupled to a reusable AgCl/Ag rod, the LOD for a solid-contact Cl^- ISE increased to $10^{-4.1 \pm 0.1}$ M, indicating that interactions of both sensing and reference electrodes with supporting substrates can affect the lower LOD.[34] This worsened LOD was consistent across ions sampled; Na^+ and K^+ gave LODs of $10^{-4.1 \pm 0.1}$ and $10^{-3.3 \pm 0.1}$ M, respectively.[34]

When detecting heavy metal ions with paper-based sampling, a jump from Nernstian to super-Nernstian response from 10^{-3}-10^{-4} M which distorts the utility of a lower LOD, has been reported. This is a similar response as that seen in macroelectrodes at very low concentrations due to ion flux across the membrane.[89] For example, in paper-based sampling with solid-contact Cd^{2+} ISEs, the LOD is reported as 10^{-5} M compared to 10^{-6} M LOD in beaker-based sampling. However, as seen in the calibration curve for paper-based sampling, the super-Nernstian jump further worsens the lower end of the working range to 10^{-3} M. While soaking of paper in an inorganic salt does not improve the lower LOD, it does resolve these super-Nernstian jumps for Pb^{2+} and Cd^{2+}, thereby extending the working range of the sampling system (see Fig. 4A).[19,27] Acidification of filter paper to a pH of 2 improved the lower LOD of Pb^{2+} ISEs slightly, but the LOD still was not as low as in beaker-based sampling.[30]

The largest improvement of the lower LOD for Pb^{2+} sensing (to $10^{-5.4}$ M) was achieved by depositing the ISM cocktail onto paper, allowing to dry overnight, and then

using for paper-based sampling with a solid-contact Pb^{2+} ISE with the standard small volume of sample. It was hypothesized that alteration of the physiochemical state of the filter paper that is in contact with the conventional ISE by coating the paper with the ISM is responsible for such an improved performance. The LOD did not improve when non-modified sampling paper was held in contact with the solid-contact ISE and submerged in a beaker of sample, indicating that the worsening is not dependent upon volume of sample solution.[28]

Lower LODs are also worsened in sampling with non-paper substrates. In textile-based sampling, Cd^{2+}, Cl^{-}, and Na^{+} had 0.1 to 1.0 orders of magnitude worsening of LOD, the degree of which depended on composition of the textile (cotton, polyester, polyamide, and blends with elastane) while there was minimal worsening of LOD for K^{+} sensing.[26,31] Similarly, for polyurethane sponge-based sampling, Cl^{-} and Pb^{2+} had substantial worsening of LOD, while K^{+}, Na^{+} and Cd^{2+} had little to no effect on LOD. While heavy metal adsorption was examined experimentally and explained the difference in effects on Pb^{2+} and Cd^{2+}, the reason for worsening in Cl^{-} sensing is yet unexplained.[29]

Lower LODs in Strip-Type Sensors

Strip-type sensors, in which only the transducer is in contact with the substrate, are tested in large volume samples and generally exhibit LODs, similar to, or within one order of magnitude of, analogous conventional ISEs.

For early strip sensors of electropolymerized PEDOT:PSS solid contact on a PET substrate, lower LODs of $10^{-8.3}$ and $10^{-6.4}$ M were achieved for Ca^{2+} and K^{+} sensing through optimization of the ratio of PEDOT:PSS and membrane thickness.[35] Strip-type

ISEs with a carbon solid contact coupled with a conventional RE also result in LOD values within an order of magnitude of analogous macro-sized ISEs for pioglitazone ion (antidiabetic drug);[20] Cu^{2+};[46] and K^+, Ca^{2+} and Cl^- sensing.[38] Interestingly, solid-contact ISEs based on carbon ink coated filter paper resulted in half an order of magnitude worsening for Ca^{2+} sensing, but 2 orders of magnitude worsening for Mg^{2+}. While these 2 strips were then incorporated into an array with an integrated RE, limits were not reported for this setup.[23]

Additionally, SWCNT-coated filter paper used as a supporting substrate also resulted in LODs in the micromolar range for K^+ and NH_4^+ 10 for pH.[21] However, in subsequent work, the same design of paper-based ISE with a Li^+ ISM gave half an order of magnitude worsening in LOD compared to the conventional ISE, showing again the effect of miniaturization is also dependent upon target ion identity. When testing artificial serum, coupling the paper-based Li^+ ISE with a paper-based RE increased the LOD slightly, from $10^{-4.2}$ to $10^{-4.1}$ M.[41]

Work has also been done to improve the lower LOD of strip-type sensors to the nanomolar range through adaptation of fabrication techniques first introduced in conventional electrodes. By coating SWCNT-coated filter paper with Au and then a poly(methyl methacrylate-*co*-decyl-methacrylate) based ISM, nanomolar detection limits were achieved for Cd^{2+}, Ag^+, and K^+.[36] Additionally, LODs on the order of 10^{-7} M for both K^+ and I^- sensing were achieved with Au-sputtered SWCNT-coated filter paper with a poly(3-octylthiophene) solid contact and then the PVC-based ISMs. Replacement of the conventional RE to a paper-based RE with an ionic-liquid-based poly(methyl

methacrylate-*co*-decyl methacrylate) reference membrane resulted in an order of magnitude worsening for Na^+ but minimal change for I^-.[42] While these methods do achieve very low LOD, they are expensive, and require Au sputtering, which is not ideal for a point-of-care device.

Lower LODs of Sensors Built on Top of the Substrate

A K^+ ISE integrated with a RE was built on a PET substrate with conductive strips of carbon ink, a layer of SWCNT functionalized with octadecylamine groups, and either a K^+ ISM or reference membrane. In these devices both the ISM and reference membrane were made of a photo-cured poly(*n*-butylacrylate), and the K^+ ISM contained, in addition to standard ionophore and ionic sites, 1 wt % ETH 500. Lower detection limits comparable to conventional solid-contact K^+ ISEs were found with both conventional RE ($10^{-6.6}$ M), and the integrated solid-contact RE ($10^{-6.5}$ M), indicating that neither part of the ISE significantly affected responses in lower concentration regions.[25]

For a sensor made of initially free-standing graphene paper strips dipped into ISM cocktails and then laid together to form an array on plastic, with no additional underlying support, there was minimal difference in LODs for K^+, Ca^{2+}, and pH sensors, although it is not clear if the data reported is from testing with a conventional or a paper-based graphene RE.[95] Additionally, an array of 4 sensors from Ag screen-printed on synthetic polypropylene paper and ISMs of polystyrene-Au ion sensing nanocomposites gave LODs of $10^{-4.2}$ and $10^{-4.3}$ M for Na^+ and K^+ in artificial urine, respectively. However, there is no data on the use of these nanocomposites-containing ISM components in conventional electrode bodies to for comparison of detection limits.[43]

Another array with a NaCl-doped poly(vinyl butyral) RE and C/Au/reduced graphene oxide/ISM for Ca^{2+} sensing gave a slightly worse LOD than in conventional setups. In the same array, a Ag/AgCl ink based Cl^- ISE resulted in an LOD of $10^{-3.3}$ M, significantly higher than the $10^{—4.8}$ M as expected from the K_{sp} of AgCl.[56] While the authors did not address attempt to explain the LOD, it may be due to Cl^- leaching from either the RE or the Ag/AgCl ink.[91]

When using a polyurethane substrate with screen printed carbon and AgCl/Ag ink, an order of magnitude worsening of the lower range (LOD not reported) of Cl^-, Na^+, and K^+ but not pH sensors was found compared to analogous conventional ISEs. This array included a RE of ionic-liquid-based reference membrane; the worsening may be due to the miniaturization of either the working or sensing electrodes.[64]

An epidermal sensor with a PET support, screen printed carbon ink as the solid contact, and drop cast ISMs resulted in a 1 mM LOD for both Na^+ and K^+ sensing.[48] While these values are more likely the lower end of the dynamic range rather than an LOD calculated from extrapolation of values below the lower limit, it is still a significant deviation from the range of conventional electrodes of similar membrane compositions.

Additionally, a comparison of the performances of the solid contacts for a Cd^{2+} ISEs built on top of a PET substrate revealed that graphene resulted in an order of magnitude improvement in the lower LOD compared to graphite..[45]

For all these devices with minimal contact between substrate and either sample solution or membranes, the slight worsening of LOD is dependent on the ion valency and identity and the solid contact used and require systemic study.

Lower LODs of Sensors with Increased Integration

Integrated single-use setups with both the sample and sensing component in direct contact with supporting substrate generally have a lower LOD that is more than an order of magnitude worse than analogous conventional ISEs. Using a paper-based sandwich-type ISE one order of magnitude worsening of dynamic range was found for Na^+, K^+, and Ca^{2+} sensing,[22] and three orders of magnitude for the LOD for ionophore-free bilirubin sensing.[52] In contrast, for a paper-based sandwich-type ISE with a 3D printed ion sensing membrane, there was no change in the dynamic range for ionophore-free tetrabutylammonium sensing.[53]

Similarly high LODs have also been found in devices with membranes embedded within the substrate material. A fully inkjet-printed paper-based device using with PVC ISMs resulted in LODs of $10^{-4.0}$ and $10^{-4.5}$ M for K^+ and Na^+, respectively.[61] While no direct data was given for analogous conventional ISEs, they are both at least an order of magnitude than other conventional rod-shaped ISEs with the same ionophores.[100] Additionally, a paper-based device with an ionic-liquid-based reference membrane and K^+ ISM resulted in an LOD of $10^{-3.1}$M K^+,[54] higher than a conventional valinomycin-based ISE. The same setup with an HHCAE membrane for Cl^- sensing gave a lower range of 10^{-3} M, similar to that of conventional devices.[55]

Devices with the same embedded design and reference membrane were also fabricated on a polyester textile with similar results. Observing an improvement in the textile-based devices compared to analogous ones, especially in membrane-free systems, a systematic study of materials was performed. It was found that both the filter

paper and Ag/AgCl ink used as transducer leached small amounts of Cl^- ions, which, due to the small sample volumes. significantly increased the concentration in samples.[91]

In another device designed as a wearable sensor, hydrophobic barriers of acrylonitrile butadiene styrene films were transferred onto a cotton shirt and an LOD for the Ca^{2+} ISE was reported as $10^{-5.2}$ M. However, it is unclear how the LOD was determined and if the electrodes and membranes were printed directly onto the cotton material or built up vertically, as in other sweat based sensors, both of which prevent direct comparisons between designs.[62]

Lower LOD of Textile-Based Sensors

A commercial carbon fiber coated with a Na^+ ISM and tested with a conventional RE resulted in an LOD of $10^{-6.3}$ M, similar to a conventional ISE. However, switching to a fiber based RE with an NaCl doped poly(vinyl butyral) membrane, a cotton pad for wicking solution, and artificial sweat the lower limit increased to about $10^{-3.5}$ M, as estimated from a calibration curve. Unfortunately, it is not possible to determine the cause of the poor LOD as so many variables changed in this second experiment and no further study was run.[70]

An integrated device with SWCNT-coated cotton fibers dip coated in either a Li^+ ISM or a reference membrane resulted in an LOD of 10^{-5} M,[67] which is similar to that reported for paper-strip type Li^+ ISEs of similar composition[41] but again higher than for a conventional solid-contact Li^+ ISE. The similarity of LOD between these 2 setups show no effect of identity of substrate on degree of worsening of LOD, perhaps because the substrates are not actually in contact with the selective sensing components or sample.

In comparison, for sensors with the same SWCNT and ISM composition, switching from filter paper to cotton yarn as the underlying substrate worsened the LOD slightly–from $10^{-5.1}$ M, $10^{-5.4}$ M, and pH 10 to 10^{-5} M, 10^{-6} M, and pH 11 for K^+, NH_4^+, and pH, respectively.[21,79] However, these LODs are relatively similar, and the largest difference is the overall worsening from analogous conventional ISEs.

CONCLUSIONS

Overall, deviations from theoretically predicted device performance have been observed more often in miniaturized devices when there is direct contact between unmodified supporting substrates and sample solutions or sensing/reference membranes. When such contact is present, the deviation also depends upon the chemical structure of the underlying support. Many modifications of supporting substrates have been shown to eliminate or lessen such effects. However, these may also increase cost and complexity of the fabrication process and therefore need to be evaluated in the overall context of the required traits of a point-of-care device. On the other hand, less deviations occur when the surface of the support is completely covered, either by a solid-contact material or hydrophobic coating. In these situations, deviations from LOD do not correlate to substrate structure and rather depend on the identity of the solid contact or ion valency.

Systematic study of interactions between supporting materials as well as miniaturization of REs have both increased understanding of the source of non-ideal performance and thereby lead to efforts to mediate deviations. Continued study of the effects of miniaturization will lead to performance that meets the needs of point-of-care devices.

Chapter 2. Potentiometric Sensors with Polymeric Sensing and Reference Membranes Fully Integrated into a Sample-Wicking Polyester Textile

Adapted from:

Herrero, E. J.; Bühlmann, P. Potentiometric Sensors with Polymeric Sensing and Reference Membranes Fully Integrated into a Sample-Wicking Polyester Textile. *Anal. Sens.* **2021**, *1*, 188–195.

PREFACE

Responding to current limitations in paper-based sensors and the increased interest in wearable sensors, we introduce here potentiometric sensors fully integrated into a knitted polyester fabric and their application in aqueous and biological samples. Single layer ion-sensing devices requiring only 30 μL of sample were fabricated using wax patterning and Ag/AgCl paint. These devices give a Nernstian response to chloride over 4 orders of magnitude—an order of magnitude improvement from analogous paper-based devices. We also report the penetration of polyester yarns with polymeric hydrophobic and hydrophilic ion-sensing and reference membranes, all fully embedded within the fabric. These results demonstrate the promise of knitted fabrics as substrates for fully-integrated potentiometric sensors with improved detection limits. They also elucidate the effect of pore structure on sensor fabrication and performance, thereby affecting how we understand both fabric- and paper-based devices.

INTRODUCTION

It is estimated that well over 1 billion clinical measurements are made with ion-selective electrodes (ISEs) each year, facilitating both diagnosis and management of many diseases, such as cystic fibrosis, cardiovascular diseases, and chronic kidney failure.[101–104] However, access to this technology in resource-limited parts of the world is limited, and there is a growing need for portable point-of-care ISEs that are characterized by low-cost, portability, and ease of use.[2,52,105] We believe that planar ISEs with all components of the potentiometric cell integrated into an underlying support substrate will help to meet the needs for ISEs for point-of-care usage.

Paper is one of the most widely used substrates for portable ISEs.[106,107] Here, we distinguish between two types of such sensors, that is, partially and fully integrated paper-based ISEs, depending upon the degree to which the potentiometric cell is integrated into the paper. For the fabrication of partially integrated paper-strip ISE's, filter paper is often coated with an electron-conducting material to serve as the solid-contact, and an ion-selective membrane is applied on top of the conductive layer.[21,36,37,41,42,108,109] Partially integrated designs include devices in which the sample makes no direct contact with the paper as well as devices with a "sandwich-like" design, in which the sampling cell is assembled from multiple separately prepared layers.[22,52] Similar to the latter are also systems in which paper is the sampling substrate but detection is performed with a traditional rod-shaped indicator electrode and either a traditional rod-shaped reference electrode[19] or a Ag/AgCl element in contact with a paper substrate coated with solid KCl.[34] Partially integrated paper-based sensors require additional assembly or special training

of the user and do not appear to be ideal as low-cost point-of-care ISEs.

To date, there are only a few examples of fully-integrated paper-based ISEs, i.e., devices that require no assembly and take advantage of wicking of the sample into paper to hold the sample. They include paper-based reference electrodes with a Ag/AgCl/KCl half cell[49] as well as devices with ion-selective and ionic-liquid reference membranes embedded into paper, with colloid-imprinted mesoporous carbon as solid contact.[54,59,60] Fully-integrated devices have also been produced with automated ink-jet printing.[61]

While readily available and inexpensive, paper has unfortunately been associated with suboptimal device properties. A sub-Nernstian response was observed in fully-integrated paper-based ISEs with a valinomycin-doped poly(vinyl chloride) (PVC)-based ion-selective membrane unless the inert and highly hydrophobic electrolyte ETH 500 was added into the sensing membrane.[54] The reason for the effectiveness of ETH 500 in this case is not known yet. Sub-Nernstian responses have also been reported for K^+-, Ca^{2+}-, and bilirubin-selective “sandwich” ISEs.[22,52] Presoaking filter paper in inorganic salts of the primary ion has been shown to overcome apparently super-Nernstian responses for Cd^{2+} and Pb^{2+} in paper-based microfluidic sampling. However, detection limits reported for these partially-integrated devices were worse than for conventional ISEs.[27] Indeed, detection limits reported for fully-integrated paper-based ISEs[54,60,61] are consistently less favorable than for conventional ISEs. While nanomolar limits of detection for Cd^{2+}, K^+, and Ag^+ have been reported for carbon nanotube impregnated paper-strip ISEs with a partially integrated design,[36] in this case the paper is not used as a wicking device and the sample is not in direct contact with paper.

The performance limitations of paper-based ISEs suggest interference from the paper substrate.[13] This may be explained by chemical interactions of target ions with organic functional groups of cellulose fibers[31,110] or inorganic impurities in filter paper.[111–113] The variable concentration of such species in different types of papers complicates the study of such effects. Moreover, it appears likely that understanding the origin of inferior detection limits is only the first of multiple steps needed to move towards improved device performance with paper-based sensors. Therefore, it seemed advantageous to us to replace paper with synthetic textiles made from molecularly pure monomers, materials in which substrate–sample interactions can be fully understood and controlled. Herein, we report the use of a knitted polyethylene terephthalate (PET) based textile as a cleaner and more well-defined material to improve the performance of single-use fully-integrated ISEs.

Wearable potentiometric ion sensors comprising a textile component have become a popular field of research,[12] with applications to coated yarns,[57,67,70,79] epidermal patches,[6437] bandages,[69] and apparel.[114–117] This also includes detection of multiple ions with one device.[116,117] However, to date, the sensing components in all these designs were printed on top of the textile, and the textiles were not designed to wick the sample, in contrast to fully-integrated paper-based devices. To the best of our knowledge, the only reports to date that use textiles for sampling describe the use of textiles soaked in sample solutions or placed in contact with skin to deliver samples to electrodes of the conventional rod-shaped design.[31,117]

In this report, we describe the design and characteristics of fully-integrated textile-

based ISEs for Cl^- sensing in small sample volumes. The successful embedding of sensing and reference membranes into a polyester fabric is explained and compared to the structural characteristics of comparable paper-based devices, and the performance of the two types of devices is compared. To our knowledge this is the first example of an ISE that both embeds membranes into a fabric and uses the fabric to wick samples into contact with both the sensing and reference membranes.

RESULTS AND DISCUSSION

Substrate Selection.

In choosing a fabric as supporting substrate for a fully-integrated potentiometric sensing device, the following properties were considered: wicking rate, wax compatibility, sample uptake, evaporation speed, and ability to control the surface chemistry of the substrate. All materials for initial screening were obtained from commercial suppliers and were selected for their high purity and hydrophilicity.

Nylon filter membranes and hydro-entangled cleanroom wipes were found not to absorb water deposited onto them, and polyethersulfone and polysulfone sheets absorbed water but were incompatible with wax patterning. Among the tested fabrics, the only ones with wicking abilities and compatible with wax patterning were the polyester cleanroom wipes from Berkshire. Comparison of the wicking speeds of three types of Berkshire polyester wipes of different fabrication patterns revealed that use of Polx1200, an unlaundered polyester wipe with no surfactants or reported surface modifications, resulted in the quickest and most uniform spreading of liquid (see Supporting Information, SI, for data). This desirable behavior of Polx1200 can be attributed to both the porous

nature of this knitted fabric and the hydrophilicity of the polyethylene terephthalate fibers that compose its yarns. Polx1200 was chosen as the substrate for all subsequent textile-based experiments.

A comparison of relevant properties of Polx1200 and Whatman 1 filter paper is shown in Table 2-1. Notably, Polx1200 is less expensive than the filter paper. It also absorbed slightly more water per gram of material than paper (4.4 ± 0.6 g water/ g Polx1200; 3.4 ± 0.7 g water/g Whatman 1 filter paper). Loss of absorbed water was assessed because evaporation can lead to an increased sample concentration and should be considered when selecting substrate materials for low-cost point-of-care devices.[110] The rates of evaporation from both Polx1200 and paper were approximately constant over the course of 5 minutes, as seen from the percent loss over time shown in Table 1, with an average rate of evaporation of 1.1 ± 0.1 μL/min for Polx1200 and 0.9 ± 0.4 μL/min for filter paper at 21 °C and 14% relative humidity. The latter value is similar to values reported previously for evaporation from filter paper.[27] Note that for a device using a liquid reference solution, evaporation similarly affects both sample and reference zones, largely cancelling out any effects from concentration changes resulting from evaporation. Also, in a solid contact design with no liquid reference solution, EMF drifts would pose a major problem only if measurements were performed over longer time periods, as the expected drift over 1 min for a 30 μL droplet is no more than 1.0 mV and 0.8 mV for Polx1200 and filter paper, respectively (see SI for the details of this assessment). Therefore, concentration changes caused by evaporation do not present any problems for sensing with single use devices, the end purpose of these textile-based

devices.

Table 2-1. Comparison of Relevant Properties of Polx1200 and Whatman Paper

Material	Cost [$/cm^2]	Uptake [g water/g material ± SD]	Water evaporation over time [% loss[a] ± SD]				
			15 s	30 s	60 s	120 s	300 s
Polx1200 (N=3)	<0.01	4.4 ± 0.6	0.1 ± 0.1	0.3 ± 0.1	0.6 ± 0.1	1.1 ± 0.3	2.7 ± 0.4
Paper (N=3)	0.04	3.4 ± 0.7	0.2 ± 0.2	0.5 ± 0.3	0.9 ± 0.4	1.7 ±0.8	3.9 ± 2.0

[a] Refers to change from initial volume of water deposited onto the respective substrate.

Structural Features of Devices with Embedded Sensing and Reference Membranes.

A textile-based device with embedded sensing and reference membranes is shown in Figure 2-1. The wax barriers were approximately 1.5 ± 0.1 mm (n= 10) wide, and sensing and reference membranes had widths of 3.5 ± 0.1 mm (n=10) and 3.5 ± 0.1 mm (n=10), respectively. Calculations based on theory and experimental data indicate that neither diffusion nor convection cause changes in the concentration of reference or sample solutions when using the dumbbell-shaped design shown in Figure 2-1a.[49]

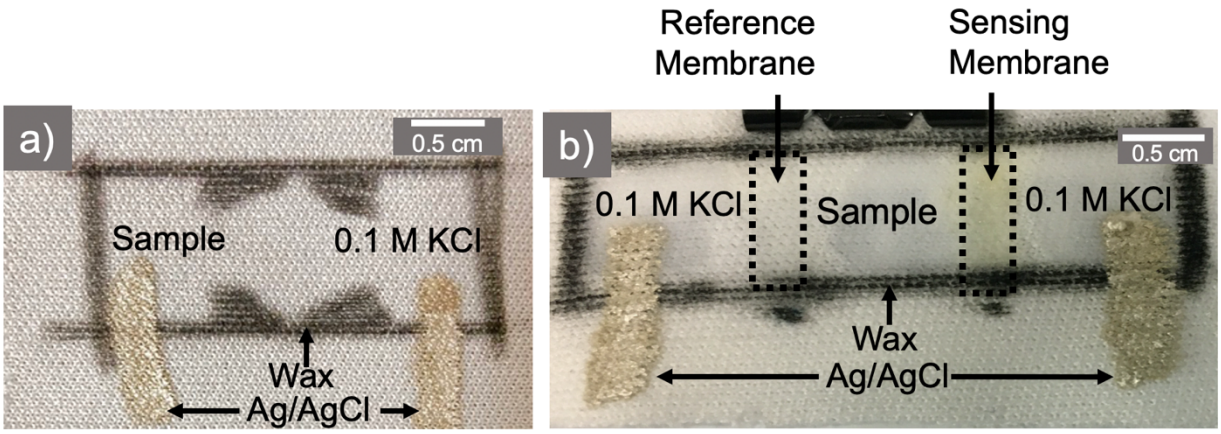

Figure 2-1. A textile-based potentiometric device (a) without integrated membranes and (b) with integrated sensing and reference membranes.

The structure of the Polx1200 textile used in this work is described by the manufacturer as a continuous knit of polyester yarns, each of which is a bundle comprising 36 individual fibers. This knit pattern results in interyarn gaps between distinct yarns and smaller interfiber gaps between the individual fibers of each yarn, as can be seen in Figure 2-2a. The wax patterning method used for these textile-based devices successfully formed hydrophobic barriers, as previously shown for paper-based devices using wax markers and inkjet printing.[50,51] However, SEM images of the wax-coated fabric in Figure 2-2b reveal that the wax layer does not fully cover interfiber or interyarn gaps, a finding that is consistent with images of wax-coated polyester fabrics by Nilghaz et al.[118] In previous work, SEM images taken of wax-coated polyester fibers revealed interyarn gaps that were not filled with wax, but no attempt was made to assess and rationalize the consequences of this finding, as discussed in the present paper. Using SEM and

calculations of pore volume fractions, Rajendra et al. and Wang et al. also found that in wax-patterned paper substrates wax coats the cellulose fibers but does not completely block pores.[119,120]

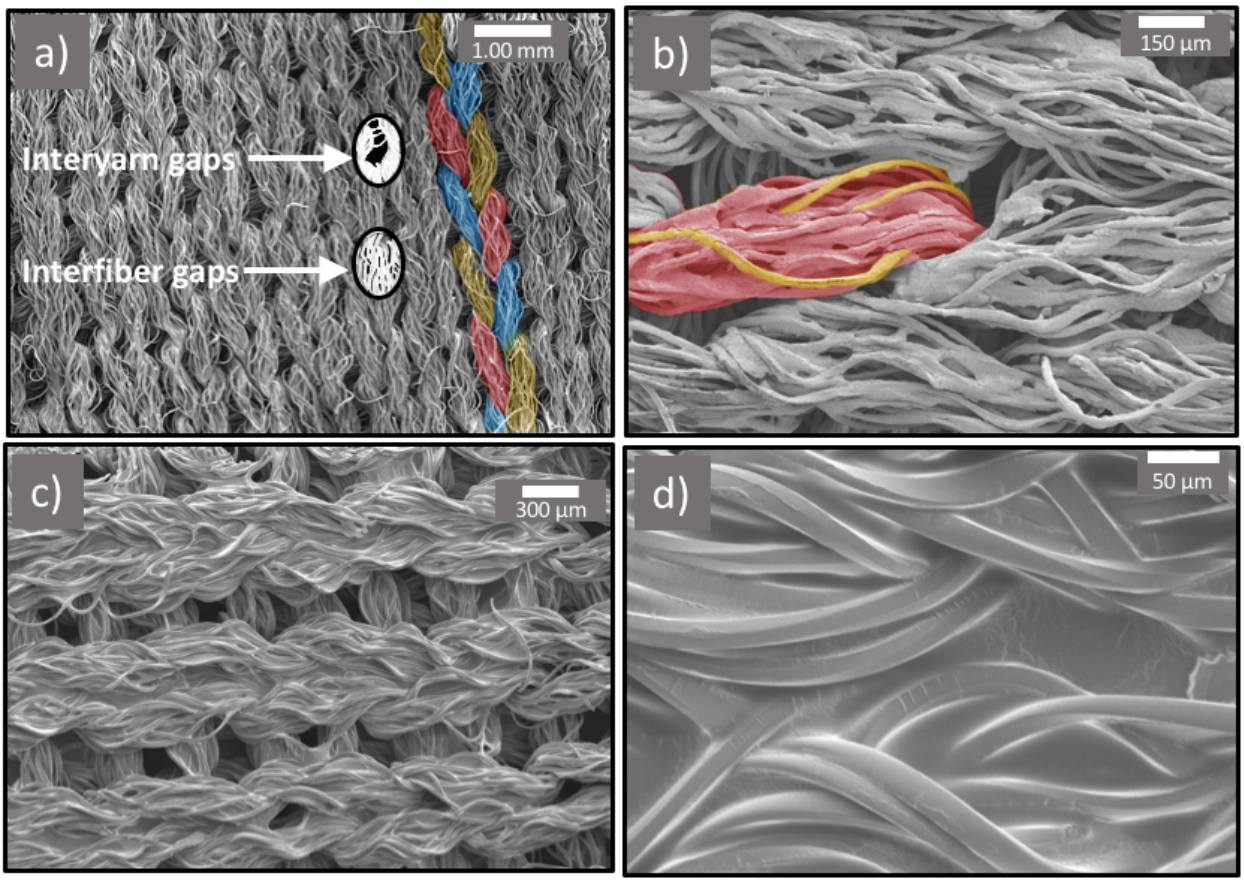

Figure 2-2. SEM images of Polx1200 devices: (a) Top view, showing interfiber and interyarn gaps in bare textile; highlighted in color are 3 distinct yarns. (b) Wax-coated fabric with a single yarn highlighted in red and a single fiber of this yarn in yellow. Shown in (c) and (d) are top views of fabric with embedded reference membrane (*o*-NPOE/PVC blend with $[C_8mim^+][C_1C_1N^-]$), with a larger magnification for (d) than for (c).

Similarly, for membrane-coated textiles, while interfiber gaps show near complete coverage by sensing and reference membrane material, the interyarn gaps remain unfilled, as seen in Figures 2-2c and 2-2d, respectively. Attempts to completely fill all interyarn gaps by increasing the number of spotting cycles, increasing the volume of membrane deposited per cycle, altering the time between cycles, or adjusting viscosity were unsuccessful. These efforts consistently increased the lateral dimension of membranes or caused membrane material to deposit on top of the textile but mostly failed to fill interyarn gaps.

This raises two questions. On one hand, one may wonder why it is so difficult to fill the interyarn gaps. On the other hand, it raises the question how the wax barriers are so effective in stopping the flow of sample solution, and why sensing and reference membranes work in potentiometric devices (as shown below) even though the wax and membrane materials do not fill all gaps. Answers to both questions come from consideration of the capillary forces acting on wax, the solutions of membrane components, and the aqueous samples and the contact angles with which these liquids wet the Polx1200 material, as shown in the following.

Treating the interyarn and interfiber gaps in textiles as capillaries, it can be predicted that a liquid that wets a textile will travel first within smaller interfiber gaps and only second along interyarn gaps.[121–123] Based on average diameters of interfiber and interyarn gaps as obtained from SEM images (see SI for calculations), we estimate the capillary force in interfiber gaps to be five times greater than in interyarn gaps. This explains why sensing and reference membrane solutions travel preferentially along interfiber gaps as opposed

to interyarn gaps. When an initial treatment of the textile only fills interfiber gaps and more membrane material is applied, the process of filling the interyarn gaps competes with the process of filling interfiber gaps that are further away from the point of deposition and have not been filled yet with these materials. Because of the larger capillary forces associated with interfiber gaps, the area covered with membrane material grows laterally, and many of the interyarn gaps remain unfilled.

It is interesting to apply the understanding of these capillary forces also to paper. In contrast to the regularly ordered interfiber and interyarn pores of Polx1200, filter paper has random spacing of interfiber pores throughout the material as the cellulose fibers are randomly oriented. Previous SEM images of ISEs with membranes integrated into filter paper show near complete filling of interfiber pores.[22,54,61] However, paper contains besides the micrometer-sized interfiber pores also intrafiber pores, which are several orders of magnitude smaller than interfiber pores but contribute substantially to total porosity. Unfortunately, SEM images are not suitable to show whether the intrafiber pores of paper are filled with ion-selective membrane material.[124] While one could expect that capillary forces pull in the ion-selective membrane material more readily into the smaller intrafiber pores than into wider interfiber gaps, this may not be true if gas trapped in those intrafiber pores cannot escape fast enough for the liquid to enter, an issue relevant in particular if there are dead-end intrafiber cavities where the solution entering the cavity also blocks the trapped gas from leaving. Importantly, the latter is not expected for a knitted fabric without intrafiber pores.

While ion-sensing and reference membranes fully fill the interfiber gaps, Figure 2-

2b shows that wax not only fails to fill most interyarn gaps but also only partially fills interfiber gaps. Capillary forces explain why, in spite of the presence of interfiber and interyarn gaps, wax barriers block the flow of aqueous samples, and why in spite of interyarn gaps the potentiometric devices with embedded sensor and reference membranes are still functional. Because the pressure in a capillary filled with a liquid is directly proportional to the cosine of the wetting angle, i.e., the angle between the liquid and the capillary wall, capillary forces are directly related to wettabilities.[123] To that end, contact angles of coated and uncoated textiles were measured in this work to evaluate the effect of the textile characteristics on wettability.

Here we report advancing and receding angles for a 12 µL droplet of water on coated Polx1200 and paper surfaces. The uncoated textile and paper are extremely hydrophilic, immediately absorbing water so that no contact angles could be measured. This can be explained by a negative capillary pressure that pulls the water into the textile. In contrast, for wax-coated Polx1200, the advancing and receding angles were 144.9 ± 2.0° and 141.1 ± 5.7°. This is clear evidence for small air pockets under the measuring droplet, as contact angles on flat surfaces do not exceed 120° even for the most hydrophobic surfaces. The relatively small difference between the advancing and receding contact angles confirms that these large contact angles are not an artefact of the measurement.[125] In combination with the results from the SEM images, this shows that the effectiveness of the wax barriers is not caused by formation of a continuous physical barrier but instead results from a combination of the poor wettability of wax by water and the high surface tension of water that prevents it from entering a multitude of small air-filled gaps in the

wax barrier. The positive capillary pressure prevents the water from penetrating the wax-coated Polx1200.

Similar results were found for Polx1200 coated with a blend of PVC and the plasticizer *o*-NOPE. The advancing and receding angles of 126.3 ± 4.4° and 123.3 ± 3.0°, respectively, are substantially smaller than for wax-coated Polx1200, but they are still somewhat larger than contact angles on a pure *o*-NPOE-plasticized PVC membrane (95.6 ± 6.8° and 94.4 ± 7.8° advancing and receding, respectively). This shows that here too positive capillary pressure prevents the sample from passing through gaps in the membrane-coated Polx1200.

In comparison, wax-coated paper had advancing and receding angles of 96.0 ± 0.5° and 82.5 ± 2.5°, which suggests a smaller role of positive capillary pressure effects in making the wax barriers effective and is consistent with a higher level of penetration of the wax into paper. However, the advancing and receding contact angles of 126.3 ± 4.4° and 123.3 ± 3.0°, respectively, for paper coated with *o*-NPOE-plasticized PVC suggest that as in the case of Polx1200 too there are some positive capillary pressure effects at play.

The important role of capillary forces in making wax barriers and reference and sensor membranes functional may raise concerns about their effectiveness in containing aqueous solutions that comprise surfactants. Blood samples, for example, contain surface-active species and are also often spiked with a surfactant in order to prevent clotting in the collection vial.[126] Therefore, we tested and found that wax barriers as well as reference and sensing membranes integrated into Polx1200 successfully contained

aqueous solutions spiked with a 0.1 M sodium dodecyl sulfate, a common surfactant (see SI for results). The apparent lipophobicity of the textile-based barriers is another significant improvement over paper-based devices, as we found in analogous experiments that paper-based wax barriers do not effectively block the flow of surfactant containing solutions, a conclusion consistent with earlier work from Ghosh et al.[127] The mechanism suggested here for blockage of fluid flow is in agreement with work by Brennan and co-workers who used silicone inks to confine surfactant-containing solutions in paper substrates and showed that these low surface energy inks do so by coating cellulose fibers rather than fully filling pores.[119,120]

Performance of Cl^- Sensing Devices with AgCl/Ag Sensors.

The preceding discussion of both the pore structure and extent of permeation of the textile by wax and membrane material as well as the physical phenomena that make wax and membrane barriers impermeable to aqueous sample ensures a thorough understanding of the electrochemical performance of these textile-based devices. In this work, potentiometric devices with and without embedded PVC-based membranes were tested, as shown in Figure 1. In measurements with these devices, the measured electromotive force, EMF, is the sum of all phase boundary potentials in the electrochemical cell.[7] Devices with two AgCl/Ag electrodes but no sensing membrane (see Figure 2a) comprise three phase boundaries that are affected by exposure to an aqueous solution. The phase boundary potential at the reference solution/AgCl/Ag interface is sample independent as it is determined by the reference solution. The liquid junction potential between the reference solution and the sample can be calculated for a

sample of known composition using the Henderson equation[87] but is minimized in work with samples of unknown concentration by use of a reference solution containing KCl at a high concentration.[87] Therefore, the only sample dependent phase boundary in devices of this type arises at the interface of the sample and the second AgCl/Ag electrode, which at room temperature responds to the activity of the Cl^- ions in the sample according to the Nernst equation: $EMF = E° - 58.2\ \mathrm{mV} \log a_{Cl^-}$. The potentiometric response of textile-based Cl^- sensing devices to varying solutions of KCl is shown in Figure 2-3. Each concentration was measured with 3 different devices, with a total of 30 devices contributing to this calibration curve. The devices gave a linear response from $10^{-4.1}$ to 10^{-1} M, with a slope of –56.8 ± 1.3 mV decade^{-1} (within error of the theoretically predicted slope) and an *E*° of -63.8 ± 3.4 mV.

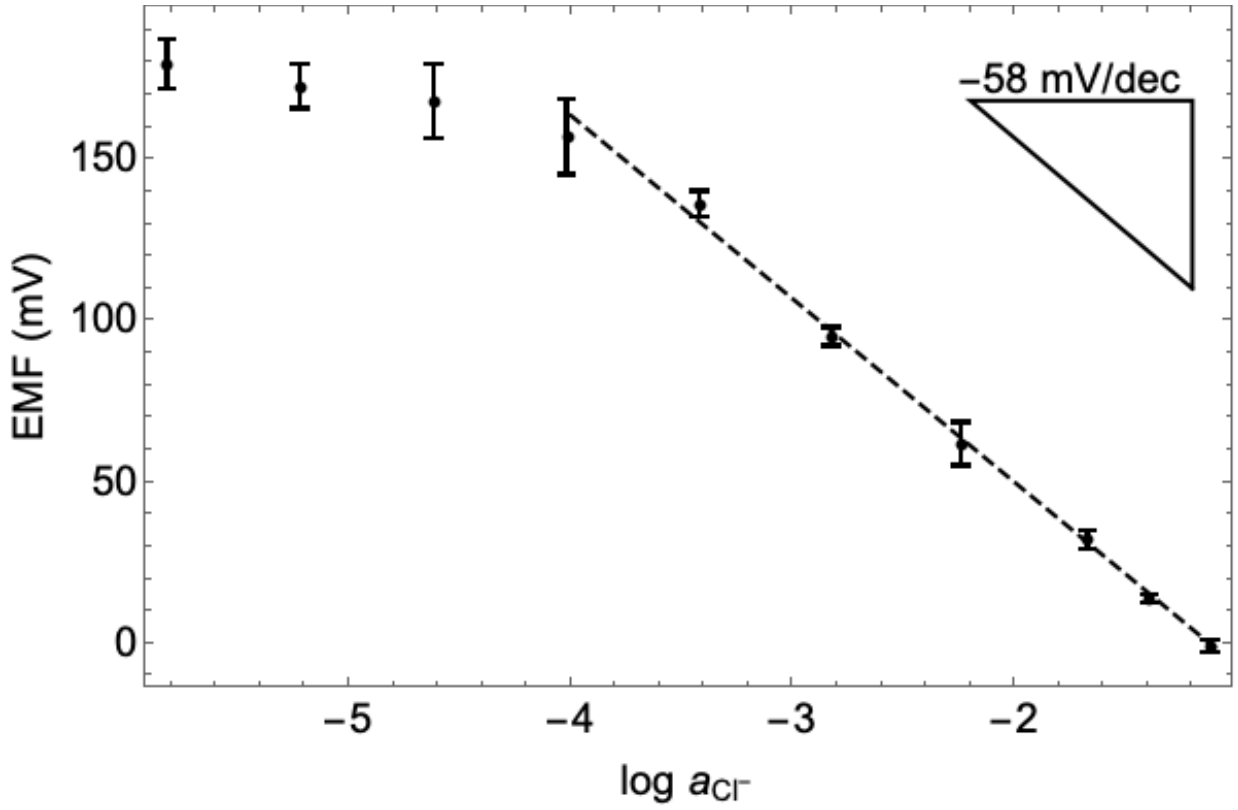

Figure 2-3. Potentiometric response of Cl^- sensing devices of the type shown in Figure 2-1a in KCl solutions.

For devices with Ag/AgCl transducers, the interfacial potential at the sensing electrode is defined by the redox reaction $\mathrm{AgCl(s) + e^- \leftrightarrow Ag(s) + Cl^-(aq)}$, and the lower limit of detection is governed by the solubility of the AgCl solid. When such an electrode is exposed to solutions containing no chloride, the activity of Cl^- at the solution electrode surface equals the square root of the solubility product of AgCl, which at room temperature is $10^{-4.8}$ M.[87] Compared to our previously reported lower limit of detection of $10^{-3.1}$ M for paper-based devices of the same design,[17] the current result of $10^{-4.1}$ M for a textile-based device is a substantial improvement and shows that the composition of the

underlying support substrate affects the lower limit of detection significantly. However, the present lower limit of detection is still slightly higher than the value of $10^{-4.8}$ M predicted by the solubility product. In order to determine the source of such variation from the theoretically predicted limit, we are currently studying adsorption of ions onto both the textile and, for comparison, paper. Interactions between ions and the textile substrate that negatively affect the limit of detection may not only be a function of the surface chemistry and porosity of the substrate material but may also be affected by minor contaminants of the substrate. Therefore, we are also investigating the possible contamination of these substrates and the AgCl/Ag paint with species that interfere with the AgCl/Ag electrode, intending to report on this complex issue in the future.

Performance of Textile-Based Devices with Embedded Membranes.

We also fabricated and tested devices with reference and ion sensing membranes embedded into the textile, as shown in Figure 2-1b. In this case, the phase boundary potentials at the reference membrane/sample and reference membrane/reference solution interfaces are sample independent and controlled by the partitioning of the ionic liquid between both phases.[128–130] The potentiometric response of devices to Cl^- in KCl solutions of varying KCl concentrations is shown in Figure 2-4. The devices gave a linear response from $10^{-3.7}$ to 10^{-1} M KCl with a slope of –55.5 ± 1.7 mV decade^{-1} and an $E°$ of -59.7 ± 4.2 mV. This response is similar to that of a conventional ISE with the same type of ion-sensing membrane (slope= –58.42 ± 0.4 mV decade^{-1}, $E°$= 18.4 ± 1.1 mV). The slight worsening in the limit of detection ($10^{-3.7}$ M as compared to $10^{-4.8}$ M) appears to be related to ion fluxes as the devices exhibited at these lower concentrations distinct

positive drift towards the expected potentials. Notably, such drift was not observed at concentrations above the detection limit, as also reflected in the much smaller error bars at higher concentrations. These results indicate that the proposed sensor is applicable for Cl^- sensing in the clinically relevant concentration range.[92]

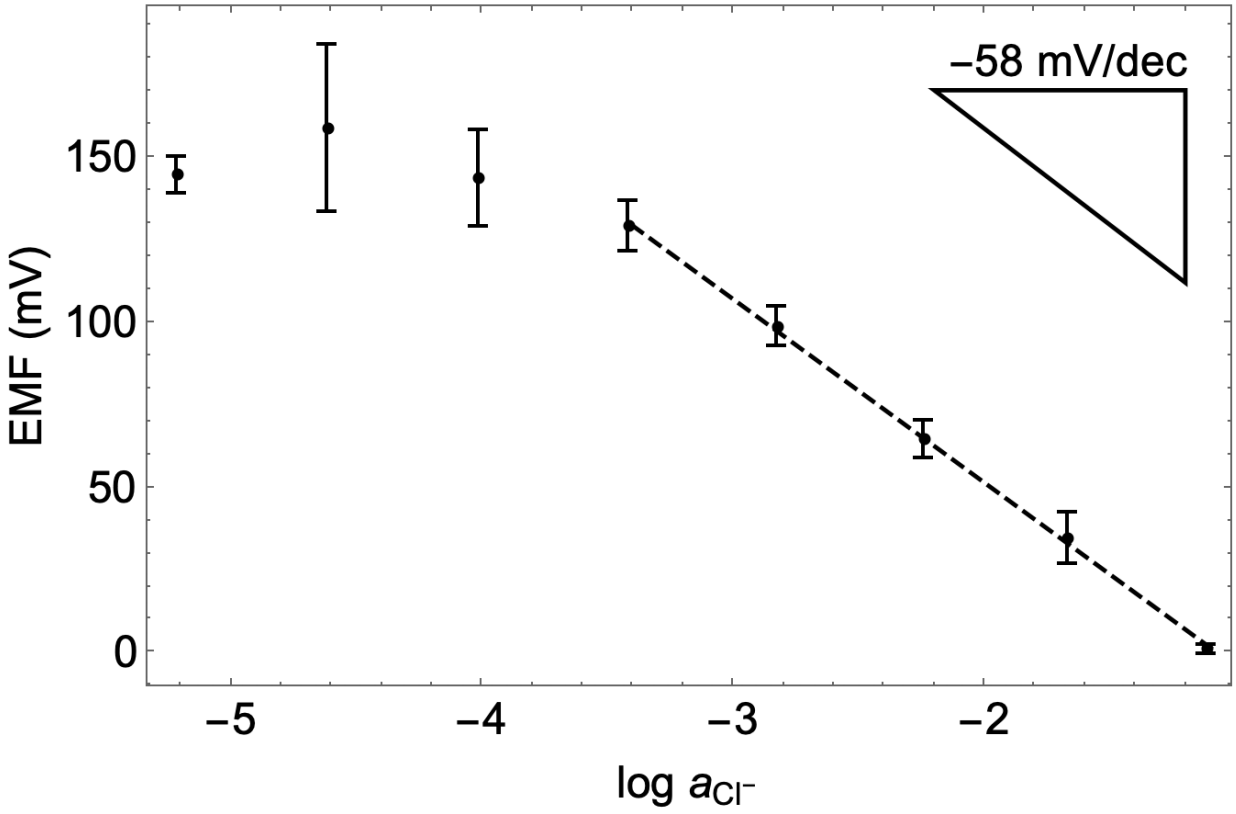

Figure 2-4. Potentiometric response to Cl^- of devices with PVC-based ion-exchanger membranes (see Figure 2-1b).

The performance of the textile-based Cl^- sensors with integrated ion sensing and reference membranes was also tested using a starting solution of undiluted blood serum, with sequential dilutions with H_2O, as shown in Figure 2-5. The devices give a linear

response with a slope of –67.2 ± 1.7 mV decade^{-1} and an $E°$ of -88.6 ± 3.5 mV in the range of from $10^{-3.1}$ to 10^{-1} M KCl, which includes the clinically relevant range for Cl^-.[131] We attribute the slightly super-Nernstian response to the relatively poor selectivity of the hydrophobic ionophore-free sensing membrane used, resulting in some interference from hydrophobic species present in the blood serum.

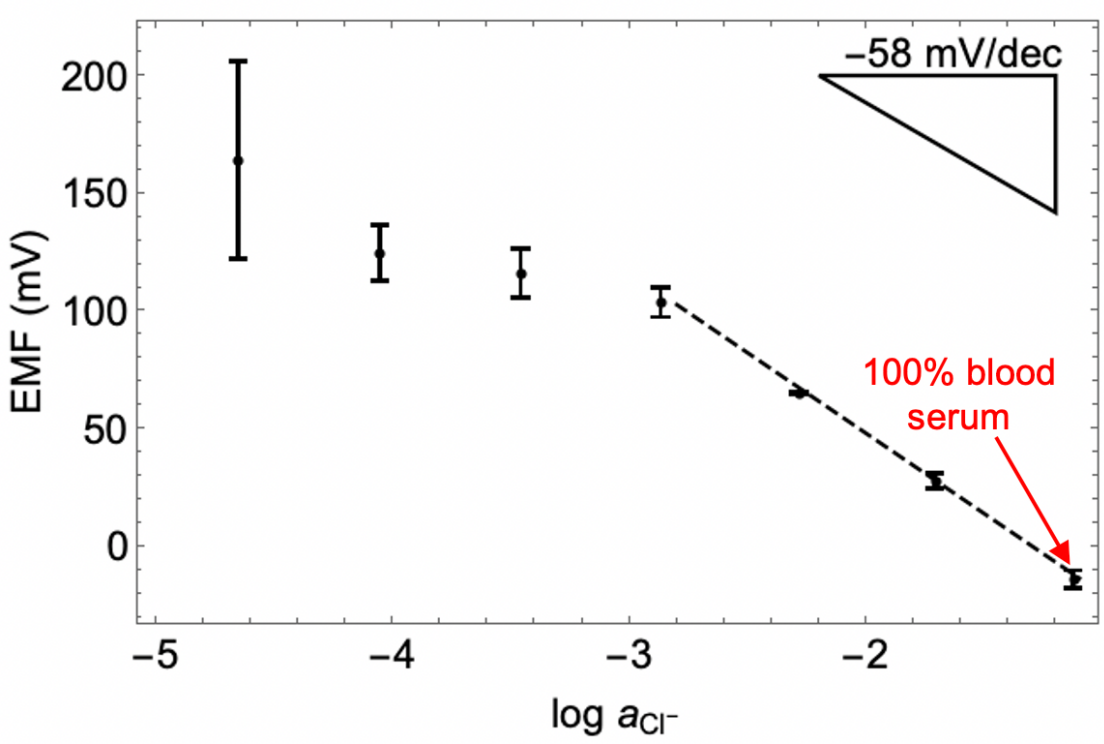

Figure 2-5. Potentiometric response to Cl^- of devices with PVC-based ion-exchanger membranes (see Figure 2-1b) in sequential dilutions of 100% blood serum.

This hypothesis was tested by replacement of the hydrophobic anion exchanger membrane with a hydrophilic high-capacity anion exchange membrane known to suffer much less from interferences caused by lipophilic ions,[132,133] as it was previously also

used in paper-based devices.[54] The potentiometric response of devices with this hydrophilic anion exchange membrane using a starting solution of undiluted blood serum, with sequential dilutions with H_2O, is shown in Figure 2-6. The devices give a linear response with a slope of –55.1 ± 1.4 mV decade^{-1} and an $E°$ of -69.7 ± 3.0 mV in the range of from $10^{-3.3}$ to 10^{-1} M KCl, which includes the clinically relevant range for Cl^-. This improved response slope suggests that the super-Nernstian response observed with the hydrophobic sensing membranes was indeed caused by their limited selectivity.

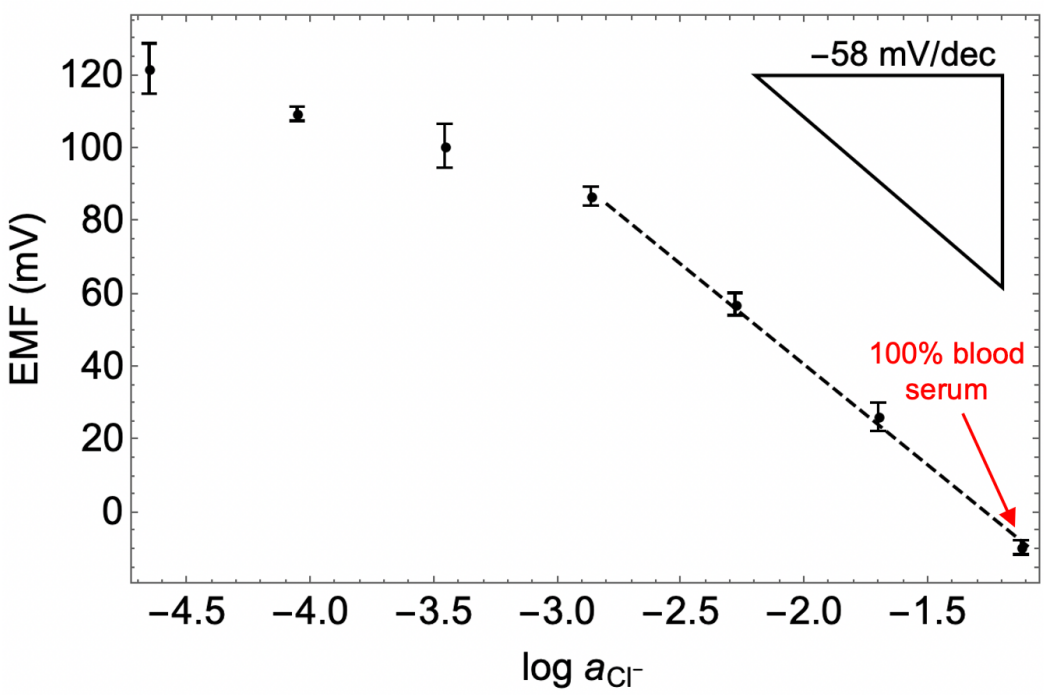

Figure 2-6. Potentiometric response to Cl^- of devices with hydrophilic anion exchange membranes in sequential dilutions of 100% blood serum (see Figure 2-1b).

CONCLUSIONS

We have shown the successful fabrication of a fully-integrated textile-based ISE

comprising reference as well as a hydrophobic or hydrophilic ion-selective membrane embedded within the knitted textile itself. The devices are easily fabricated and compatible with undiluted blood serum. Ongoing efforts in our laboratory are testing the modification of hydrophobic sensing membranes with ionophores to detect other clinically relevant ions.

Interestingly, the experimentally observed unfilled interyarn gaps in the membrane-coated textile along with the Nernstian responses of the resulting devices show that it is not necessary to fill all interyarn gaps to prevent leaks in or around the hydrophobic ion sensing and reference membranes embedded into the fabric. This can be explained by capillary forces. A notable advantage of the knitted polyester textile as the sensor platform is that this synthetic material has a well-defined structure and high purity. For chloride measurements, this resulted in a limit of detection which is not only well below the clinically relevant range[92] but also significantly lower than previously reported for paper-based devices.[22]

Acknowledgements

This work was supported by the National Science Foundation (CHE-1710024) to P.B. as well as a Graduate Research Fellowship from the National Science Foundation to E.J.H. Parts of this work were carried out in the Characterization Facility, University of Minnesota, which receives partial support from NSF through MRSEC (DMR-2011401) and the NNCI (ECCS-2025124) programs.

SUPPORTING INFORMATION

Materials.

Reagents were purchased from the following sources: Fumion FAA-3 ionomer anion exchanger from FuMA-Tech GmbH (Bietigheim-Bissingen, Germany), inhibitor-free anhydrous tetrahydrofuran (THF), methanol, tridodecylmethylammonium chloride, and sodium dodecyl sulfate from Sigma-Aldrich (St. Louis, MO, USA), high molecular weight poly(vinyl chloride) (PVC) and *o*-nitrophenyl octyl ether (*o*-NPOE) from Fluka (Buchs, Switzerland), the ionic liquid 1-methyl-3-octylimidazolium bis(trifluoromethylsulfonyl)imide (referred to here as $[C_8mim^+][C1C1N^-]$) from Fisher Scientific (Pittsburg, PA, USA), Ag/AgCl ink (AGCL-675; consisting according to the material data safety sheet of 40–60% silver, 10–25% silver chloride, 25–50% γ-butyrolactone, and 5–15% urethane acrylate oligomer) from Nayaku Advanced Materials (Westborough, MA, USA), and Autonorm freeze-dried blood serum from SERO (Stasjonsveien, Norway). Seven different textiles were obtained for initial substrate screening: Polx1200, Capsure-LP, and Microseal-VP polyester continuous knit filament cleanroom wipes from Berkshire Corporation (Great Barrington, MA, USA), asymmetric polysulfone sheets and hydrophilic polyethersulfone membrane sheets (5.00 μM pore size) from Pall corporation (Westborough, MA, USA), polyamide-based nylon filter membranes (0.45 μM pore size) from Sigma Aldrich (St. Louis, MO, USA), and polyester hydro-entangled, non-woven cleanroom wipes from Contec Industries (Spartanburg, SC, USA). Whatman grade 1 filter paper was obtained from Sigma-Aldrich (St. Louis, MO, USA). Deionized water was purified to a resistivity of 18.2 MΩ cm with a Milli-Q PLUS reagent-grade water system

(Millipore, Bedford, MA, USA).

Substrate Selection Methods.

To test the wax compatibility of each fabric, a 0.5 cm wide, 3.0 cm long microfluidic channel was drawn onto both the front and back of these substrates using a Sharpie Peel Off China Marker (Atlanta, GA, USA). The fabrics were then placed in an oven for 10 min at 100 °C, according to standard procedures for hydrophobic wax patterning.[50,51] Tests of wax compatibility were made with each material, specifically noting the ability to form hydrophobic barriers to contain water stained with small amounts of food coloring (McCormick, Hunt Valley, MD, USA). To measure wicking rates for fabrics compatible with wax printing, 25 µL droplets of the dilute food coloring solution were deposited onto the end of the wax-patterned channel, and the time it took for the solution to travel 2.0 cm was recorded. Each experiment was performed in triplicate. Polx1200 wicked aqueous solutions the fastest (7 ± 2 s), while Microseal-VP wicked aqueous solutions in 63.7 ± 15 s, and Capsure-LP exhibited a very variable wicking speed,-with solution travelling to the 2 cm mark in 80 s, 200 s, and then not at all in a third trial.

Characterization of Polx1200.

A basic hydrolysis of a sample of Polx1200 was performed using a modified procedure from the literature to assess the identity of Polx1200 as polyethylene terephthalate (PET) and detect in this commercial polymer any possible monomeric units differing from terephthalate and ethylene glycol.[134] Several strands of the fabric were placed in 2.0 mL of D_2O comprising 0.12 M NaOD and heated to reflux. A sample was removed at 20 h, filtered with a 0.45 µm syringe filter, and a ^1H NMR spectrum was

recorded using a 400 MHz Bruker Avance III HD spectrometer (see Figure 2-S1). The peak at 7.88 ppm corresponds to the aromatic hydrogens in the terephthalate units, and the peak at 3.67 ppm corresponds to the ethylene group of ethylene glycol. The peak at 4.79 ppm results from HDO and is characteristic of the solvent. The absence of other peaks confirms that no other monomers were used in any substantial amount to prepare the Polx1200 polymer.

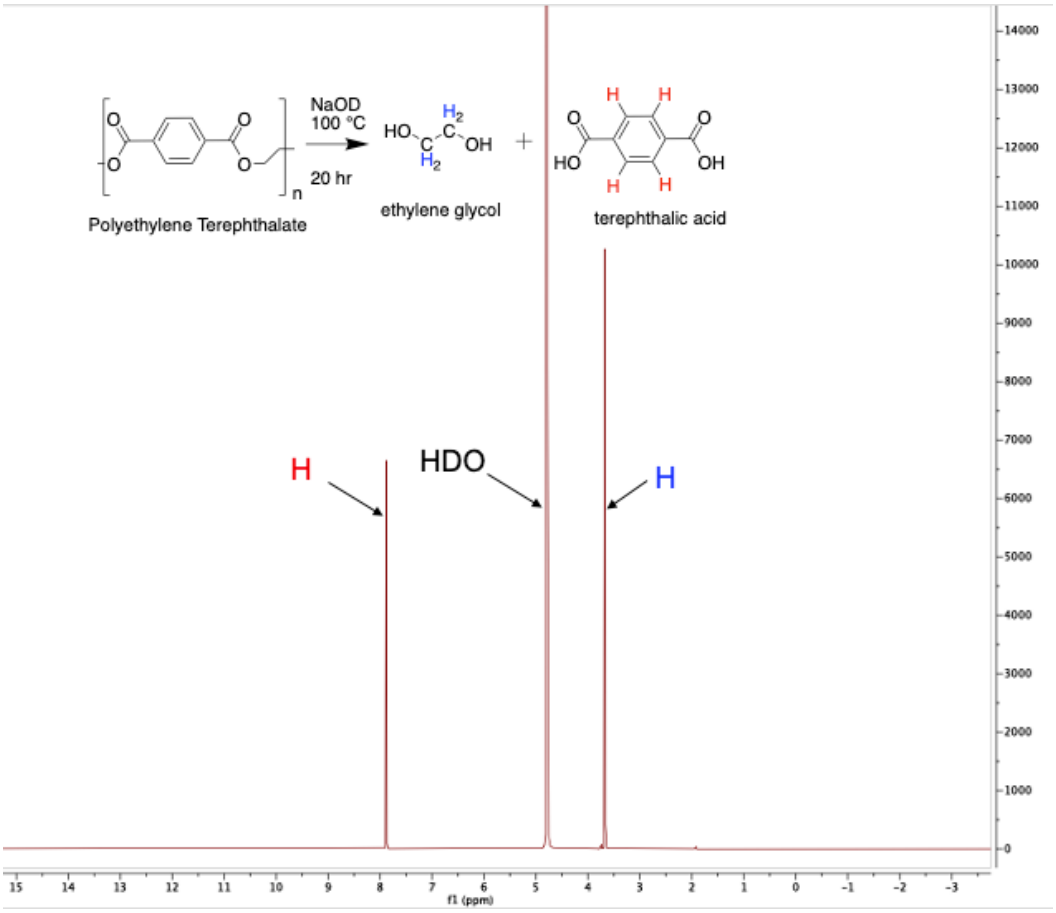

Figure 2-S1. ^{1}H NMR spectrum of basic hydrolysis of Polx1200 in D_2O comprising 0.12 M NaOD.

Precursor Solutions for the Preparation of Sensor and Reference Membranes.

All sensing membranes were prepared following literature protocols.[54] Precursor solutions for Cl^- ion sensing membranes were prepared by dissolving 204.3 mg PVC, 403.6 mg *o*-NPOE, and 33.4 mg tridodecylmethylammonium chloride in 3.0 mL THF. Precursor solutions for reference membranes were prepared by dissolving 42.0 mg $[C_8mim^+][C_1C_1N^-]$, 87.2 mg PVC, and 87.0 mg *o*-NPOE in 1.5 mL THF. The Fumion FAA-3 ionomer anion exchanger that was used to prepare the hydrophilic high-capacity anion exchange membranes was obtained from the supplier in the Br^- form. To exchange the Br^- for Cl^-, the membrane was conditioned sequentially in aqueous solutions of 1 M KCl for 1 day and 1 mM KCl for 2 days and then dried overnight at 100 °C. Precursor solutions were then obtained by dissolving 85.6 mg of the Cl^- loaded membrane in 3 mL methanol, heating gently, and passing through a 5 µm syringe filter.

Fabrication of Polyester-Based Sensors.

Microfluidic zone barriers were hand drawn in matching patterns on both sides of the textile using a Sharpie Peel Off China Marker. For each of the two electrical connections, Ag/AgCl ink was applied to one side of the textile using a rubber tipped paintbrush (Royal Sovereign Ltd, UK) to achieve uniform coverage. This was followed by curing for 10 min at 100 °C. For initial Cl^- sensing designs, a dumbbell-shaped wax pattern was drawn, with separate reference and sample zones as well as a central contact area, as introduced by Lan and co-workers.[49]

For subsequent Cl^- sensing devices, a rectangular wax pattern was drawn, and both sensing and reference membranes were deposited into the textile.[54] Solutions of the

membrane components were applied to the textiles using a micropipette. Three cycles consisting of deposition of a 7 µL aliquot of the appropriate solution on each the front and the back of the textile were completed for all devices, with a 10-minute waiting period between cycles. Membrane-coated filter papers for contact angle measurements were prepared in the same way.

Additional Notes on Membrane Deposition.

Several parameters were explored in the optimization of the method for membrane deposition onto fabric. While previous reports[54,60] cite the use of glass capillaries to deposit the solutions of the sensor and reference membrane components, this work found that use of micropipettes resulted in improved accuracy in the patterning of membranes deposited into the textile. For each cycle, each individual device was spotted with membrane solution on the front of the textile and then immediately on its back, before moving on to the next device. This prevented solvent from evaporating from the top before making the application on the back.

Conventional ISEs.

Membranes were prepared by pouring 1.5 mL of the THF solutions containing the membrane components into a flat-bottomed glass Petri dish (diameter 25 mm), covering the dishes with cardboard, and allowing the THF to evaporate overnight. Circular membranes (diameter 12 mm) were cut out of the master membrane the following day using a cork borer. Circular membranes were then mounted into house-made ISE bodies,[135] with an inner filling solution of 1.0 mM KCl in contact with a AgCl-coated Ag wire as inner reference.

Potentiometric Measurements.

Electrode potentials were measured using an EMF 16 high-impedance voltmeter (input impedance 10 TΩ) controlled by EMF Suite 1.03 software (Lawson Labs, Malvern PA). Two alligator clips were used to connect each device to the voltmeter. The textile-based devices were placed on top of a sheet of PVC and held in place with binder clips (see Figure 2-S2). For each device, 30 µL each of the aqueous sample and reference solutions were simultaneously deposited into the respective zones. For devices with reference and sensing membranes, an aliquot of reference solution was deposited into the zones including a AgCl/Ag sensing element and an aliquot of sample was deposited into the zone between the sensing and the reference membrane. A series of blood serum samples with various Cl^- concentrations was prepared by sequential dilution of an undiluted blood serum solution, with a certified Cl^- concentration of 99 mM. After solutions were deposited onto the textile-based devices, it took approximately 30 s for solutions to fully wet the fabric; the recorded response was the average EMF over the following 30 s. The potentiometric response of conventional ISEs stabilized within less than 30 s; the reported response here too was the EMF over the following 30 s. Activity coefficients were calculated according to a two-parameter Debye-Hückel approximation,[88] and EMF values were corrected for liquid-junction potentials with the Henderson equation.[87]

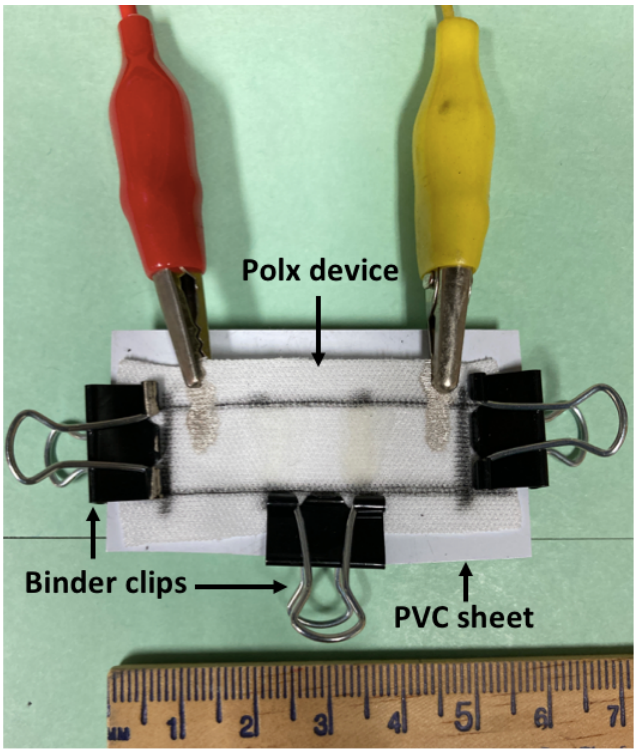

Figure 2-S2. Experimental setup for measurements with membrane-based devices. The PVC sheet provides mechanical support for the textile, and binder clips hold the textile flush with the PVC.

Device Characterization.

Structural features of devices were characterized by scanning electron microscopy (SEM, S-4700, Hitachi, Tokyo, Japan) with an accelerating voltage of 1.0 kV. Contact-angle measurements were performed with a contact-angle goniometer (Erma, Tokyo, Japan) using the needle-in-contact method.[136] With this method, a droplet of water is brought into contact with the test surface using a micrometer syringe, and the volume of the drop is first increased stepwise, with measurement of the advancing contact angle

after each step, followed by stepwise removal of solution and measurements of the receding contact angles after each removal step. Reported contact angles represent contact angles measured when either the successive volume increases or decrease no longer affect the measured contact angle.

Surfactant Compatibility.

Two solutions of 0.1 M sodium dodecyl sulfate (a total concentration significantly above the critical micelle concentration) were stained with either red or green food dye to visualize the ability of wax barriers as well as sensor and reference membranes to contain solutions. Aliquots of 25 µL of the colored solutions were added to the outer zones of Polx1200-based devices comprising both sensing and reference membranes, as shown in Figure 2-S3a. As Figure 2-S3c shows, after 30 min the dye was still contained by the wax barrier and the sensing membrane. However, the dye started to stain the reference membrane in the second device. This shows that both the wax barriers and the PVC-based sensor membranes are an effective barrier blocking transfer of aqueous solutions even if they contain a surfactant. Three reasons lead us to believe that the reference membranes too contain aqueous solutions well and that the colored ionic components of the food coloring enter the reference membrane only because they exchange for ionic liquid ions transferring into the aqueous sample. First, the ionic liquid doped reference membranes consist of 81% (w/w) PVC and plasticizer and, therefore, have a matrix that closely resembles that of sensor membranes. Second, such membranes have been shown to respond in a Nernstian manner when the ionic liquid cation was added at high concentrations into the sample.[128] Third, while the food coloring started to stain the

reference membranes over a period of several minutes, even after 24 h and using very concentrated solutions of food coloring, no coloring was observed to fully penetrate the reference membrane and stain the untreated textile on the side opposite to the solution of the food coloring.

We also studied the effectiveness of wax barriers in paper-based systems, and saw that the surfactant solution began to visibly penetrate barriers after 5 min, as shown in Figure S3E. This inability of paper-based wax barriers to contain surfactants is in agreement with previous reports.[119,127]

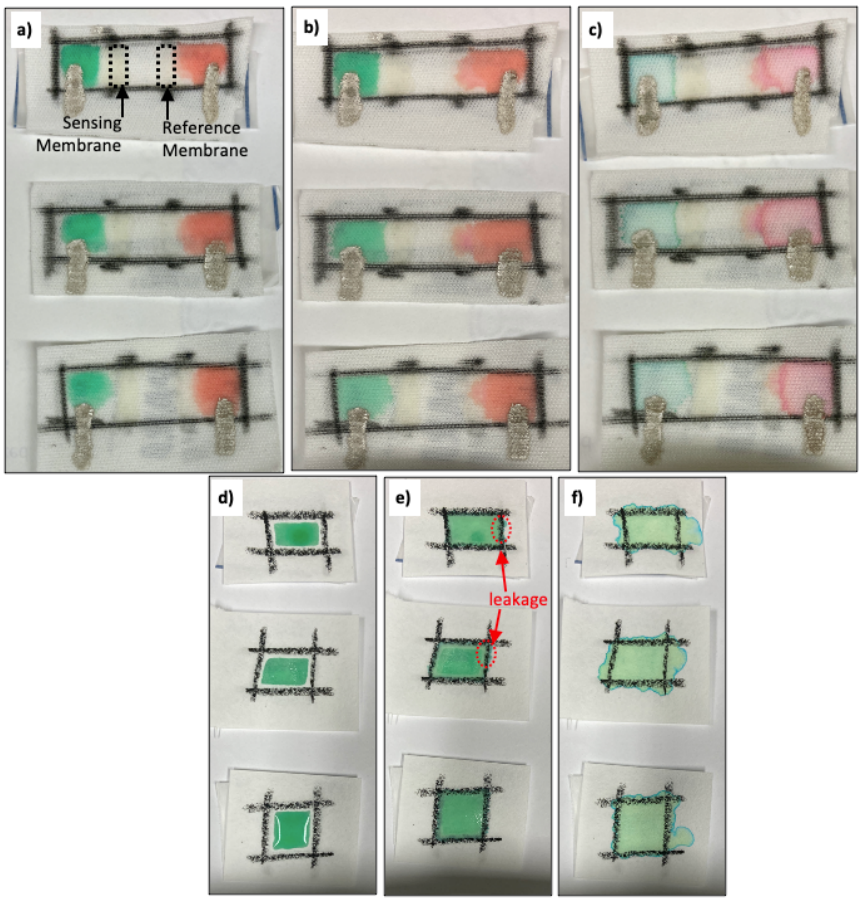

Figure 2-S3. Surfactant compatibility of PVC-based membranes and wax barriers in Polx1200 (a-c) and paper (d-f) at 6 s (a,d), 5 min (b,e) and 30 min (c,f). For (a) to (c), sensing membranes are on left of the textile devices and reference membranes on the right (i.e., the positioning is opposite to that of the device shown in Figure 2-1b).

EMF Drift Assessment.

The EMF drift over time due to evaporation of sample solution from Polx1200 and paper substrates was estimated using the Nernst equation:

$$\Delta EMF = \text{-}58.1\ mV\ Log\frac{c(t=0)}{c(t)} = \text{-}58.1\ mV\ Log\frac{V(t=0)\text{-}tR}{V(t=0)} \qquad (2\text{-}S1)$$

where c(t=0) is the initial concentration, $c(t)$ the concentration at time t, $V(t=0)$ the original sample volume, and R the rate of evaporation. The experimentally determined rates of evaporation were 1.86 x 10^{-8} L s^{-1} and 1.59 x 10^{-8} L s^{-1} for Polx1200 and paper, respectively. Inserting these values for the evaporation rate and a sample volume of 30 µL into Equation 2-S1 gives the plot of the predicted EMF drift over time as shown in Figure 2-S4. This graph shows an approximately constant drift for the first 5 min, followed by a continuously increasing drift as the complete evaporation of the sample is approached. After 1 min, the EMF drifts are 1.0 mV and 0.8 mV for Polx1200 and filter paper, respectively.

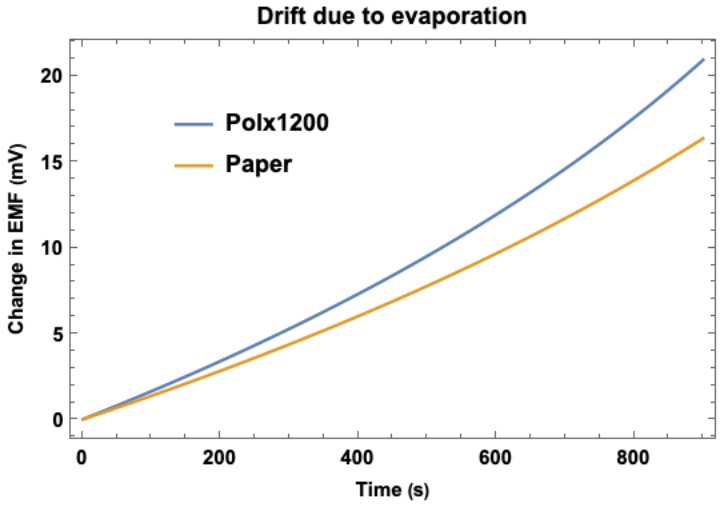

Figure 2-S4. EMF drift resulting from evaporation of water from Polx1200 or paper based potentiometric devices, as predicted on the basis of the experimentally determined rates of evaporation and a starting volume of 30 µL.

Capillary Force Calculations.

In order to compare the magnitude of capillary forces in channels formed by interfiber and interyarn gaps, those gaps were modelled as capillaries of constant width.[123] The pressure in a capillary, p_c, is defined by the Washburn Equation,

$$p_c = \frac{2\gamma \cos\theta}{r_c} \tag{2-S2}$$

where γ is the surface tension of the liquid in the capillary, θ is the wetting angle, and r_c is the radius of the capillary. It follows that the ratio of the capillary pressures in two capillaries can be computed as

$$\frac{p_1}{p_2} = \frac{\frac{2\gamma_1 \cos\theta_1}{r_1}}{\frac{2\gamma_2 \cos\theta_2}{r_2}} \tag{2-S3}$$

Assuming that in Polx1200 the wetting angles and surface tensions are equal for interfiber and interyarn gaps because fibers and yarns have the same surface chemistry, the ratio of the capillary pressures in interfiber gaps and interyarn gaps as defined by Equation 3 simplifies to

$$\frac{p_{\text{interfiber gap}}}{p_{\text{interyarn gap}}} = \frac{r_{\text{interyarn gap}}}{r_{\text{interfiber gap}}} \tag{2-S4}$$

The widths of channels created by both interyarn and interfiber gaps were measured at five distinct points in an SEM image of Polx1200, as denoted by the yellow and blue lines, respectively, in Figure 2-S5. The average diameter of interyarn and interfiber gaps were determined to be 140 ± 38 μm and 28 ± 9 μm, respectively, which yields upon insertion into Equation 2-S4 a capillary force five times greater in interfiber gaps than in interyarn gaps.

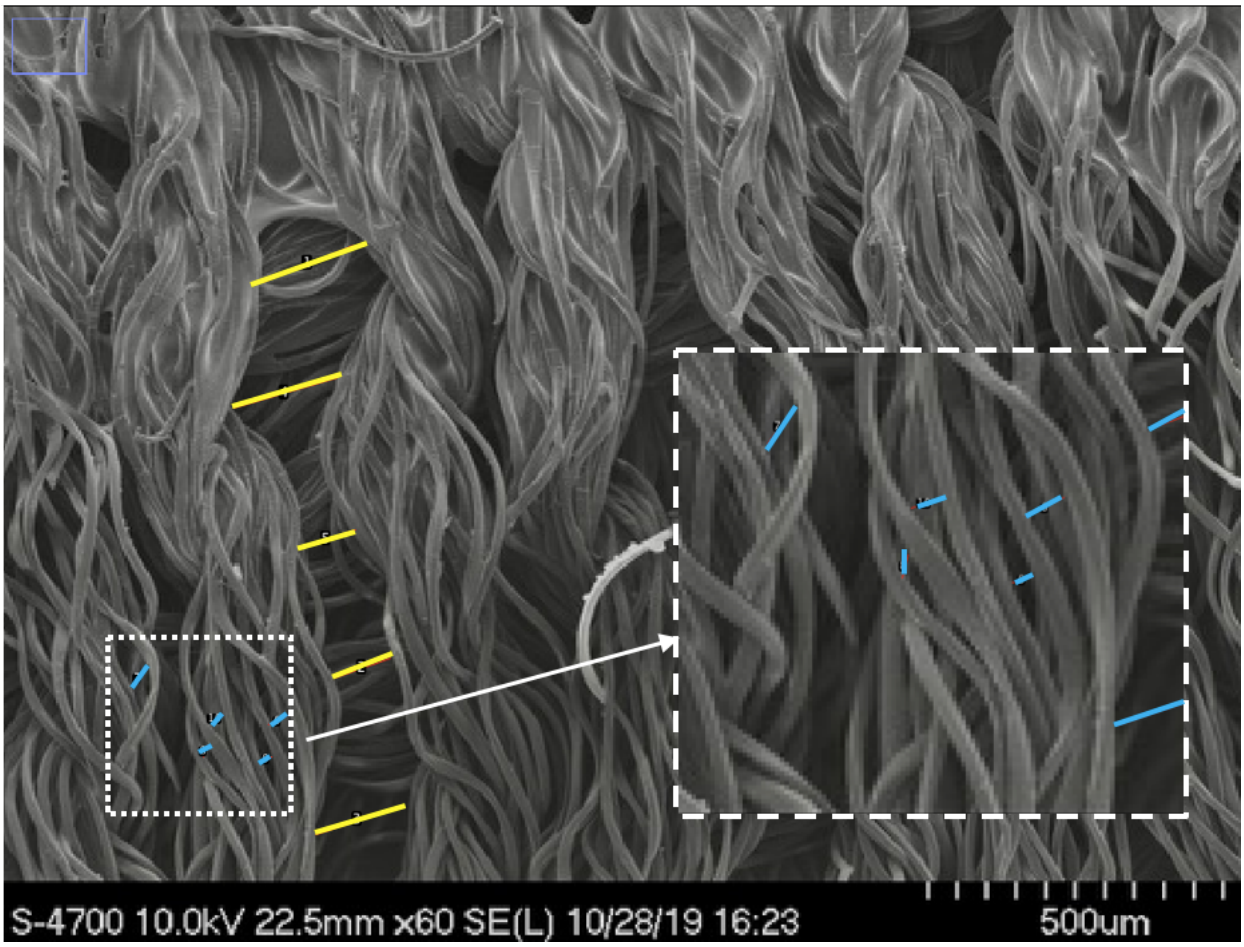

Figure 2-S5. SEM image of Polx1200 annotated for interfiber (blue) and interyarn (yellow) pore widths.

Chapter 3. The Effect of Paper on the Detection Limit of Paper-Based Potentiometric Chloride Sensors

Eliza J. Herrero, Blair K. Troudt, and Philippe Bühlmann

Adapted From:

Herrero, E. J.; Troudt, B. K.; Bühlmann, P. The Effect of Paper on the Detection Limit of Paper-Based Potentiometric Chloride Sensors. *Anal. Chem.* **2022**, *94*, 14898–14905.

Contributions: B.K.T. contributed with the design and fabrication of capillary reference electrodes. E.J.H. performed all the other experimental work.

PREFACE

While paper is an excellent material for use in many other portable sensors, potentiometric paper-based sensors have been reported to perform worse than conventional rod-shaped electrodes, in particular in view of limits of detection (LODs). Reported here is an in-depth study of the lower LOD for Cl^- measurements with paper-based devices comprising AgCl/Ag transducers. Contamination by Cl^- from two commonly used device materials—a AgCl/Ag ink and so-called ashless filter paper—was found to increase the concentration of Cl^- in paper-contained samples far above than what is expected for the spontaneous dissolution of the transducer's AgCl, thereby worsening lower LODs. In addition, for the case of Ag^+, the commonly hypothesized adsorption of

metal cations onto filter paper was found not to significantly affect the performance of AgCl/Ag transducers. We note that in the context of chemical analysis, metal impurities of paper are often mentioned in the literature, but Cl^- contamination of paper has been overlooked.

INTRODUCTION

High mechanical stability, biodegradability and a low cost make paper an attractive material for the design and fabrication of analytical devices.[80,137] Filter paper in particular has long been used in chemical analysis due to its ability to wick solutions through capillary action, whether for the urine test strips developed first in 1880,[13,81,138–140] for the pioneering work with paper chromatography in the early 1900s,[141] or for the electroanalytical Kodak Ektachem slides of the 1980s.[15] The current popularity of paper-based devices resulted to a large extent from the simple and affordable wax printing and melting techniques used to create hydrophobic barriers and control liquid flow, as introduced by the Whitesides and Lin groups in 2009.[81,137] The term “paper-based device” does not have a single definition, though. Rather, it has been used in a generic manner to describe any device in which at least one component is made of paper.[142] The most common role of paper is sample collection and wicking, with sensing components either attached to, printed on top of, or integrated into the paper itself.

In the field of potentiometric sensors, paper has been used either to hold the sample (such as in strip-type sensors dipped into sample solutions to collect samples),[21,37,93] to wick samples to conventional rod-shaped electrodes,[19,34] or to serve as a platform

substrate onto which the sensing components are placed.[54,59,60] Although many paper-based devices of this type respond linearly in the clinically relevant range, many have either lower LODs worse than conventional rod-shaped ion-selective electrodes (ISEs) or exhibit non-Nernstian response slopes. For sandwich-based designs, in which the sensing membrane is placed between two pieces of filter paper, a worse LOD was found for both a divalent anion (bilirubin)[52] and a monovalent cation (K^+)[22]. For more integrated setups, in which membranes are embedded into the filter paper, an order of magnitude or more worsening of LOD was observed for Cl^- and K^+.[54,59,61] Nanomolar lower LODs have been achieved with strip-type paper-based sensors for Cd^{2+}, Ag^+, and K^+, but only when the paper components of those devices were coated with carbon nanotubes and were not in direct contact with the samples.[36] A worsened lower LOD has been reported even when paper is only the sample holder to measure Cd^{2+}, Pb^{2+}, Ag^+, and K^+ with large rod-shaped ISEs.[17–19,27] Paper sampling was also found to result in super-Nernstian responses when detecting Cd^{2+} and Pb^{2+} with solid-state and solid-contact ISEs, respectively.[27] Such deviations from the theoretically predicted response slope are indicative of interactions between paper and the target ion or kinetically limited processes, restricting device reproducibility. While pre-treating paper with inorganic salts of the target ions resulted in Nernstian response slopes, the lower LODs of such devices were still worse than for conventional potentiometric sensors.[27]

We describe here limitations of paper-based potentiometric sensors with different types of AgCl/Ag and AgBr/Ag transducers. In an ideal system, the lower LOD of these solid-state ISEs is determined by dissolution of the silver halide into the aqueous sample,

which is controlled by the very low solubility product of the silver halide.[87] However, we observed higher than expected LODs for Cl^- sensing. We show here that Cl^- contamination from AgCl/Ag ink is a key factor in worsening of the lower LOD, as is, surprisingly, Cl^- contamination of the paper.

We wondered whether Cl^- contamination of samples also results from interactions of Ag^+ with paper, lowering the activity of free Ag^+ and increasing solubility of AgCl. Indeed, as early as 1960, Pickering and co-workers reported adsorption capacities of Whatman filter paper for Cu^{2+}, Pb^{2+}, Cd^{2+}, Zn^{2+}, and Ni^{2+} on the order of 4 □g/g paper, values that are reduced in acidic solutions and solutions with high backgrounds of K^+ or Mg^{2+} salts.[143] They also noted an increased concentration of Mg^{2+} and Ca^{2+} in solutions after exposure to paper. This led them to conclude that adsorption of heavy metal ions to paper results from ion exchange with H^+, Mg^{2+} and Ca^{2+}, all ions that are probably present in filter paper mostly as counter ions to the many carboxylate groups of the cellulose polymer chains.[143] More recent work showed that treatment of paper pulp with peroxide and alkaline solutions increases the adsorption of divalent cations to paper, both treatments that increase the number of carboxylate groups.[144,145] Consistent with these observations, Ota et al. showed that the transport of cations through cellulose-based materials with negatively charged surfaces is significantly decreased as compared to other types of paper.[110] While evidence for the interactions of various cations with filter paper is plenty, only few equilibrium parameters, such as binding constants describing cations to paper, have been reported. Metal adsorption onto cellulose nanomaterials has been quantified with a view to water remediation, but such studies reported adsorption to

functionalized rather than non-functionalized cellulose such as filter paper.[146–148] To this end, we also quantified binding of Ag^+ to paper.

EXPERIMENTAL SECTION

Materials.

Reagents were purchased from the following sources: KCl, $AgNO_3$, citric acid, and Whatman grade 1 filter paper from Sigma-Aldrich (St. Louis, MO, USA); sodium citrate dihydrate from Mallinckrodt (St. Louis, MO, USA); unflavored gelatin from Kraft (Chicago, IL, USA); AgCl/Ag ink (AGCL-675; consisting, according to the supplier's material data safety sheet, of 40–60% silver, 10–25% AgCl, 25–50% γ-butyrolactone, and 5–15% urethane acrylate oligomer) from Nayaku Advanced Materials (Westborough, MA, USA); Polx1200 polyester continuous knit filament cleanroom wipes from Berkshire Corporation (Great Barrington, MA, USA); and gold disk electrodes (2 mm diameter; embedded into an inert Kel-F polymer shaft) from CH Instruments (Austin, TX, USA). In-house deionized water was purified to a resistivity of 18.2 MΩ/cm with a Milli-Q PLUS reagent-grade water system (Millipore, Bedford MA, USA) and used for all experiments involving water.

Paper Adsorption Studies.

Six stock solutions of $AgNO_3$ in the range from 10^{-5} to 10^{-2} M were prepared. For both paper and textile analysis, 6 g of material was separately added to 25 mL of each $AgNO_3$ solution. After 2 min, an aliquot of the solution was removed with a plastic syringe, and the concentration of Ag in these samples was determined with an iCAP 7600 inductively coupled plasma optical emission spectrometer (ICP-OES; ThermoFisher,

Waltham MA, USA).

Fabrication of Paper-Based Sensors.

Microfluidic zone barriers were hand-drawn in matching patterns on both sides of paper or textile substrates using China Wax pencils (Sharpie brand, Atlanta, GA, USA). For each of the two electrical connections, AgCl/Ag ink was applied to one side of the paper or textile using a rubber-tipped paintbrush (Royal Sovereign, UK) to achieve uniform coverage. This was followed by curing for 10 min at 100 °C in ambient atmosphere to both melt the wax and allow it to permeate through the thickness of the substrate as well as to let evaporate the solvent contained in the AgCl/Ag ink. For devices comprising AgCl or AgBr coated Ag wires and AgCl coated Ag plates, no AgCl/Ag ink was applied.

Ink-Coated Gold Electrodes.

The 2 mm diameter gold disk electrodes were polished over polishing cloths with aqueous dispersions of alumina (0.3 and 0.05 μm, Buehler, Lake Bluff, IL, USA). They were then cleaned in piranha solution (concentrated sulfuric acid and 30% hydrogen peroxide solution in a 3:1 ratio). *Caution: piranha solution is a strong oxidizing reagent, is highly corrosive, and should be handled with care*. The electrodes were then cleaned by ultrasonication in water and ethanol and dried with a flow of nitrogen. A continuous coating of the AgCl/Ag ink was applied using a rubber-tipped sculpting brush and allowed to dry overnight. A double-junction type external reference electrode (DX200, Mettler Toledo, Switzerland; 3.0 M KCl saturated with AgCl as inner filling solution and 1.0 M LiOAc as bridge electrolyte) was used for measurements with this type of electrodes.

Potentiometric Measurements.

Electrode potentials were measured using an EMF 16 high-impedance voltmeter (input impedance 10 TΩ) controlled by EMF Suite 1.03 software (Lawson Labs, Malvern PA, USA). For devices with a AgCl or AgBr coated Ag wire as transducer, small holes were made in the reference and sample zones of the paper and the wires were inserted through these holes (Figure 3-S1, Supporting Information). When using a AgCl/Ag plate, the plate was held flush against the paper with binder clips. (See the Supporting Information for the preparation of AgCl coated Ag wires and plates.) Two alligator clips were used to connect the devices to the voltmeter, and all devices were placed on top of a sheet of PVC and held in place with binder clips for stability. Both the plates and wires were stored in 0.1 M KCl solution saturated with AgCl when not in use and washed with H_2O before each use and between uses. For each device, 20 μL each of the aqueous sample and reference solution were simultaneously deposited into the respective zones. It took approximately 30 s for the solutions to fully wet the paper; the recorded response was the average EMF over the following 30 s. Activity coefficients were calculated according to a two-parameter Debye-Hückel approximation,[88] and EMF values were corrected for liquid-junction potentials with the Henderson equation.[87]

For measurements with acidic sample solutions, 0.55 M citrate buffer (pH 2.4) was used. This concentration was chosen to ensure that the paper would not affect the pH, as the concentrations of acidic groups on cellulose nanofibers and pulp have been reported as 100 μmol/g cellulose[147] and 50-200 μmol/g pulp,[145,149–151] respectively (approximately equivalent to a 0.1 M concentration when a 20 μL droplet of sample is placed onto a 2

cm^2 section of paper, as typical for the work described here).

Leaching of Cl^- from Paper and Textile.

To determine its Cl^- content, 2.3 g filter paper was dry ashed, dissolved in 10 mL 10 wt % HNO_3, and analyzed with the mercury(II) thiocyanate method, using a Lachat QuikChem8500 flow injection analyzer.[152] To assess the possibility of Cl^- contamination of aqueous samples upon brief contact with filter paper or pieces of textile, 35 mL of H_2O was exposed to 10 g of paper or textile. After 5 min, a water sample was removed using a separate plastic syringe and analyzed for Cl^-.

Leaching of Cl^- from Ink.

To assess leaching of Cl^- from AgCl/Ag ink, 6 glass vials were coated on their inner walls with AgCl/Ag ink and dried overnight under vacuum. Then, 4 mL water was added to each vial and stirred with a magnetic stir bar for 5 min. Then, the solution was removed and analyzed potentiometrically for Cl^- using a AgCl/Ag coated Ag wire as ISE and a capillary reference electrode (AgCl/Ag, 3.0 M KCl inner filling solution).[153]

RESULTS

Performance of AgCl/Ag Ink Transducers in Absence of Paper.

For this work, a commercial AgCl/Ag ink was initially used to prepare Cl^- sensors because such inks are commonly used as ion-to-electron transducers in paper-based electrochemical devices.[22,52,54,59,137,154] Besides Ag nanoparticles and AgCl, this ink also contained according to the supplier a urethane acrylate oligomer and γ-butyrolactone. We

first examined the performance of the AgCl/Ag ink using 100 mL beakers to contain the samples. For this purpose, commercial rod-shaped electrodes were coated with a layer of the AgCl/Ag ink, the solvent was allowed to evaporate, and potentiometric measurements with the thus prepared ISEs were performed with respect to a conventional double-junction reference electrode. Lower LODs were determined by extrapolation of the linear EMF response to the value observed when no target ion was added to the sample, as this is standard practice in the ISE literature.[99]

In this type of electrochemical cell, the only phase boundary potential expected to depend on the sample is at the interface of the sample and the AgCl.[87] Consequently, the measured electromotive force (EMF) depends on the activity of Cl^- ions according to the Nernst equation, $EMF = E° - 58.2$ mV log a_{Cl^-} (response slope for room temperature). The lower LOD is expected for both Cl^- and Ag^+ to be $10^{-4.9}$ M, as given by the square root of the solubility product of AgCl (1.6×10^{-10} M^2).[87]

The ink-coated Au electrodes responded to Cl^- with a lower LOD of $10^{-4.8 \pm 0.1}$ M Cl^- (n=3), and to Ag^+ with a lower LOD of $10^{-5.0 \pm 0.1}$ M Ag^+ (n=4), as shown in Figure 3-S1. These values are within error of what theory predicts, confirming that in the absence of paper these ISEs perform in an ideal manner. Therefore, we proceeded to use paper-based devices using the same AgCl/Ag ink.

Performance of Paper-Based Devices with AgCl/Ag Ink Transducers.

A dumbbell-shaped wax pattern was drawn onto rectangular pieces of ashless filter paper to define separate reference and sample zones as well as a central contact area (see Figure 3-1A and Figure 3-S2 of the Supporting Information), as introduced by Lan et

al.[49] For potentiometric measurements, 20 µL 0.1 M KCl reference solution was applied to the rectangular area in contact with the reference electrode, and 20 µL sample solution was applied to the rectangular zone in contact with the indicator electrode. The solutions were then allowed to wick into the diamond-shaped contact area to contact one another (see Figure 3-1A). This procedure results in three phase boundary potentials affected by the deposited solutions. The size of the liquid junction potential that arises at the phase boundary between the 0.1 M KCl reference solution and the sample solution can be predicted using the Henderson equation and is kept small by use of a highly concentrated solution of KCl.[87] The phase boundary potential at the reference solution/AgCl/Ag interface is determined by the concentration of the reference solution, and is, therefore, independent of the sample. Consequently, the measured EMF (which comprises the sum of all phase boundary potentials) only varies with the phase boundary at the sample/AgCl/Ag interface, which depends upon the Cl^- concentration in the sample as predicted by the Nernst equation.

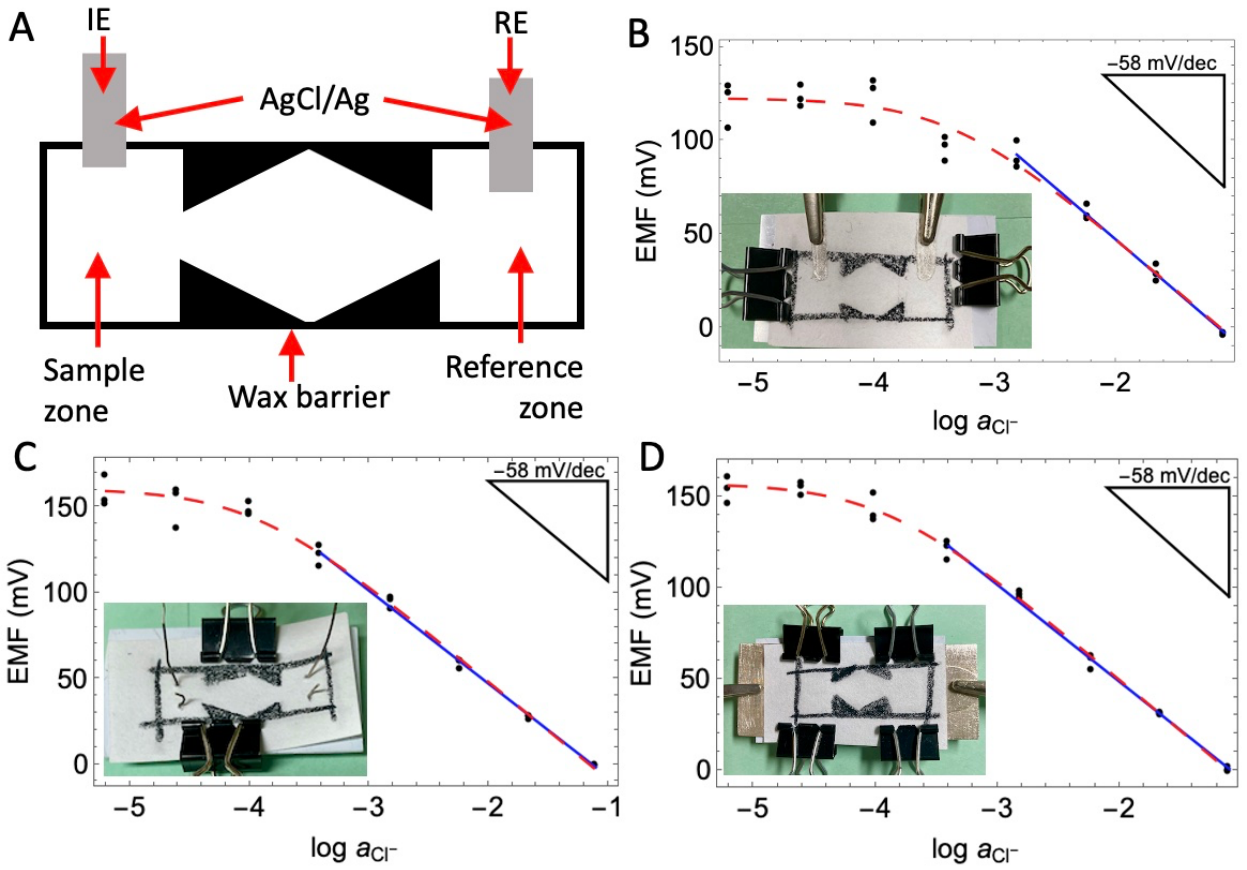

Figure 3-1. (A) Schematic of paper-based devices used (RE: reference electrode, IE: indicator electrode). Potentiometric responses to KCl solutions as measured with Cl^- sensing devices with (B) ink, (C) wire, and (D) plates as AgCl/Ag transducers; insets show photographs of the corresponding device setups. Blue solid lines are fits of the linear portions of the response curve, and red dashed lines are non-linear fits of all data using a modified Nicolskii–Eisenman equation accounting for a lower LOD (i.e., $EMF = E° - 58.2$ mV log (a_{Cl^-} + LOD), where a_{Cl^-} is the activity of Cl^- in the sample).

The potentiometric responses to Cl^- of paper-based devices with AgCl/Ag ink

transducers are shown in Figure 3-1B–D and Table 3-1. Each concentration was measured with 3 different devices. Because these are single-use devices, a total of 24 devices contributed to each calibration curve. Use of these paper-based devices with AgCl/Ag ink directly applied to the paper resulted in a lower LOD of $10^{-3.4 \pm 0.3}$ M Cl^-, as shown in Figure 3-1B. This LOD is significantly higher than the value of $10^{-4.9}$ M, as expected from the solubility of AgCl and as indeed observed in the beaker-based measurements. However, it is consistent with detection limits previously reported for paper-based potentiometric devices comprising electrodes prepared with a AgCl/Ag ink.[22]

Table 3-1. Potentiometric responses to Cl^- of devices with different types of AgCl/Ag transducers (see Figure 3-1).

AgCl/Ag Form	Setup	Slope (mV/decade)	LOD (M)
Ink	Paper-based	–55.3 ± 4.0	$10^{-3.4 \pm 0.3}$
Ink	Textile-based[55]	–56.8 ± 1.3	$10^{-4.1 \pm 0.1}$
Ink	Paper-based (acidic solutions)	–63.4 ± 2.5	$10^{-3.3 \pm 0.2}$
Ink	Textile-based (acidic solutions)	–61.1 ± 5.0	$10^{-3.9 \pm 0.3}$
Ink	Au electrodes in beaker	–54.9 ± 0.5	$10^{-4.8 \pm 0.1}$
Ink*	Au electrodes in beaker*	+54.4 ± 1.4	$10^{-5.0 \pm 0.1}$
Wire	Paper-based	–54.2 ± 2.0	$10^{-4.0 \pm 0.2}$
Wire	Paper-based (0.01 wt % gelatin)	–53.4 ± 2.4	$10^{-3.5 \pm 0.2}$
Wire	Textile-based	–55.0 ± 1.0	$10^{-4.4 \pm 0.1}$
Wire	Beaker	–57.5 ± 0.4	$10^{-4.9 \pm 0.1}$
Wire	Beaker*	+55.7 ± 0.8	$10^{-4.8 \pm 0.1}$
Plate	Paper-based	–54.2 ± 2.0	$10^{-3.9 \pm 0.1}$
Plate	Beaker	–58.6 ± 1.2	$10^{-4.8 \pm 0.1}$

*Data corresponds to Ag^+ sensing

Characterization of the AgCl/Ag Ink.

Given the discrepancy in the results from the experiments with, on one hand, the beakers and, on the other hand, the paper-based devices, we characterized the ink in view of impurities. For that purpose, 4 mL water was added to reaction vials previously coated on their inside walls with AgCl/Ag ink, and, after 5 min of stirring, those water samples were transferred into other vials for potentiometric determination of the Cl^- concentration using a AgCl/Ag wire transducer as indicator electrode. Water stored for 5

min in non-coated control vials did not contain any measurable Cl^-, but water stored for 5 min in the ink-coated vials contained $10^{-3.7\pm 0.1}$ M Cl^- (n=3). This corresponds to 90 ± 30 ppm leachable Cl^- in the ink, and we note that there may well be more Cl^- leaching into samples if the leaching time were longer. Because the Cl^- concentration in the aqueous sample exceeded the value predicted by the solubility of AgCl considerably, it follows that most of this leachable Cl^- is present in the ink in a form other than AgCl. To the best of our knowledge, there are no previous reports of Cl^- contaminants in commercial AgCl/Ag inks with which to compare this value.

These result show that while ppm level reagent impurities in the AgCl/Ag ink do not affect measurements in large samples, they cannot be ignored for measurements with microfluidic devices and even for sample volumes of a few milliliters. Assuming an extent of mass transfer comparable to that observed in the experiments with the internally coated vials, leaching of Cl^- from the 3 mg of ink on a paper-based device into a 20 µL droplet of pure H_2O deposited would result in a $10^{-3.5}$ M Cl^- concentration. This value is very close to the observed lower LOD for paper-based devices with transducers prepared from AgCl/Ag ink. It follows that using a commercial AgCl/Ag ink such as the one used here can significantly worsen the lower LOD for Cl^-.

Performance of Cl^- Sensing Devices with Alternative AgCl/Ag Transducers.

To determine whether the observed worsening of the lower LOD in paper-based devices is unique to the AgCl/Ag ink we used, or whether it occurs also for other types of AgCl/Ag electrodes integrated into paper-based devices, we used Ag wires and plates, both electrochemically AgCl coated and differing from one another only in their area of

contact with paper (see insets of Figures 3-1C and 3- D). Specifically, the wires and plates contacted approximately 0.1 and 2.0 cm^2 of paper, respectively.

As for the AgCl/Ag ink transducers, the performance of the AgCl/Ag wires and plates was first measured in 100 mL sample volumes with a conventional double-junction reference electrode. The lower LODs and slopes for both Cl^- and Ag^+ were all within error consistent with theory (see Table 3-1), showing no evidence for sample contamination by the transducers.

The potentiometric responses of paper-based devices with a AgCl/Ag wire or AgCl/Ag plate transducer to varying concentrations of KCl are shown in Figure 1C-D. Devices using a AgCl/Ag wire or plate gave a lower LOD of $10^{-4.0 \pm 0.2}$ M Cl^- and $10^{-3.9 \pm 0.1}$ M Cl^-, respectively, both worse than expected based on the solubility product of AgCl. While these two transducers differ in the contact area between electrode and paper by a factor of 20, the lower LODs were within error of one another, suggesting that the paper-induced worsening of the LOD is not affected by the area of the filter paper/electrode interface.

While typically AgCl coated Ag wires were stored in KCl solution, control experiments were also performed by immersing these transducers into deionized water for 1 h before and after each measurement to rule out contamination of samples from KCl solution adhering to these transducers. However, results thus obtained provided no evidence for such a mode of sample contamination (for details, see the Supporting information). It was also hypothesized that convection in samples might affect the lower LOD, influencing how quickly contaminants might be dissolved into the samples closeby

to the transducers. However, experiments with paper-based devices and samples that contained in addition to KCl also 0.01 wt % gelatin gave LODs that did not differ from experiments without gelatin (see the Supporting Information for full experimental details). As gelatin is well known to suppress convection,[155] we conclude that convection is not relevant in this system.

It is interesting to note that for all transducers tested, the standard deviation of the measured EMF was invariably larger at Cl^- concentrations below the devices' LOD, as seen in Figure 3-1B-D. This has not been previously reported and suggests that the interference introduced by the filter paper depends on parameters that are of lesser importance to the EMF response at higher Cl^- concentrations. This and the observed increase in response time at the lower LOD may be related to a slow rate of leaching of Cl^- out of the paper substrate.

Performance of Br^- Sensing Devices with AgBr/Ag Transducers.

Clearly, while use of the AgCl/Ag ink resulted in the most pronounced worsening of the lower LOD for Cl^-, some LOD worsening is also observed for paper-based devices with AgCl/Ag wire and plate transducers. This raised the question whether the worsening of the lower LOD for paper-based devices is unique to AgCl/Ag transducers, or whether it is also observed for other silver halide transducers. To address this question, we used AgBr coated Ag wires with KBr solutions as samples, as shown in Figure 3-S4 and Table 3-S1. Analogous to the observations with AgCl/Ag transducers for the detection of Cl^-, paper-based devices measuring Br^- also had a lower LOD ($10^{-5.5 \pm 0.3}$ M) worse than what is expected from the square root of the AgBr solubility product (5.35×10^{-13} M^2), i.e., 10^-

$^{6.1}$ M. However, the extent to which paper worsened the LOD for Br^- was less pronounced than for Cl^- (see the Supporting Information for full data). Indeed, the slight worsening of the lower LOD for Br^- sensing with AgBr/Ag transducers appears to be the result of the same Cl^- contamination that also affects Cl^- sensing, as discussed further below.

Adsorption of Ag^+ to Filter Paper.

All the results described above are consistent with a lower LOD affected by a Cl^- concentration in samples higher than what is predicted by the solubility of AgCl. We wondered whether that may be explained by the adsorption of Ag^+ to filter paper, increasing the overall solubility of AgCl in a medium comprising paper. Indeed, adsorption of metal cations onto negatively charged cellulose is often posited as an explanation for the performance limitations of paper-based devices.[19,27,81]

To investigate this hypothesis, filter paper was suspended in aqueous $AgNO_3$ solutions of varying concentrations, and aliquots of the equilibrated solutions were then removed and analyzed for silver by ICP-OES. From this data, the extent of Ag^+ adsorption to the paper was determined by difference. The amount of Ag^+ adsorbed onto filter paper as a function of the equilibrium concentration of $AgNO_3$ is shown in Figure 3-2, with a fit based on Langmuir adsorption theory. The fit gives a maximum surface coverage of 9.0 x 10^{-4} ± 1.7 x 10^{-4} g Ag/g filter paper (8.3 μmol Ag/g filter paper), with an equilibrium constant for adsorption of 500 ± 300 M^{-1}.

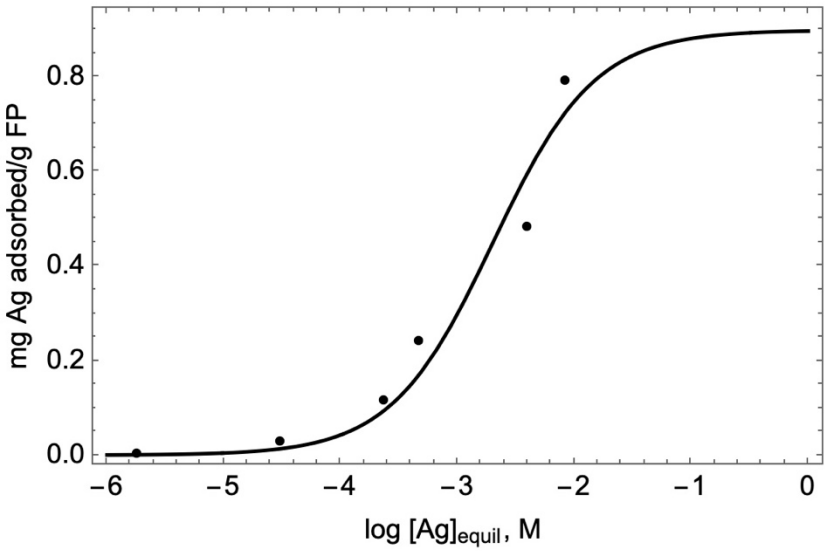

Figure 3-2. Adsorbed amount of Ag^+ per g filter paper (FP) versus logarithm of the equilibrium concentration of Ag (black dots), as determined by ICP-OES, along with a fit based on Langmuir adsorption theory (solid black line) for adsorption of Ag^+ onto filter paper.

While there are not enough points in the higher concentration range of the adsorption data shown in Figure 3-2 to conclusively distinguish between a Langmuir or Frumkin type adsorption process, the relevant Ag^+ concentration range for understanding lower LOD interferences in biological samples using paper-based $Cl^–$ sensors with AgCl transducers is well below 1 mM Ag^+. This readily follows from the solubility product of AgCl ($1.6 \times 10^{–10}$ M^2), which at the surface of a AgCl transducer predicts concentrations of Ag^+ below 1 mM for any sample that contains more than $10^{–6.8}$ M $Cl^–$.

Given the weak affinity of Ag^+ for paper as evident from Figure 3-2, the purity of the filter paper, and the reported concentration of carboxyl groups of 50-100 µmol/g filter

paper,[145,146,149,151] it appears likely that this type of Ag^+ adsorption is related to carboxylic acid groups of cellulose. Pickering attributed the adsorption of divalent cations to filter paper to an ion exchange with metals on the paper,[143] but the concentrations of metals in ashless filter paper as reported by commercial suppliers are only in the low ppm range.[156] Therefore, in a system with ashless filter paper, the cations that exchange with Ag^+ are more likely hydronium ions formed by deprotonation of carboxylic acid groups, which, based on their similarity to gluconic acid, may be estimated to have pK_a values of about 4 and are, therefore, expected to dissociate readily. The equilibrium constant for Ag^+ adsorption to filter paper, as evident from Figure 3-2, is very small, but it is larger than the extremely small formation constant of the 1:1 complex of Ag^+ and acetate of only 0.73 M^{-1}.[157] Given the relatively high concentration of carboxyl groups in paper of 50-100 µmol/g, it is possible that adsorbed Ag^+ ions electrostatically interact with more than one carboxylate group.

As can be seen from Figure 3-2, there is less than 0.1 mg Ag^+ adsorbed per gram filter paper for any concentration of Ag^+ in the sample lower than 1 mM. A fit of the equilibrium concentration of Ag^+ versus the total Ag^+ concentration in the system for data below 1 mM results in a slope of 0.67 ± 0.04 (see Figure 3-S5). This predicts a decrease in the equilibrium concentration of Ag^+ by 0.2 logarithmic units, which is expected to increase the concentration of Cl^- in equilibrium with a AgCl transducer in an otherwise Cl^- free sample by an analogous 0.2 logarithmic units. However, we see experimentally an increase in the lower Cl^- LOD in paper-based devices that is much more significant (see Table 3-1 and discussion above). This shows that while there is some very weak Ag^+

adsorption, this effect is far too weak to explain the worsened lower LOD that we observed in paper-based devices.

The weakness in binding of Ag^+ to cellulose needs to be understood not only by the weak affinity of Ag^+ for carboxylate groups as ligands but also as the result of competition with hydronium ions. We observed that solutions of 1 x 10^{-5} to 1 x 10^{-2} M $AgNO_3$ had an average pH of 6.0 ± 0.3 before exposure to filter paper and 5.2 ± 0.2 after addition of filter paper. A moderate level of acidity of these solutions is expected also as the result of equilibration with the atmosphere, as at 25 °C and 1 atm the solubility of CO_2 in water is 0.57 mg/L,[158] which with the pK_a of carbonic acid[157] of 6.352 results in a pH of 5.6. The very slight acidification of the $AgNO_3$ solutions upon addition of filter paper is nevertheless noteworthy and is consistent with Ag^+ versus hydronium ion exchange.

Weak binding of Ag^+ to cellulose and competition for adsorption with hydronium ions is also consistent with the observed effect of the pH on the Cl^- response. This is shown by the performance of paper-based devices with AgCl/Ag ink, which were also tested with reference and sample solutions prepared in 0.55 M citrate buffer at pH 2.4. These devices had a lower LOD of $10^{-3.3 \pm 0.1}$ M Cl^-, a slope of –63.4 ± 2.5 mV / decade. There was no significant change in lower LODs using paper substrates when samples of lower pH were measured. If adsorption onto a negatively charged substrate were to explain the observed lower LODs, then an improved lower LOD would be expected. Therefore, these findings indicate that the interaction of carboxylate groups with Ag^+ does not explain the worsened lower LODs for Cl^- of paper-based interferences.

Chloride Impurities in Filter Paper.

As we determined that Ag^+ adsorption to paper does not facilitate the dissolution of AgCl from AgCl/Ag transducers, we further examined the paper substrate itself, again looking for impurities. While filter paper is often referred to as a pristine material, it is not free from impurities. Previous studies of various industrial filter papers have detected metal ions as well as anionic impurities such as $Cl^–$, $SO_4^{2–}$, and $NO_3^–$, species that may have already been present in the raw cellulose or were introduced in the manufacturing process.[159–161] So-called ashless filter paper for analytical chemistry purposes is typically characterized by suppliers in view of alkali, earth alkali, and heavy metal ion content, but halide concentrations are not normally reported. Therefore, we analyzed filter paper using dry-ashing followed by detection with the mercury(II) thiocyanate method, giving the $Cl^–$ content of filter paper as 20.1 ± 2.2 μg $Cl^–$/g (n=3). While the supplier's documentation for the Whatman grade 1 filter paper used in this work does not mention chlorine as a possible contaminant, the current value is close to the value of 11.55 μg Cl/g filter paper reported many years ago for Whatman 41 filter paper, which is also cellulose based.[161]

To confirm that the thus detected $Cl^–$ in paper can be leached into aqueous samples, filter paper was immersed in H_2O for 5 min. This relatively short time period was chosen because, when using paper-based devices, measurements are typically taken within 1 min of deposition of the sample onto the device, as evaporation of water begins right away and eventually starts to affect sample concentrations; typically, after 5 min almost all solution has evaporated.[55] Analysis of purified water revealed no measurable $Cl^–$ prior to contact with filter paper but after exposure to filter paper for 5 min, a $Cl^–$concentration

of 14.6 ± 0.6 μg Cl^-/g filter paper was found (n=3).

The source of this Cl^- may be related to the bleaching process that is used in papermaking to clean pulps, remove lignin, and increase both the absorbency and brightness of paper.[162] While the Hg^{2+} used in the mercury(II) thiocyanate method for Cl^- analysis may bind anionic oxygenated chlorine species, the solubilities of Ag^+ species such as perchlorate and hypochlorite are very high,[157] making the precipitation of such salts—and, thereby, interference with the silver halide transducer—an unlikely cause for the observed worsening of the lower LOD for Cl^-. We also note that if impurities of oxygenated chlorine species were present to a significant degree so as to oxidize silver metal and, thereby, raise the Ag^+ concentration, this would lower rather than raise the LOD for Cl^-. This suggests that Cl^- contamination is indeed the main cause of LOD deterioration.

Using the value of 14.6 ± 0.6 μg Cl^-/g filter paper found by soaking of paper in H_2O for 5 min, leaching of Cl^- from paper would lead to a concentration of $10^{-3.4 \pm 0.1}$ M Cl^- in a 20 μL droplet of pure H_2O in the sample zone of 2 cm^2 (see SI for calculations). As this matches the experimentally found lower LOD for paper-based devices with AgCl/Ag ink, it appears likely that the contamination of paper with Cl^- is the dominant cause for observed lower LOD in Cl^- sensing.

To determine whether leachable Cl^- ions can be removed from filter paper by simple rinsing, paper was submerged in H_2O for 5 min, removed from the suspension, rinsed with H_2O, and submerged again in H_2O for a total of three 5-min soaks, dried overnight, and then used for sensor fabrication as normal. This pretreatment did not improve the

lower LOD as compared to untreated paper, indicating that the three 5-min soaks are not sufficient to remove all leachable Cl^-. More vigorous attempts to remove Cl^- ions from the filter paper were hindered by disintegration of the paper.

The contamination of samples by Cl^- leaching from the paper substrate also affected the Br^- measurements with AgBr/Ag transducers described above. For the Br^- measurements shown in Figure 3-S4, Cl^- is an interfering ion that contaminates the sample, worsening not only the lower LOD for Br^- but, as a result of the kinetics of leaching, also reducing the reproducibility of the measured EMF near and below the lower LOD. Given a selectivity coefficient of $\log K^{\mathrm{pot}}_{\mathrm{Br,Cl}}$ of –2.5, as it can be obtained from the ratio of the solubility products of AgBr and AgCl,[87] a detection limit of $10^{-5.9 \pm 0.1}$ M Br^- is estimated for samples contaminated with $10^{-3.4 \pm 0.1}$ M Cl^-. The experimentally observed lower LOD of $10^{-5.5 \pm 0.3}$ M for Br^- is slightly worse, but this difference appears well within the range of error often caused by the well-documented Hulanicki effect[163] (that is, a deviation of the EMF of silver halide ISEs from the thermodynamically predicted value at the lower LOD).

Whatman 1, the paper used in this work, has been used in a number of studies on paper-based ISEs. To explore whether there is something unique to Whatman 1, we also fabricated devices with three other types of filter paper previously reported for use in paper-based ISEs. However, there was no improvement in the LOD for chloride with any of these alternative devices (see the Supporting Information for full results). Indeed, one of the three alternative filter papers provided a slightly worsened LOD for chloride. This suggests that low level chloride contamination of filter paper is quite common.

Considering the possibility of a different supporting substrate, we also performed experiments using both AgCl/Ag ink and AgCl coated Ag wires as transducers using the textile fabric Polx1200 as device substrate instead of the filter paper. Polx1200 is a knitted sample-wicking polyester textile designed for use as a cleanroom wipe that was previously used as a supporting substrate for ISEs.[55] Textile-based devices using AgCl/Ag transducers exhibited lower LODs of $10^{-4.1 \pm 0.1}$ and $10^{-4.4 \pm 0.1}$ for ink and wire transducers, respectively. This is still not as low as predicted by the solubility product of AgCl in water, but it is an improvement over paper-based devices (see the Supporting Information for full discussion of results). Noting this favorable property of Polx1200, we also considered the wax barriers as a possible source of contamination. However, using textile-based devices without wax barriers, we saw no improvement in device performance (see the Supporting Information for details), confirming that the wax barriers do not negatively affect the LOD for chloride.

CONCLUSIONS

Our results show that Cl^- contamination of samples from both a commercial AgCl/Ag ink and filter paper explains the sub-optimal performance of paper-based potentiometric Cl^- sensors. While both AgCl/Ag ink and so-called ashless filter paper have sufficiently high enough purities for use with large sample volumes, leaching of Cl^- significantly worsens the LOD in devices with sample sizes on the order of microliters and even a few milliliters. Improved lower LODs for Cl^- may be obtained by use of device substrates with a higher purity, such as synthetic textiles, and the preparation of AgCl coated Ag

electrodes directly by oxidation of Ag. More careful formulation of AgCl/Ag inks may also be considered. Notably, adsorption of Ag^+ onto negatively charged cellulose was confirmed to occur at very high Ag^+ concentrations but has only a minimal effect on potentiometric Cl^- sensing. This work demonstrates the sensitivity of small-volume potentiometric devices both to sample depletion by interaction with the platform substrate and to contamination from impurities of the sensing membrane and the platform substrate. These are problems that can, however, be avoided if materials are thoughtfully selected, for example, by the replacement of paper by a textile as the platform substrate[55] or cautious selection of silver inks of higher purity.

SUPPORTING INFORMATION

Materials.

Reagents were purchased from the following sources: iron (III) chloride, nitric acid, potassium bromide, hydrochloric acid, and Whatman quantitative filter paper (grade 589/2 white ribbon) from Sigma-Aldrich (St. Louis MO, USA); 0.5 mm diameter Ag wire from Alfa-Aesar (Ward Hill MA, USA); and Ahlstrom-Munksjö qualitative filter paper grade 74 and Sartorius quantitative filter paper grade 388 from Thermo Fischer Scientific (Waltham MA, USA).

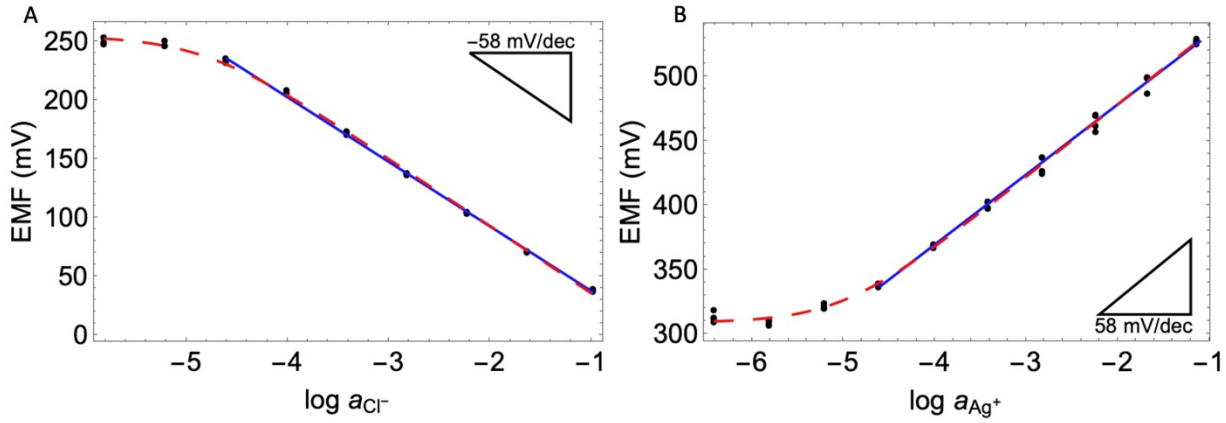

Figure 3-S1. Potentiometric response in beakers with Au electrodes coated with AgCl/Ag ink in (A) KCl solutions and (B) $AgNO_3$ solutions. Blue solid lines are fits of the linear portions of the response curve, and red dashed lines are non-linear fits using a modified Nicolskii–Eisenman equation, accounting for a lower LOD (i.e., $EMF = E° - 58.2$ mV log (a_{Cl^-} + LOD), where a_{Cl^-} is the activity of Cl^- in the sample).

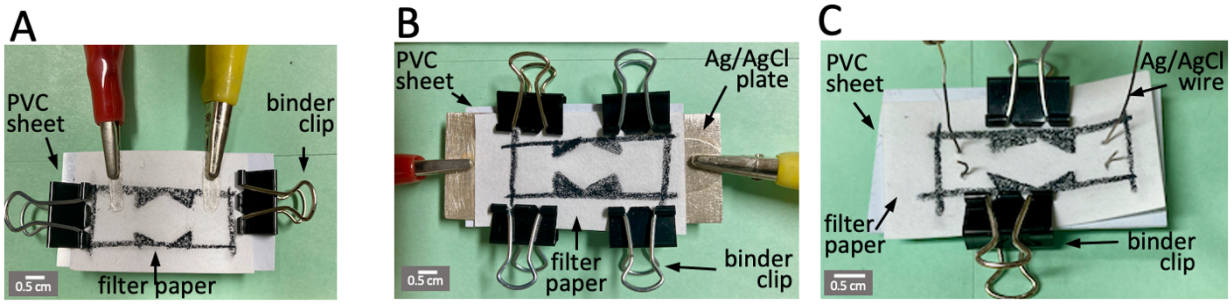

Figure 3-S2. Device setups for Cl^- sensing devices using (A) Ag/AgCl paint, (B) Ag/AgCl plates, and (C) Ag/AgCl wires as transducers.

Preparation of AgCl and AgBr coated Ag wires and Ag plates.

Ag plates and wires were cleaned with 3 M HNO_3 and rinsed with deionized H_2O. They were then placed in a 0.1 M HCl, 1 M $FeCl_3$, solution for 5 min, again rinsed with deionized H_2O, and finally aged in a 0.1 M KCl solution saturated with AgCl for 2 days.

AgBr coated Ag wires were prepared electrochemically, with a Ag wire (cleaned as above) as the cathode in a solution of 0.1 M KBr and a Pt mesh as counter electrode. A current of 0.2 mA/cm^2 was applied for 2 h, followed by aging of the AgBr for 2 days in a solution of 0.1 M KBr saturated with AgBr.

Potentiometric response of AgCl/Ag wires as transducers upon storage in deionized water.

To rule out possible contamination of electrodes by KCl storage solutions, wires were soaked for 1 h in deionized water before potentiometric measurements, and devices were tested in solutions of increasing concentrations, rather than decreasing, as for the experiments shown in Figures 3-1 and 3-2C. This type of cleaning of the AgCl/Ag coated wires and measurement procedure gave a lower LOD of $10^{-3.7\pm 0.3}$ M, which did not represent an improvement and confirmed that the wires as used in prior experiments were not contaminated with KCl from the 0.1 M KCl solution in which the AgCl/Ag wire transducers were stored between experiments.

Potentiometric responses of AgCl/Ag transducers in 0.01 wt.% gelatin solutions.

Considering convection in the sample solution surrounding AgCl/Ag transducers and a possible effect of convention on potentiometric responses, paper-based devices were tested with sample and reference solutions containing 0.01 wt % gelatin, which is well

known to minimize convection in aqueous samples.[155] All solutions used in these experiments were prepared with a 0.01 wt % gelatin background to maintain a constant concentration of gelatin throughout the experiment. Measurements were taken as for other paper-based devices too; 20 µL droplets of sample and reference solution were deposited onto the sample and reference zones, respectively. Devices using AgCl/Ag wire transducers integrated into paper-based devices gave a lower LOD of $10^{-3.5 \pm 0.2}$ M Cl^-, as compared to $10^{-3.4 \pm 0.3}$ in the absence of gelatin. This indicates that convection is not a major factor and cannot explain the higher-than-expected lower LODs of paper-based devices.

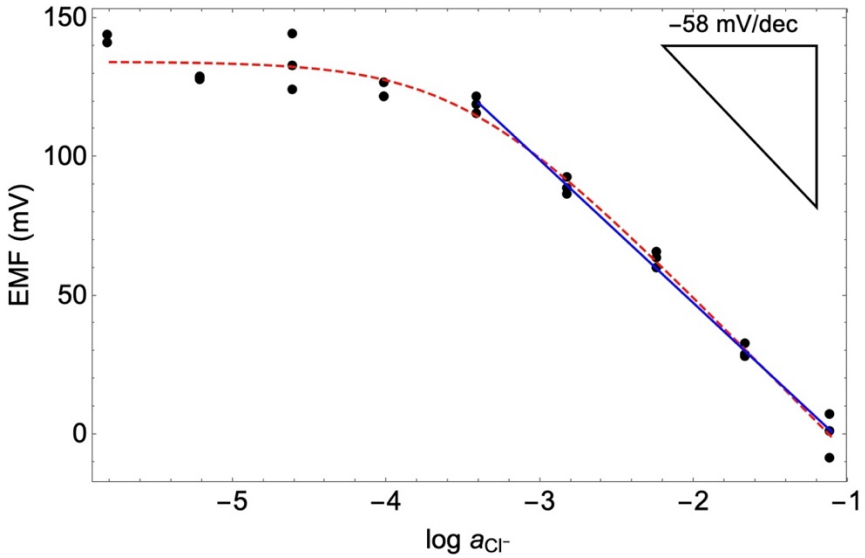

Figure 3-S3. Potentiometric response of paper-based Cl^- sensing devices using AgCl/Ag wires (as shown in Figure S1C) with 0.01 wt % gelatin in both the sample and reference solutions. The blue solid line is a fit of the linear portion of the response curve, and the red dashed line is a non-linear fit of all data using the Nicolskii–Eisenman equation, accounting for the LOD.

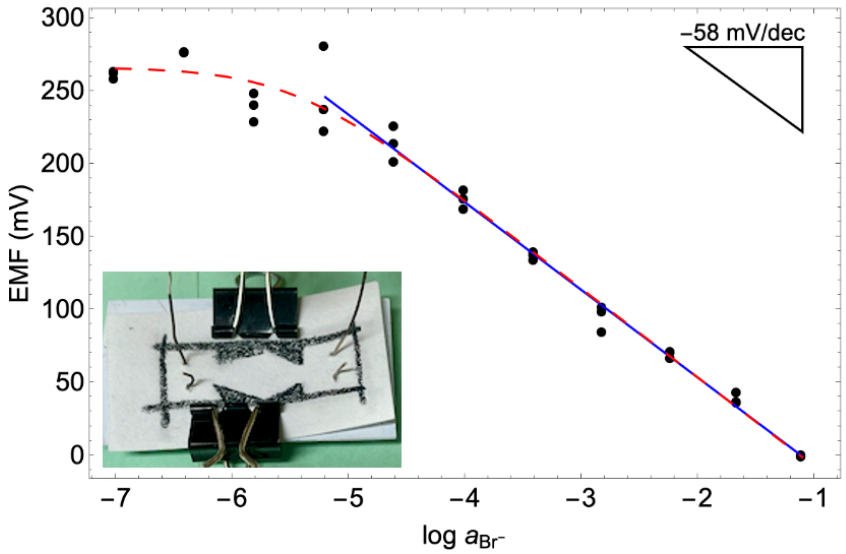

Figure 3-S4. Potentiometric response of paper-based Br^- sensing devices using AgBr/Ag wires as transducers in KBr solutions; inset shows pictures of the device. The blue solid line is a fit of the linear portion of the response curve, and the red dashed line is a non-linear fit using the Nicolskii–Eisenman equation, accounting for the LOD.

Table 3-S1. Potentiometric response to Br^- for different device setups with AgBr/Ag wire transducers.

Device Setup	Slope (mV/decade)	LOD (M)
Beaker	–59.3 ± 0.4	$10^{-6.0 \pm 0.1}$
Paper	–60.1 ± 2.3	$10^{-5.5 \pm 0.3}$
Textile	–56.0 ± 1.5	$10^{-5.6 \pm 0.3}$

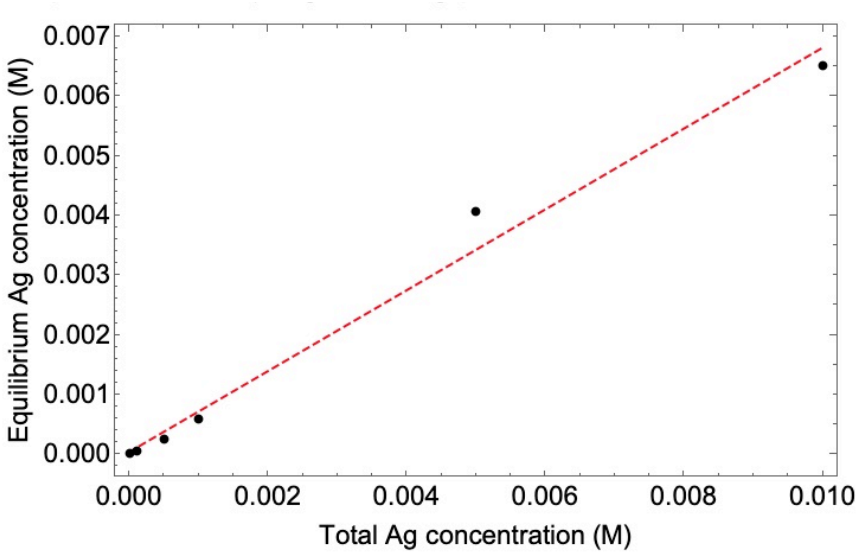

Figure 3-S5. Equilibrium concentration of Ag in deionized water after2 min exposure to filter paper as a function of initial total Ag concentration in the sample, as determined by ICP-OES. The red dashed line is a fit of the data; it has a slope of 0.67 ± 0.04.

Maximum Concentration of Cl^- in a 20 µL Sample in Contact With Filter Paper:

The concentration of Cl^- in the typical sample volume (20 µL) on a paper-based device was calculated as follows. Multiplication of the weight of filter paper per unit area, ρ_{FP}, with the area, A_{FP}, of paper in contact with the sample gives the weight of the paper in contact with the sample, $\rho_{FP} \times A_{FP}$. This term is multiplied with the Cl^- content of paper in mol/g as found by ICP-OES, $C_{Cl^-,FP}$, giving the maximum amount of Cl^- that could leach from paper into a 20 µL sample. Finally, division by the sample volume, V_S, gives the

maximum concentration of Cl^-, $C_{Cl^-,sample}$, that may result from Cl^- leaching from paper into the sample:

$$\rho_{FP} \times A_{FP} \times C_{Cl^-,FP} \times V_S^{-1} = C_{Cl^-,sample} \qquad \text{(3-S1)}$$

In our experiments, A_{FP} was 2 cm^2, the manufacturer reported a value of 8.7 mg/cm^2 for ρ_{FP}, the droplet size used was 20 μL, and as described in the manuscript, we determined $C_{Cl^-,FP}$ as 0.41 mol/g. Insertion of these values into Equation 3-S1 gives the value $10^{-3.4}$ M as reported in the manuscript.

Performance of Devices Using Alternative Papers.

The filter paper used in this manuscript was Whatman grade 1, as is commonly used in paper-based ISEs.[22,36,37,52,61] Alternative filter papers were chosen because their use was reported previously in the literature: Ahlstrom grade 74,[21] Whatman grade 589/3,[54,59,164] and Sartorius grade 388 filter paper.[27,30,32] Devices were fabricated using wax barriers and AgCl/Ag ink as transducer, as shown in Figure 3-S2. Lower limits of detection for chloride were $10^{-2.3 \pm 1.2}$, $10^{-2.3 \pm 0.5}$, and $10^{-3.6 \pm 0.9}$ M for Ahlstrom grade 74, Whatman grade 589/3 and Sartorius grade 388 filter paper, respectively. Responses of these devices are shown in Figure 3-S6 and confirm that the lower LOD is not improved by the use of alternative filter papers of different manufacturers or pore sizes. Contamination of the samples by Cl^- is most likely an artifact from chloride impurities left in these filter papers from the manufacturing process.

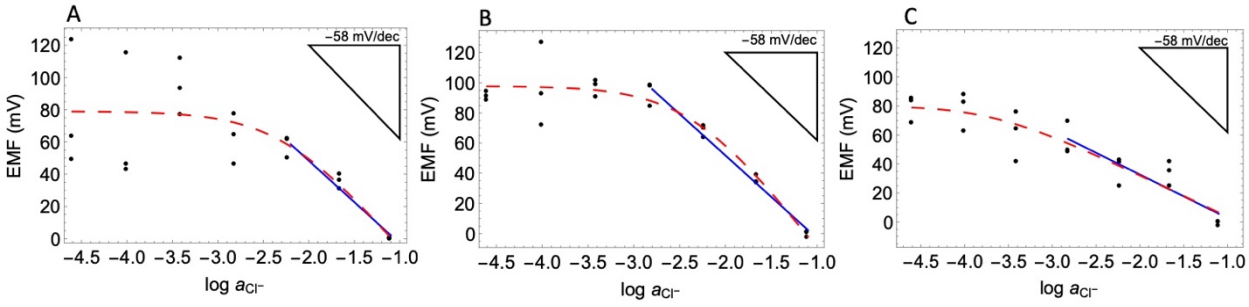

Figure 3-S6. Potentiometric response of paper-based Cl^- sensing devices with AgCl/Ag ink (as shown in Figure S1A) using (A) Ahlstrom grade 74, (B) Whatman grade 589/3 and (C) Sartorius grade 388 filter paper. The blue solid line is a fit of the linear portion of the response curve, and the red dashed line is a non-linear fit of all data using the Nicolskii–Eisenman equation, accounting for the LOD. Lower LODs were $10^{-2.3 \pm 1.2}$, $10^{-2.3 \pm 0.5}$, and $10^{-3.6 \pm 0.9}$ M for (A), (B), and (C), respectively.

Performance of textile-based devices.

The experiments using AgCl coated Ag wires as transducers were performed in the same manner using as the platform substrate the textile Polx1200 instead of paper. Polx1200 is a knitted sample-wicking polyester textile that was previously used as a supporting substrate for ISEs.[55] Textile-based devices using a AgCl/Ag wire as the transducer gave a lower LOD of $10^{-4.4 \pm 0.1}$, and AgBr/Ag wires resulted in a lower LOD of $10^{-5.6 \pm 0.2}$, as shown in Table 3-2. Both for Br^- and Cl^- sensing with Polx1200 devices this represents a worsening of the LOD by 0.5 logarithmic units, a value within error the same as for Br^- sensing with paper but again much smaller than for Cl^- sensing with paper-based devices. When using reference and sample solutions prepared in 0.55 M citrate

buffer at pH 2.4, textile-based devices had a lower LOD of $10^{-3.3 \pm 0.2}$ M Cl^-, a slope of –61.1 ± 5.0 mV decade^{-1}, and an *E*° of –67.1 ± 12.4 mV. It is interesting to note the increased standard deviation in slopes for textile-based devices when using acidic sample solutions as compared to pH neutral solutions of KCl, a change which is not observed for the paper-based platform. Dry ashing of Polx1200 resulted in 2.1 ± 1.1 ppm Cl^-, while soaking of the material in water, as done with paper, resulted in no measurable Cl^-.

Table 3-S2. Potentiometric responses to Cl^- of different devices using a textile support.

Type of Ag/AgCl	Slope (mV/decade)	*E*° (mV)	LOD (M)
Wire	–55.0 ± 1.0	–61.4 ± 2.6	$10^{-4.4 \pm 0.1}$
Wire (acidic solutions*)	–61.1 ± 5.0	–67.1 ± 12.4	$10^{-3.9 \pm 0.3}$
Ink[55]	–56.8 ± 1.3	–63.8 ± 3.4	$10^{-4.1 \pm 0.1}$

*KCl solutions prepared in citrate buffer at pH 2.4

Performance of textile-based devices without wax.

To test if wax interferes with device performance, devices without wax barriers were fabricated. Instead, pieces of Polx1200 textile were cut into the previously mentioned dumbbell shape to define reference and sample zones and control liquid flow (see inset in Figure 3-S7). Devices using this free-standing textile and AgCl/Ag wires had a lower LOD of $10^{-4.2 \pm 0.1}$ M Cl^-, a slope of –56.1 ± 2.5 mV/decade, and an *E*° of –57.2 ± 6.7 mV, as shown by Figure 3-S7.

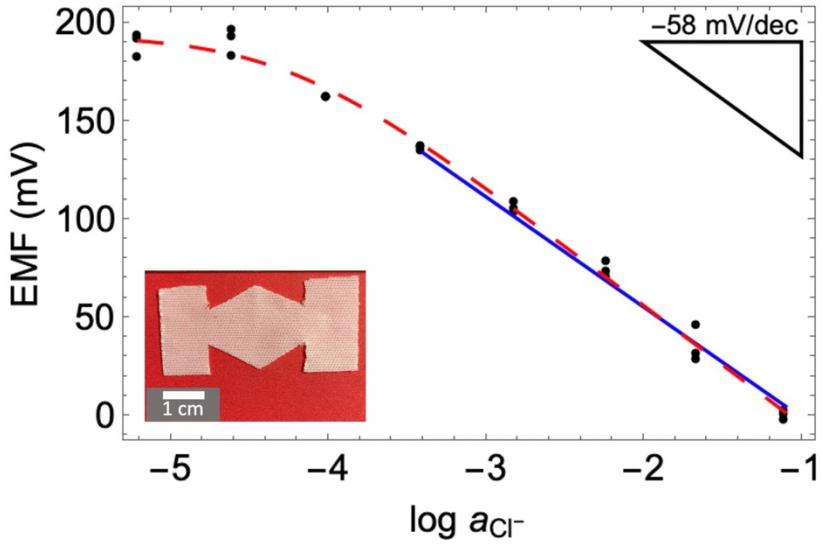

Figure 3-S7. Potentiometric response of textile-based Cl^- sensing devices using AgCl/Ag wires and no wax; inset show a picture of a cut textile on a red background. The blue solid line is a fit of the linear portion of the response curve, and the red dashed line is a non-linear fit of all data using the Nicolskii–Eisenman equation, accounting for the LOD.

Chapter 4. Hydrophilic Redox Buffers for Textile-Based Potentiometric Sensors

Eliza J. Herrero, Takumi Goto, and Philippe Bühlmann

Contributions: Takumi Goto evaluated possible redox buffers and proposed the use of the cobalt terpyridine complex.

PREFACE

One of the barriers to the widespread use of ion-selective electrodes (ISEs) in resource-limited areas is the need for frequent recalibration of such devices. The incorporation of a redox buffer to minimize the effect of redox-active impurities in the system has previously been shown to significantly improve reproducibility. To date, however, there have been no examples of redox buffers compatible with anion sensing that can be incorporated into the inner filling solution of an ISE. Here, we introduce a novel hydrophilic redox buffer, cobalt(II/II)bis(terpyridine), and show the improvement of the standard deviation of E^0 of chloride sensors from 2.7 to 0.3 mV upon introduction of the redox buffer into the inner filing solution of conventional, rod-shaped electrodes. The redox buffer is also compatible with a textile-based sensing platform, and progress has been made towards incorporation of the complex into a textile-based platform with embedded ion-sensing and reference membranes. As only a surprisingly small number

of hydrophilic redox buffers have been reported in the literature, the cobalt(II/II)bis(terpyridine) redox buffer may also find applications outside of the field of ISEs.

INTRODUCTION

There is a need for ion-selective electrodes (ISEs) that can be used in mobile settings with limited resources.[1,2] A large focus of work in this area has been on the miniaturization of ISEs, with variations in the degree of incorporation of the sample holder, reference electrode (RE) and ion-sensing electrode. These include paper- and textile-based sampling with conventional sensing and reference electrodes,[18,31] paper- and thread-based strip-type ISEs dipped into sample solutions,[21,3657] sandwich-type ISEs in which a sensing membrane is held in place between two pieces of filter paper,[22,52,53] and paper- or textile-based devices with membranes integrated into the underlying support substrate.[54,55,59]

A key characteristic for ISEs designed for use in resource-limited areas is high ease-of-use, particularly elimination of the need for frequent and individual calibrations, which require additional equipment and trained users. While the term “calibration-free” does not have an agreed upon definition, it is generally evaluated in terms of the standard deviation (SD) of the standard potential, E^0, which is defined as the potential measured at a primary ion activity of 1.[4,5,7] For example, for diagnostic tests, the U.S. Food and Drug Administration mandates a maximum acceptable error for Na^+ of ± 4 mM within the range of 80-200 mM, which translates to a 0.7 mV acceptable standard deviation for a sodium

ISE,[92] while manufacturers of clinical mainframe analyzers, which are recalibrated very frequently, strive for substantially narrower confidence intervals.

While most research into improving the reproducibility of ISEs is performed with conventional, rod-shaped ISEs, there is a growing amount of work on the development of miniaturized ISEs with improved reproducibilities. One such method, first shown for rod-shaped solid-contact K^+ ISEs, is the short-circuiting of multiple ISEs to a single RE.[98] This method was also used for miniaturized, carbon-fiber based Na^+ ISEs and lowered the E^0 SD from 37.6 to 1.45 mV (n=4) for sampling in aqueous solution against a conventional double-junction RE.[70] While a carbon-fiber based RE was also developed and used for testing in an integrated setup with artificial sweat, repeatability was reported only for slope; visual inspection of the calibration plot suggests a worsened SD of E^0.[70] Improvements in reproducibility were also achieved through optimization of the fabrication methods of strip-type paper-based ISEs prepared from a filter paper coated with carbon nanotubes and poly(3-octylthiophene) as a solid contact, along with plasticized poly(vinyl chloride) (PVC) ion-selective membranes. The SD of the potential of 3 K^+-selective devices in the same solution was lowered from approximately 10 mV to approximately 2 mV by using cyclohexanone rather than tetrahydrofuran (THF) as the solvent for membrane cocktails and performing a single step for the application of both the carbon nanotubes and the poly(3-octylthiophene) onto the filter paper.[37] This improved methodology of fabricating strip-type sensors was also used to achieve a SD of 1 mV or less for both Na^+ and K^+ ISEs in both aqueous and artificial sweat samples.[21,24]

Another method for improving the reproducibility of low-cost miniaturized ISEs is the

use of a molecular redox buffer to control the potential at the interface of the inner filling solution and the electron conducting inner electrode. A redox buffer contains both the reduced and oxidized form of a redox couple and resists changes in the EMF of a solution, just as a traditional pH buffer resists changes in the pH of a solution. Redox buffers such as the thiol disulfide couple are inherent components of the cells of any living organism, as they maintain the stable redox potential needed for their survival. Redox buffers are also well known in geochemistry, and have been used in thermal cells for thermal energy harvesting.[165]

Early uses of molecular redox buffers for ion-selective potentiometry include the incorporation of hydrophobic Co(II/III)tris(phenanthroline) in both ion-selective and reference membranes,[166,167] cobalt(II/III)tris(4,4′-dinonyl-2,2′-bipyridyl) in ion-selective membranes,[168] and both cobalt(II/III)tris(4,4′-dinonyl-2,2′-bipyridyl) and 7,7,8,8,-tetracyanoquinodimethane and the corresponding anion radical in underlying solid contacts in ISEs.[60] In all these cases, the use of the redox buffers improved the reproducibility of E^0. In an effort to the improve reproducibility of *miniaturized* paper-based ISEs, the hydrophobic redox buffer comprising 7,7,8,8-tetracyanoquinodimethane and the corresponding anion radical was incorporated into both Cl^- sensing and reference membranes.[60] Unlike for conventional electrodes, where this buffer resulted in an E^0 SD of 4.3 mV without conditioning, translation into the paper-based device resulted in poor linearity (E^0 SD was not reported). Incorporation of cobalt(II)porphyrin and cobalt(III)corrole, which do not form a redox pair, into the transduction layer of paper-based K^+ ISEs also resulted in an improvement in the E^0 SD in, although additional work

suggested the presence of low level redox-active impurities in the reagents resulted in an EMF which was actually controlled by a redoxbuffer.[90,96] Additionally, incorporation of potassium ferrocyanide with a known impurity of potassium ferricyanide in a ratio of 6.9 to 1 was incorporated into the transduction layer of screen-printed K^+ ISEs.[97] Besides hydrophobic redox buffers, the hydrophilic ferrocyanide/ferricyanide redox couple was also used, in this case by incorporation into a hydrogel miniaturized inner filling solution in a conventional cation-selective electrode to significantly improve the E^0 SD.[169]

Despite the surge in recent work in redox buffers for ISEs, there have been no hydrophilic redox buffers that can be used for anion sensing with the recently proposed fully integrated paper- and textile-based ISEs.[54,55] In this paper, therefore, we expand the scope of applications of redox buffers to aqueous systems for anion sensing, such as the clinically relevant chloride ion. In addition to the standard requirement of redox buffers to contain a chemically stable reduced and oxidized species, which requires a relatively small standard redox potential, a redox couple used as component of the inner filling solution of an anion-selective ISE must also be water-soluble and it cannot comprise an anionic species or else it is likely to interfere with anion sensing through distribution into the anion-selective membrane.

EXPERIMENTAL METHODS

Materials

Reagents were purchased from the following sources: inhibitor-free anhydrous THF, methanol, tridodecylmethylammonium chloride, $CoCl_2 \cdot 6H_2O$, Br_2, and KCl from Sigma (St. Louis, MO, USA); high molecular weight PVC and *o*-nitrophenyl octyl ether (*o*-

NPOE) from Fluka (Buchs, Switzerland); 2,2′:6′,2″-terpyridine and the ionic liquid 1-methyl-3-dodecylmidazolium bis(trifluoromethylsulfonyl)imide (referred to here as [$C_{12}mim^+$][C1C1N$^-$]) from Fisher Scientific (Pittsburg, PA, USA), deuterium oxide from Cambridge Isotope Laboratories (Andover, MA, USA), Au wire from Alfa Aesar (Ward Hill, MA, USA), and Polx1200 polyester continuous knit filament cleanroom wipes from Berkshire Corporation (Great Barrington, MA, USA). In-house deionized water was purified to a resistivity of 18.2 MΩ/cm with a Milli-Q PLUS reagent-grade water system (Millipore, Bedford, MA, USA) and used for all experiments involving water.

Redox buffer preparation

Co(II)bis(terpyridine) chloride was prepared from $CoCl_2$•H_2O and the commercially available terpyridine using a modified literature procedure.[170] Oxidation to Co(III) was performed with Br_2 as oxidant, using a modified literature procedure.[171] ^{1}H NMR spectroscopy was performed with a 500 MHz Bruker Avance III HD spectrometer (Bruker, Billerica, MA). Details of the synthesis and characterization are included in the Supporting Information (SI).

Precursor Solutions for the Preparation of Sensor and Reference Membranes

All sensing membranes were prepared following literature protocols.[54] Precursor solutions for Cl^- ion sensing membranes were prepared by dissolving 60.0 mg PVC, 120.0 mg *o*-NPOE, and 10.0 mg tridodecylmethylammonium chloride in 1.0 mL THF. Precursor solutions for reference membranes (RMs) were prepared by dissolving 30.0 mg [$C_{12}mim^+$][$C_1C_1N^-$], 60.0 mg PVC, and 60.0 mg *o*-NPOE in 1 mL THF.

Fabrication of Conventional ISEs

Membranes were prepared by pouring 1.25 mL of the THF solutions containing the membrane components into a flat-bottomed glass Petri dish (diameter 25 mm), covering the dishes with cardboard, and allowing the THF to evaporate overnight. Circular membranes (diameter 12 mm) were cut out of the master membrane the following day using a cork borer. Circular membranes were then mounted into custom-made ISE bodies,[135] with an aqueous inner filling solution containing 2.5 mM $[Co(terp)_2]Cl_2$, 2.5 mM $[Co(terp)_2]Cl_2$, and 1 mM KCl in contact with a Au wire as inner reference. For electrodes with an ionic-liquid-based RM, the inner filling solution was saturated with the ionic liquid. Either a double-junction type external RE (DX200, Mettler Toledo, Switzerland; 3.0 M KCl saturated with AgCl as inner filling solution and 1.0 M LiOAc as bridge electrolyte) or a capillary RE (AgCl/Ag, 3.0 M KCl inner filling solution),[153] as specified in the text, was used for measurements with this type of electrode.

Fabrication of Textile-Based Electrodes

Textile-based devices were fabricated using a previously reported method.[55] Microfluidic zone barriers were hand drawn in matching patterns on both sides of the textile using a Sharpie Peel Off China Marker. This was followed by curing for 10 min at 100 °C. For initial experiments, a dumbbell-shaped wax pattern was drawn, with separate reference and sample zones as well as a central contact area, as introduced by Lan and co-workers.[49] For electrodes with embedded membranes, solutions of the membrane components were applied to the textiles using a micropipette. Three cycles, consisting each of deposition of a 7 µL aliquot of the appropriate solution on the front and the back

of the textile, were completed for all devices, with a 10-min waiting period between cycles. The Au wire used as an electrical contact in these devices was inserted through interyarn gaps into the textile (see Fig. 4-S3B).

Potentiometric Measurements

Electrode potentials were measured using an EMF 16 voltmeter (input impedance 10 TΩ) controlled by EMF Suite 1.03 software (Lawson Labs, Malvern PA, USA). For textile-based devices, a Au wire was inserted in each side of the device through gaps in the textile. Two alligator clips were used to connect the device to the voltmeter, and all devices were placed on top of a sheet of PVC and held in place with binder clips for stability. For each device, 25 μL each of the aqueous sample and reference solution were simultaneously deposited into the respective zones. It took approximately 30 s for the solutions to fully wet the textile; the recorded response was the average EMF over the following 30 s. All devices were used only once, and each sample was measured in triplicate. Activity coefficients were calculated according to a two-parameter Debye-Hückel approximation,[88] and EMF values were corrected for liquid-junction potentials with the Henderson equation.[87]

RESULTS AND DISCUSSION

Selection of the Redox Buffer

In our search for a hydrophilic redox buffer compatible with anion sensing, we considered commercially available buffers as well as several other metal and organometallic complexes but identified fundamental issues with most of them. Commonly used commercially available redox buffers include ZoBell's solution ($Fe(CN)_6^{3-}$

$^{/4-}$), which is incompatible with anion sensing because of the negative charge of the redox buffer species, quinhydrone, which is not stable over time, and Light's solution ($Fe(NH_4)(SO_4)_2$), which requires acidic conditions. Considering their standard redox potential, we also considered metal chloride salts such as $CuCl_2$/CuCl and $CrCl_3$/$CrCl_2$. However, CuCl has a poor solubility in water (K_{sp} of 1.72×10^{-7}), and Cr^{2+} is easily oxidized under ambient conditions, preventing their possible use.[157] After a thorough literature survey, we identified and synthesized both the reduced and oxidized species of cobalt(II/II)bis(terpyridine) chloride, as shown in Fig. 4-1 (see SI for detailed synthesis and cyclic voltammogram).[172]

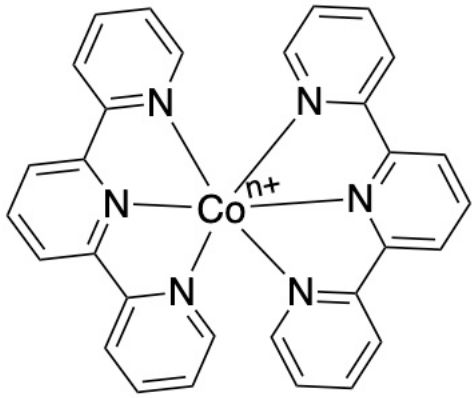

Figure 4-1. Structural formula of cobalt(II/III)bisterpyridine (n=2 or 3).

In contrast to previously introduced redox buffers that have been incorporated into an ion-selective membrane,[166–168] solid contact,[60,173] or hydrogel,[169] the present hydrophilic redox buffer is designed to be incorporated into the inner filling solution of an

ISE and to control the potential at the electron conductor/inner filling solution interface. The potential at the interface of the electron conductor and inner filling solution will depend on the ratio of the reduced to oxidized species present in the solution, as predicted by the Nernst equation, $E = E^0 - 58.2\ \text{mV} \log \frac{c_{red}}{c_{ox}}$, where c_{red} and c_{ox} represent the concentration of the reduced and oxidized species, respectively, and E^0 is the standard redox potential.[166] To confirm this relationship, solutions with c_{red}/c_{ox} of 1:1, 1:5, and 5:1, with a constant total concentration of 5 mM, were prepared. A Au wire was used as the working electrode and a capillary RE (AgCl/Ag, 3.0 M KCl inner filling solution) was used to accommodate small sample volumes (1.0 mL).[153] The EMF, which results from the sum of all of the phase boundary potentials across the system was then measured. The EMF of each solution was found to depend on log c_{red}/c_{ox}, with a slope of -56.9 ± 0.6 mV/decade (n=3) (Fig. 4-2C). This value agrees with the Nernst equation and confirms that the phase boundary potential at the interface of the Au wire and the solution is determined by the ratio of the reduced to oxidized species of the redox buffer, that is, the redox buffer serves its intended purpose.

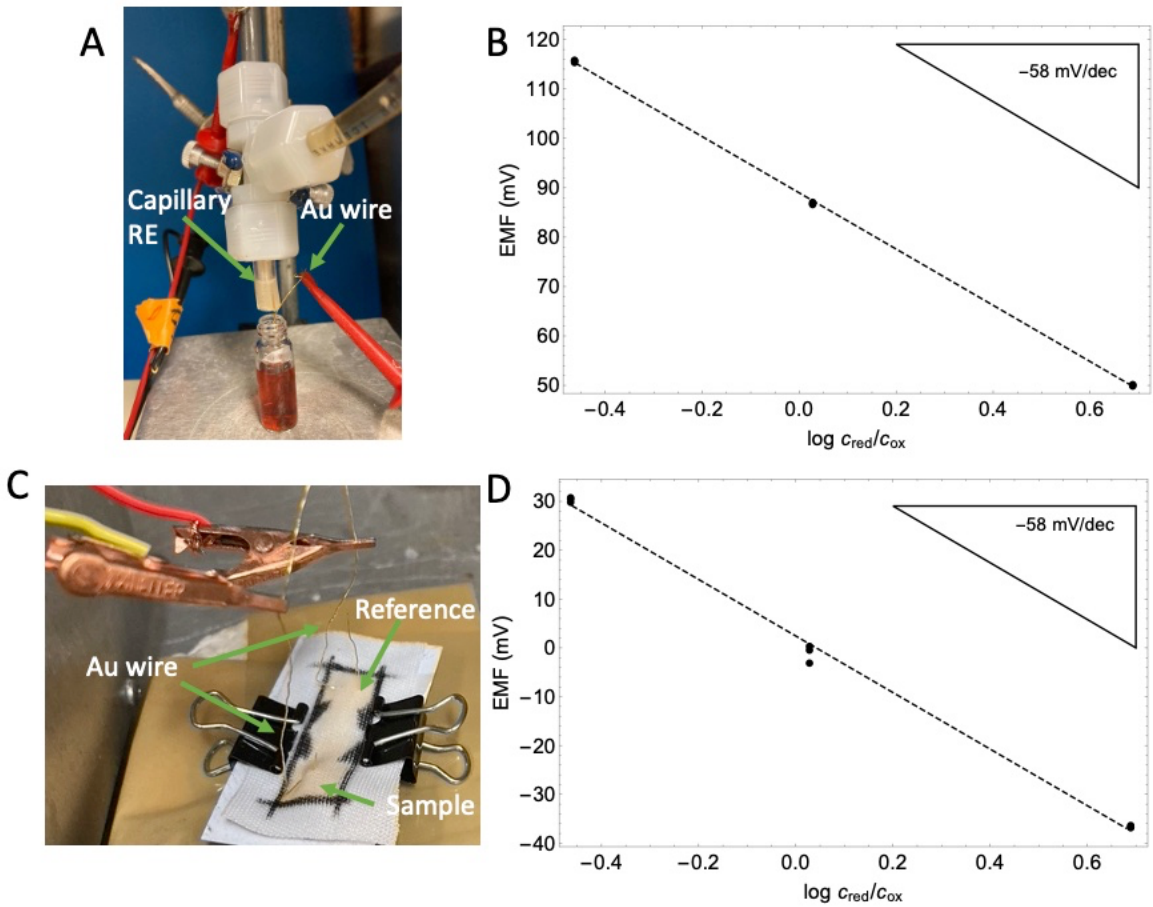

Figure 4-2. Photograph of conventional setup for measuring EMF dependence on ratio of Co(II)(terpyridine)$_2$ and Co(III)(terpyridine)$_2$ (A) and corresponding potentiometric response (B), photograph of textile-based sampling setup for measuring EMF dependence (C) and corresponding potentiometric response (D). A larger version of the photographs is available in Figure 4-S4.

Conventional Electrodes with Inner Filling Solutions Comprising Redox Buffer

Upon confirmation of the ability of the redox buffer to control the phase boundary potential at the interface to the inner reference electrode, the redox buffer was incorporated into the inner filling solution of electrodes with sensing membranes

comprising plasticized PVC as polymer matrix and tridodecylmethylammonium chloride as anion exchanger. In the first set of electrodes, such an anion exchange membrane was affixed to a Tygon tube, with an inner filling solution of 2.5 mM each of Co(II)(terpyridine)$_2$ chloride and Co(III)(terpyridine)$_2$ chloride as well as 1 mM KCl, and a Au wire as electron conductor. In this case, the phase boundary potential at the Au wire/inner filling solution interface is well controlled and the only sample dependent phase boundary potential of the electrochemical cell is the one between the sample and the ion-sensing membrane. Therefore, at room temperature the electrodes are expected to respond to the activity of Cl^- in the sample solutions according to the Nernst equation: $EMF = E^0 - 58.2\ \text{mV} \log a_{Cl^-}$.[7] Electrodes of this kind gave an experimental response slope of –59.9 ± 0.1 mV/decade, consistent with theory, and an E^0 of 12.9 ± 0.3 mV (n=5) (see Fig. 4-3). In contrast, electrodes with an inner filling solution of 1 mM KCl and a Ag/AgCl wire as transducer gave a SD of E^0 of 2.7 mV (n=5). The significant improvement in the SD of E^0 upon introduction of the redox buffer confirms the ability of the redox buffer to control the potential at the interface of the electron conductor and the inner filling solution.

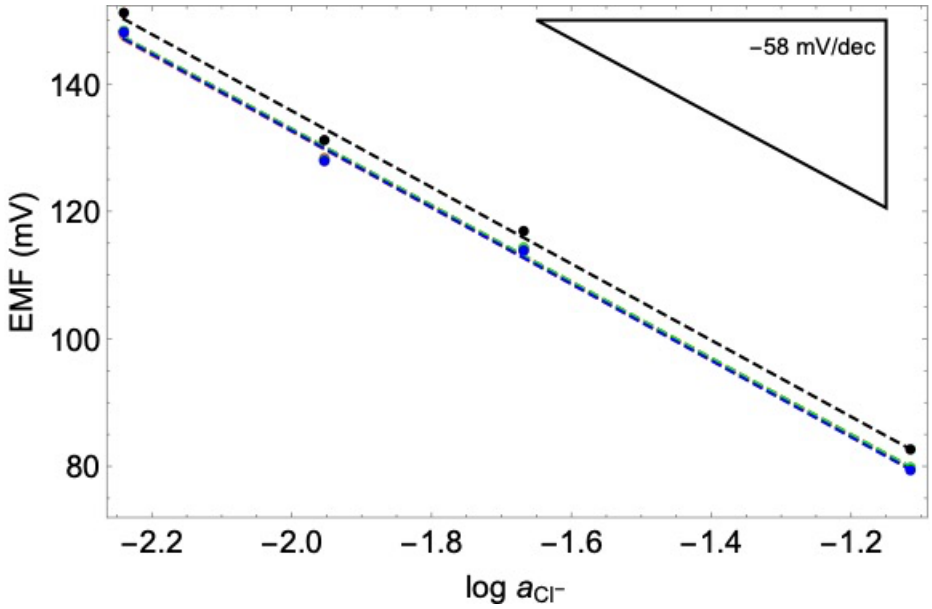

Figure 4-3. Potentiometric response of conventional electrodes comprised of a Cl^- ion-sensing membrane and with a redox buffer containing inner filling solution (n=5).

Keeping in mind the final goal of integrating this redox buffer into a planar design in which ionic-liquid-based RMs are used,[42,54,55] we also examined the compatibility of the proposed redox buffer with such RMs. For this purpose, an ionic-liquid-based RM was affixed to a Tygon tube with an aqueous inner filling solution comprising 2.5 mM each of Co(II)(terpyridine)$_2$ chloride and Co(III)(terpyridine)$_2$ chloride, 1 mM KCl, and the ionic liquid at saturation concentration, as well as a Au wire as electron conductor. In this case, the phase boundary potential at the sample/reference membrane interface is controlled by the partitioning of the ionic liquid between the two phases and does not depend on the sample composition. When measured with respect to a conventional reference electrode, the response slopes of this ionic-liquid-based reference electrode to any type of ion should be ideally 0 mV/decade. Electrodes of this kind resulted in a theoretically predicted

slope of 0.4 ± 0.1 mV/decade and an E^0 of –16.6 ± 1.9 mV (n=4) when tested in sample solutions of 0.01 to 85 mM KCl (See Figure 4-S4B). Analogous electrodes without the redox buffer but a chloride containing inner filling solution in contact to a Ag/AgCl wire as transducer exhibited a response of 0.2 ± 0.4 mV/decade and E^0 of 105.2 ± 10.0 mV (n=3) when tested in sample solutions of 0.01 to 85 mM KCl ((See Figure 4-S4A). With macrosized ionic-liquid-based reference membranes, a somewhat large E^0 standard deviation has also been observed before.[167] As with the chloride ion-sensing membrane, introduction of a redox buffer significantly improves reproducibility, as seen in the reduction of the SD of E^0.

Textile-Based Devices with Redox Buffer

The ability of the redox buffer to improve reproducibility in textile-based electrodes was also tested. As in conventional electrodes, initial experiments were designed to confirm the dependence of the potential at the Au/redox buffer solution interface on the ratio of reduced to oxidized species present. A dumbbell-shaped wax pattern was drawn onto rectangular pieces of a polyester textile to define separate sample and reference zones[49] and a Au wire was woven through as electron conductor (see Figure 4-S1B). For potentiometric measurements, 20 µL of a reference solution of 1:1 c_{red}/c_{ox} was applied to the reference zone while 20 µL of a sample solution was applied to the sample zone. The three sample solutions contained either 1:1, 1:5, or 5:1 c_{red}/c_{ox}, with a constant total concentration of 5 mM. In these devices, the only sample dependent phase boundary potential is that between the sample solution and the Au wire. The potentiometric response of electrodes of this kind is shown in Figure 4-2D; as these are single-use

sensors, each data point represents a separate device. The EMF of each solution was found to depend on log c_{red}/c_{ox}, with a slope of –57.9 ± 2.3 mV/decade (Fig. 4-2D), confirming the ability of the redox buffer to control the potential when the redox buffer solution is in direct contact with the textile of a textile-based sensor device.

The compatibility of textile-based devices with polymeric reference and ion-sensing membranes embedded into the polyester textile was also assessed, as previous work has shown that miniaturization of ISEs can result in performance limitations.[54,91] Initial experiments included devices containing a single membrane, either reference or ion-sensing to separate reference from sample zones. In exploring the compatibility of the redox buffer with ion-sensing membrane infused textiles, it was found that the phase boundary potential at the Au/redox buffer interface depends on the concentration of the KCl in solution. However, this relation does not affect performance of devices with both sensing and reference membranes and is therefore not a problem. Additionally, it was found that the RM contributed significant to irreproducibility of the textile-based devices, and optimization of membrane composition may improve results. The reader is directed to the SI for a full discussion of results of this work.

Returning to the double membrane design introduced previously for both paper and textile-based sensors (shown in Fig. 4-4A),[54,55] the reference solutions in contact with the Au wire contain 100 mM KCl, and 2.5 mM each of Co(II)(terpyridine)$_2$ chloride and Co(III)(terpyridine)$_2$ chloride, while the sample solutions with varying amounts of KCl are only in contact with the sensing and the reference membrane but not the inner electrodes. Therefore, theory suggests that the only sample dependent phase boundary potential to

be that between the sensing membrane and the sample, resulting in a slope of –59 mV/decade. Indeed, devices of this kind gave a within error Nernstian slope of –58.5 ± 5.2 mV/decade (E^0 of –38.0 ± 10.7 mV), and a lower LOD of $10^{-3.0 \pm 0.6}$ M Cl^-. Unfortunately, the improved reproducibility in E^0 observed for conventional electrodes with an inner filling solution containing the hydrophilic Co(II/III)bis(terpyridine) buffer did not translate to this final textile-based device. One possible explanation for this is a poorer half-cell potential of the ionic-liquid-based RM when combined with a textile device (see SI for data). Future work will therefore explore the effect and further optimization of the reference membrane composition.

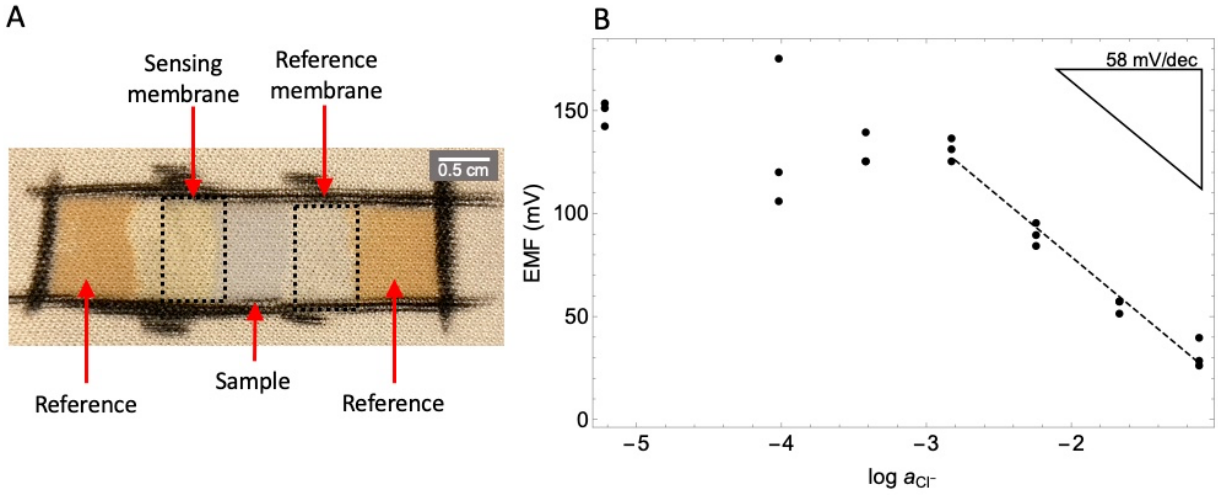

Figure 4-4. Labelled photograph of textile-based device with reference and sensing membrane (A) and potentiometric response to solutions of varying concentration of Cl^- (B).

CONCLUSIONS

While redox buffers have long been used in chemical biology and as standards for

redox probe calibration solutions, there has been no hydrophilic redox buffer based on cationic or electrically neutral redox-active species that can be used for the fabrication of anion-selective ISEs. To address the need for such a redox buffer, we showed here that cobalt(II/II)bisterpyridine chloride is a promising candidate for a redox buffer in anion sensing ISEs to improve reproducibility. The complex is obtained through a single step synthesis with minimal purification and is stable in both the reduced and oxidized forms. When incorporated into the inner filling solution of conventional Cl^- ISEs, the redox buffer reduces the E^0 SD from to 2.7 to 0.3 mV. The complex is also shown to be compatible with ionic liquid-based RMs and textile-based platforms. While current results show the improvements in reproducibility do not translate to textile-based devices that contain both sensing and reference membranes, future work will address this final step. This complex may also find use as an alternative to unstable calibration solutions and other applications of redox buffers.

SUPPORTING INFORMATION

Materials

Reagents were purchased from the following sources: methanol, isopropyl alcohol, hexanes, Dowex 1 x 8-100 Ion Exchange Resin, ammonium tetrakis(3-chlorophenyl)borate, and tetraoctylammonium bromide from Sigma (St. Louis, MO, USA); terpyridine (2,2′:6′,2″-terpyridine) from Fisher Scientific (Pittsburg, PA, USA), glassy carbon electrodes and gold disk electrodes (2 mm diameter; embedded into an inert Kel-F polymer shaft) from CH Instruments (Austin, TX, USA); Fumion FAA-3 ionomer anion exchanger from FuMA-Tech GmbH (Bietigheim-Bissingen, Germany).

Synthesis of Co(II)(terpyridine)$_2$ Chloride

The synthesis of this compound was performed by modification of a literature procedure.[170] 55.7 mg of $CoCl_2$•$6H_2O$ (1 equiv.) and 119.5 mg of terpyridine (2.2 equiv.) were dissolved in 15 mL methanol, and the resulting solution was refluxed for 3 h and then stirred at room temperature overnight. After the evaporation of methanol, the product was washed three times with hexanes to remove any unreacted terpyridine. After the evaporation of the hexanes, the product was analyzed with ^{1}H NMR spectroscopy (see Figure 4-S1). The peaks at 7.40-9.15 ppm are the aromatic hydrogens of the terpyridine complex.

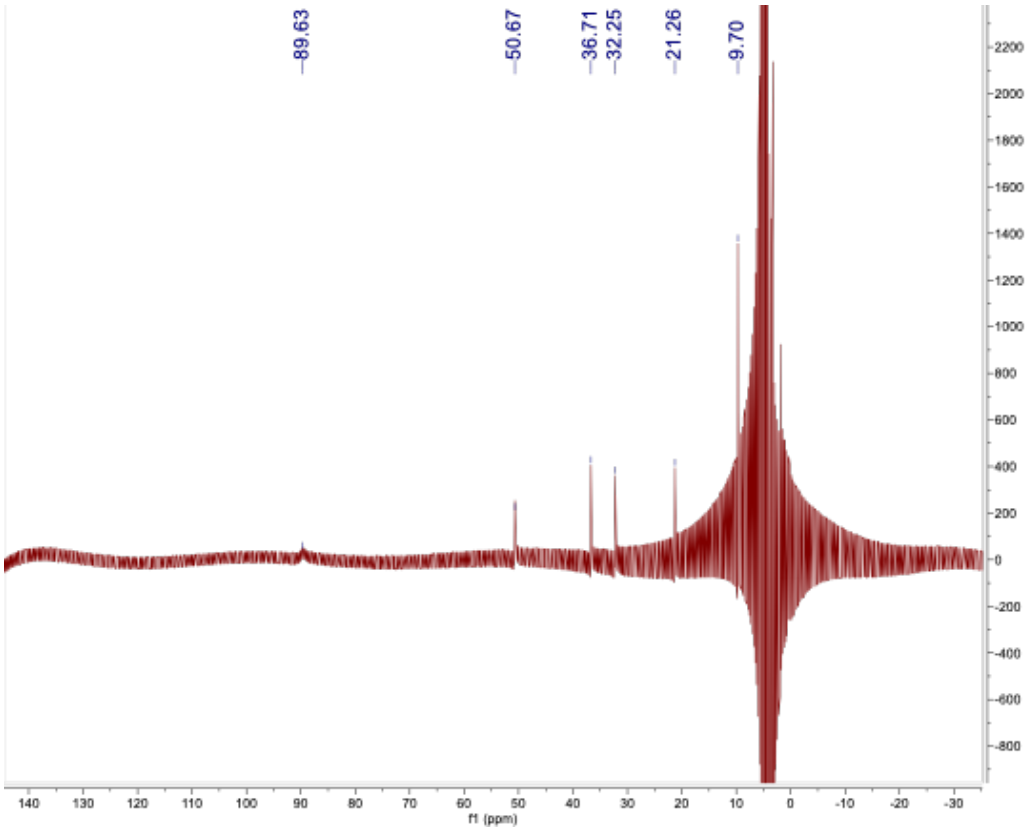

Figure 4-S1. ^{1}H NMR spectrum of Co(II)(terpyridine)$_2$ chloride in D_2O.

Synthesis of Co(III)(terpyridine)$_2$ Chloride

55.5 mg of $CoCl_2$•$6H_2O$ (1 equiv.), 118.63 mg of terpyridine (2.2 equiv.) and 6.0 µL Br_2 (1. equiv.) were dissolved in 15 mL methanol, and the resulting solution was refluxed for 3 h and then stirred at room temperature overnight. An ion exchange was performed with Dowex 1 x 8-100 Ion Exchange Resin Cl^- loaded resin to exchange the Br^- counter ions for Cl^-. After evaporation of methanol, the product was washed three times with hexanes to remove any unreacted terpyridine. After the evaporation of the hexanes, the product was analyzed with ^{1}H NMR spectroscopy (see Figure 4-S2).

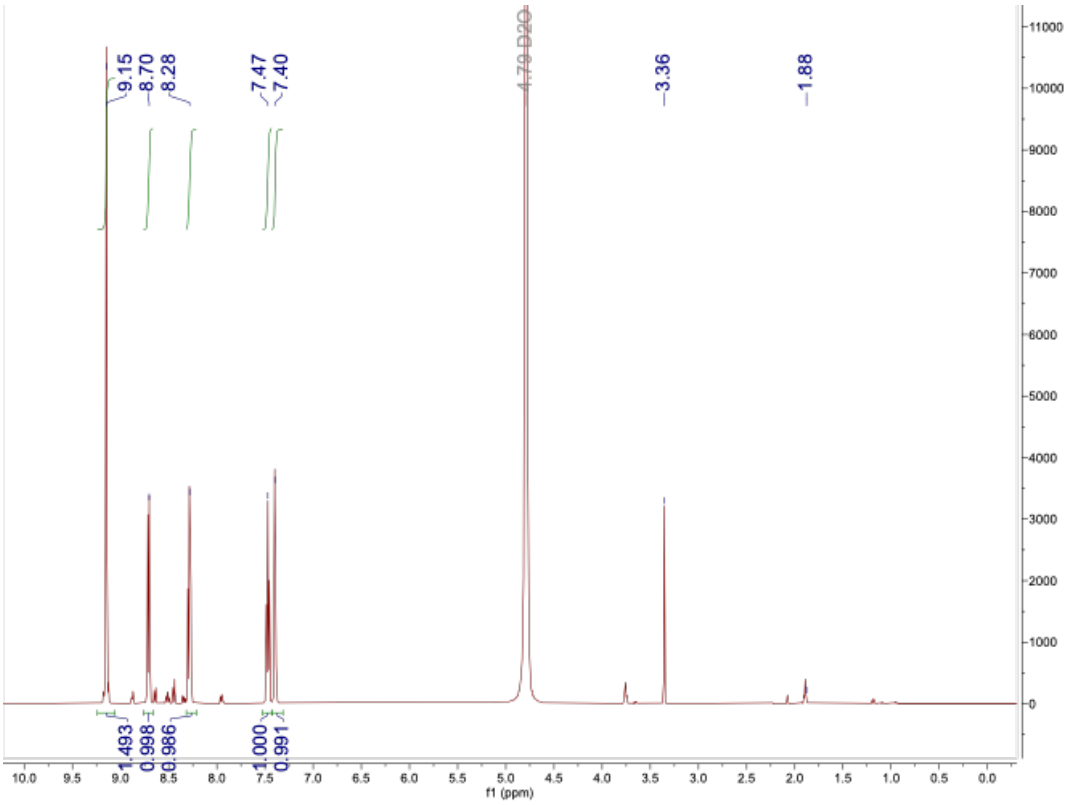

Figure 4-S2. ^{1}H NMR spectrum of Co(III)(terpyridine)$_2$ chloride in D_2O.

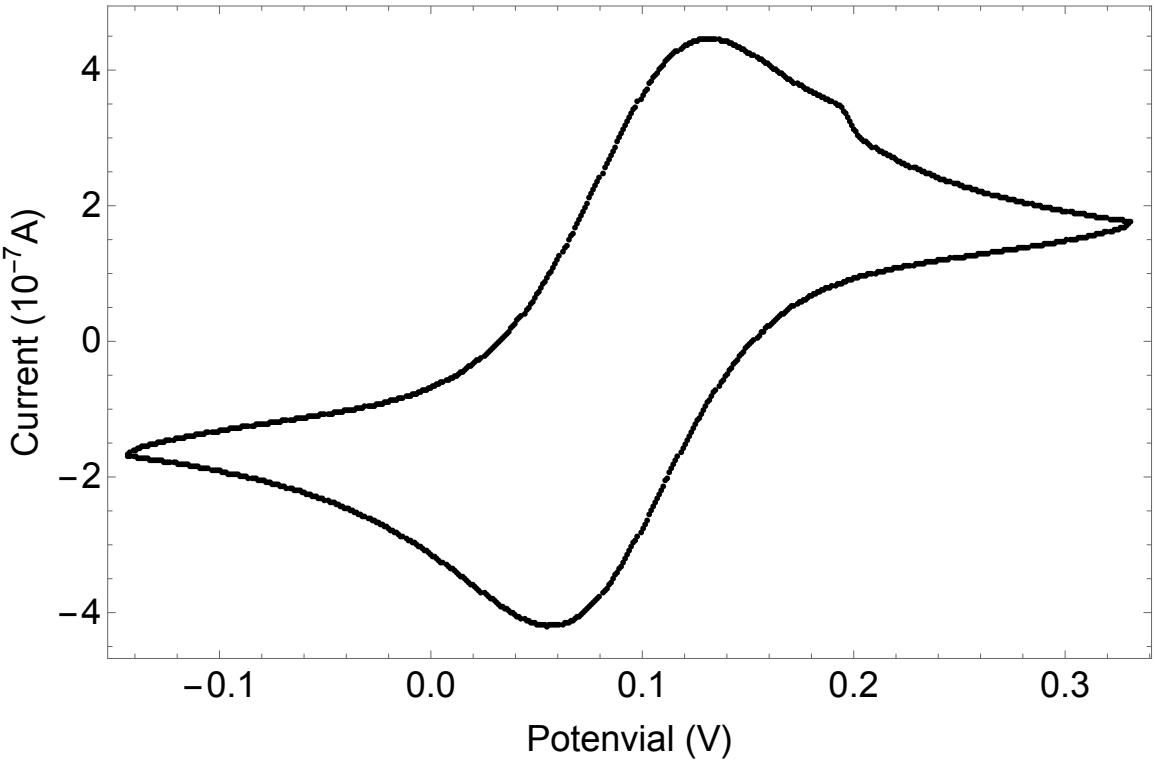

Figure 4-S3. Cyclic voltammogram of an aqueous solution containing 2.5 mM Co(II)(terpyridine)$_2$Cl$_2$, 2.5 mM Co(II)(terpyridine)$_2$Cl$_3$, and 100 mM KCl, using a AgCl/Ag wire in 3 M mM KCl saturated with AgCl solution as the reference electrode (with a porous glass junction), a platinum wire as the counter electrode, and a glassy carbon disc as the working electrode. Scan rate 0.1 V/s.

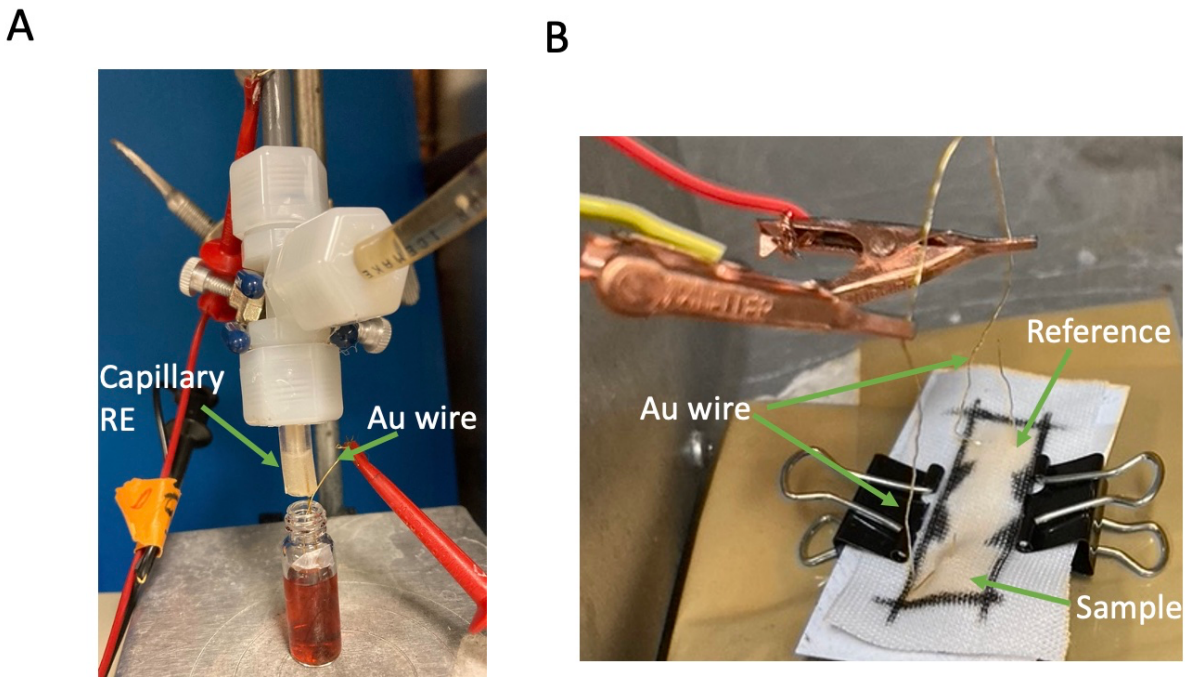

Figure 4-S4. Larger version of the Figure 1 of the main text. Photograph of setups for membrane-free devices in a glass vial (A) and on a textile platform (B).

Fabrication of Single-Membrane Textile-Based Devices

Microfluidic zone barriers, polymeric membrane coated textile and conductive strips were fabricated according to the same procedure used for textile-based electrodes with two membranes to define sample and refence zones, as described in the main section of the manuscript. Two 2 mm gold disk electrodes were used as electrical contacts; they were placed on top of the sample and reference zones and clamped into place. Two alligator clips were used to connect the device to the voltmeter, and all devices were placed on top of a sheet of PVC and held in place with binder clips for stability (see Fig 4-S5).

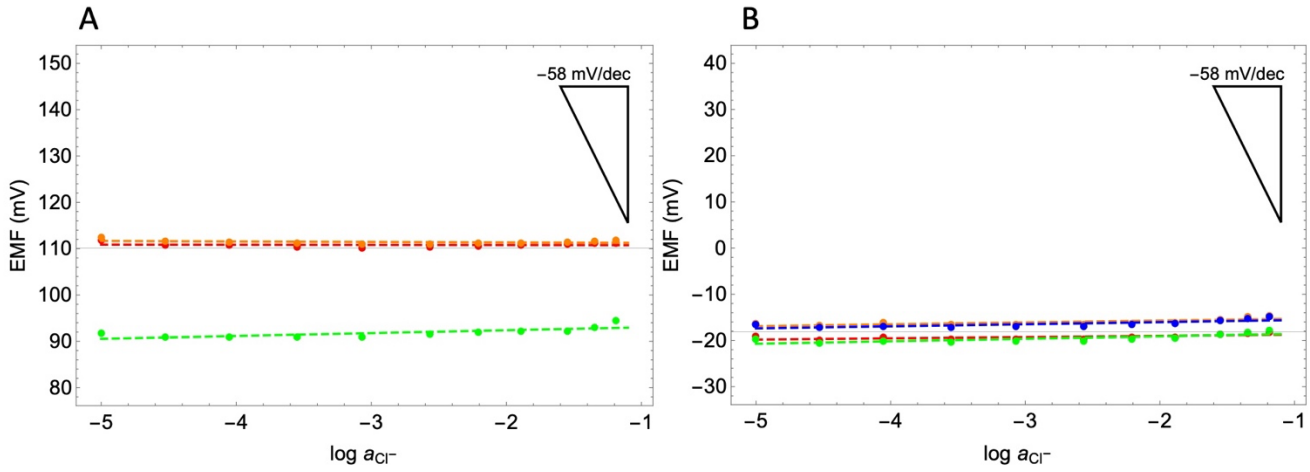

Figure 4-S5. Potentiometric response of conventional electrodes composed of an ionic liquid-based reference membrane and an inner-filling solution without a redox buffer (n=3) (A) and with a redox buffer (n=4) (B).

Before use, the gold disk electrodes were polished over polishing cloths with aqueous dispersions of alumina (0.3 and 0.05 μm, Buehler, Lake Bluff, IL, USA). They were then cleaned in piranha solution (concentrated sulfuric acid and 30% hydrogen peroxide solution in a 3:1 ratio). *Caution: piranha solution is a strong oxidizing reagent, is highly corrosive, and should be handled with care.* The electrodes were then cleaned by ultrasonication in water and ethanol and dried with a flow of nitrogen.

Performance of Single-Membrane Textile-Based Devices with Redox Buffer

To evaluate the compatibility of the ion-sensing membrane integrated into the textile along with the aqueous redox buffer, we fabricated devices with an ion-sensing membrane to define sample and reference zones (Fig. 4-S5). Solutions that contained

100 mM KCl were used as the reference solutions, while the concentration of KCl in the sample solutions was varied. For this particular test, both types of solutions also contained a constant background of 2.5 mM of Co(II)(terpyridine)$_2$ chloride and 2.5 mM Co(III)(terpyridine)$_2$ chloride. In this configuration, the only phase boundary potential that is expected to change is the one between the sample solution and the ion-sensing membrane; a response slope of –59.2 mV/decade to the chloride activity in the sample solution is expected. However, the devices responded in a sub-Nernstian manner, with a slope of 44.6 ± 4.1 mV/decade and an E^0 of 45.7 ± 6.9 mV. Several hypotheses were proposed to explain this non-ideal response slope, including a high resistance of ion-sensing membranes, the partitioning of the redox buffer into the sensing membrane, and finally a dependence of the Au/sample potential on the ionic strength of the solution. We tested each hypothesis and report the results below.

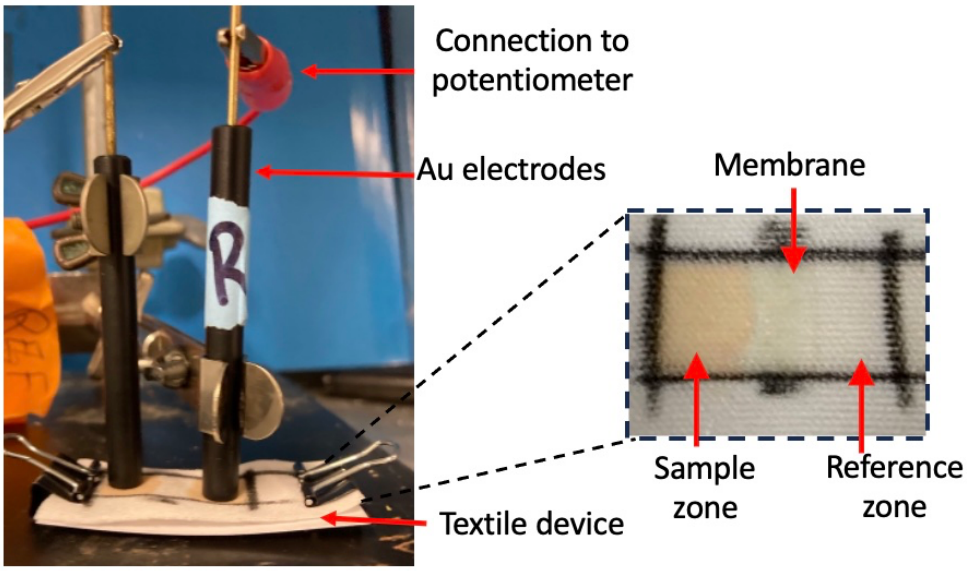

Figure 4-S6. Photograph of setup for a textile-based device with a single membrane, and solution deposited into the sample zone to highlight sample containment by the sensing membrane and the wax pencil barriers.

Previous work in our group showed that the addition of 20 wt % of an inert electrolyte, tetradodecylammonium tetrakis(4-chlorophenyl)borate (ETH 500), to a K^+ ion selective membrane integrated into a paper-based device improved a sub-Nernstian slope in K^+ sensing, an effect thought to be possibly due to a reduction in the resistance of devices.[54] This compound is, however, expensive ($273/g at Sigma on Aug 23 2023), especially when used in high amounts. We therefore performed an ion exchange from two less expensive salts, ammonium tetrakis(3-chlorophenyl)borate and tetraoctylammonium bromide, to obtain an analogous inert electrolyte, tetraoctylammonium tetrakis(3-chlorophenyl)borate. 95.70 mg of ammonium tetrakis(3-

chlorophenyl)borate and 135.24 mg of tetraoctylammonium bromide were separately dissolved in isopropyl alcohol. Upon mixing of the solutions, a white precipitate immediately formed. This precipitate was filtered off, washed three times with methanol and vacuum dried overnight. After the evaporation of the methanol, the product was analyzed with ^{1}H NMR spectroscopy (see Figure 4-S6). Devices fabricated with 20 wt% tetraoctylammonium tetrakis(3-chlorophenyl)borate in the sensing membrane still resulted in a sub-Nernstian slope of 49.1 ± 4.2 mV/ decade (E^0 of 55.8 ± 7.0 mV). Interestingly, the resistance of devices remained within error of each other 17.9 ± 7.0 MΩ for salt-free membranes and 31.0 ± 9.70 MΩ for 20 wt% salt containing membranes.

We also tested single-membrane devices with Fumion FAA-3 ionomer, a polyether ether ketone based hydrophilic high capacity anion exchange membrane known to suffer less from interferences caused by lipophilic ions.[132,133] The membrane was previously used in both paper and textile-based chloride ISEs and was prepared according to the reported methodology.[54,55] However, devices with the hydrophilic anion exchange membrane also resulted in a sub-Nernstian slope of –41.8 ± 4.7 mV/decade (E^0 of 44.8 ± 7.8 mV), indicating that the low slope was not due to the hydrophilic redox buffer partitioning into the sensing membrane.

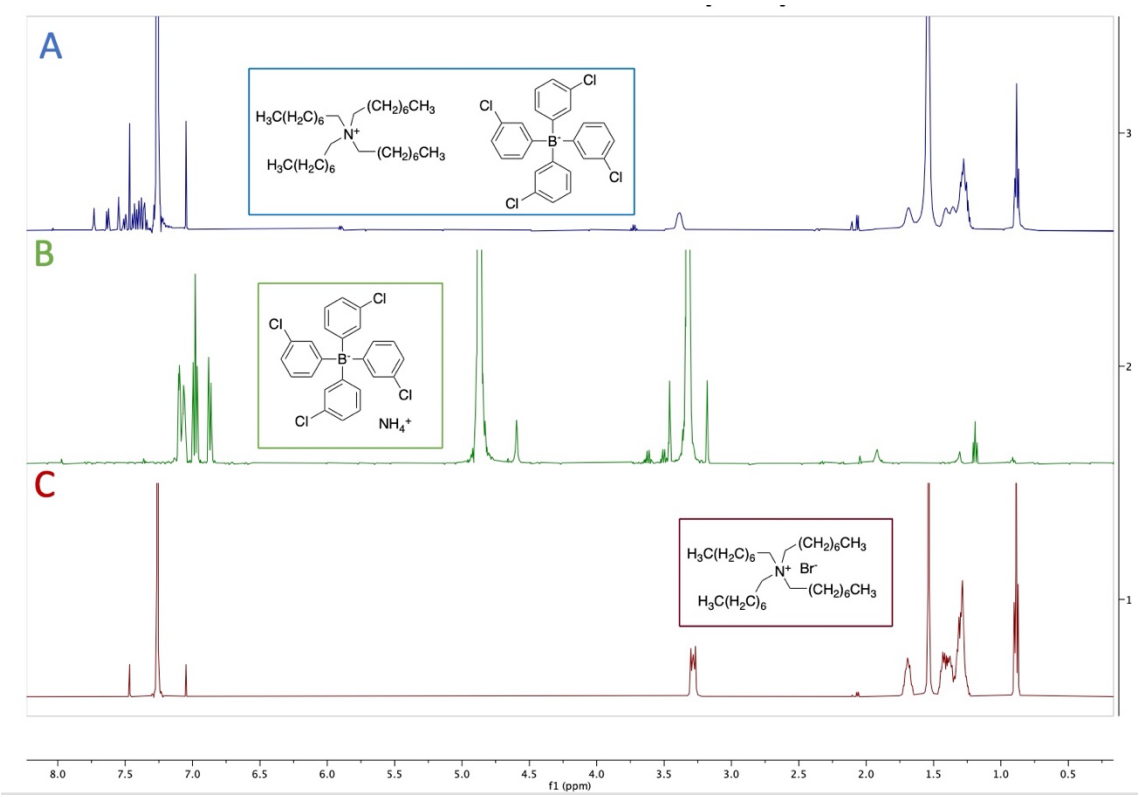

Figure 4-S7. ^{1}H NMR of tetraoctylammonium tetrakis(3-chlorophenyl)borate in CDCl3 (A), ammonium tetrakis(3-chlorophenyl)borate in MeOD (B), and tetraoctylammonium bromide in CDCl3 (C).

At this point, we hypothesized that the KCl in the solution might be affecting the activity of the redox buffer ions and, consequently, the potential at the Au/redox buffer interface. To test this hypothesis, we fabricated membrane-free devices (see Fig. 4-S4B) and tested with a reference solution comprising 100 mM KCl, 2.5 mM Co(II)(terpyridine)$_2$ chloride, and 2.5 mM Co (III)(terpyridine)$_2$ chloride. The sample solutions contained a constant 2.5 mM each of Co(II)(terpyridine)$_2$ chloride and Co (III)(terpyridine)$_2$ and a varying concentration of KCl. In this configuration, the potential at the Au/solution interface

should again be constant as both the reference and sample solutions contained a constant 1:1 ratio of the oxidized and reduced cobalt complex. The EMF values were corrected for liquid-junction potentials at the interface of the two solutions with the Henderson equation. Therefore, the potential was expected to be independent of the Cl^- concentration in the samples. Surprisingly, devices with this setup responded to changes in Cl with a slope of –22.5 ± 3.9 mV/decade, suggesting that the Au/solution interface is not independent of the Cl^- concentration.

In order to test this new hypothesis, we conducted an experiment in which the potential of a sample of 2.5 mM each of Co(II)(terpyridine)$_2$ chloride and Co(III)(terpyridine)$_2$ was monitored while spiking with a stock solution comprising 1 M KCl, 2.5 mM Co(II)(terpyridine)$_2$ chloride, and 2.5 mM Co(III)(terpyridine)$_2$ chloride. A Au wire was used as the working electrode along with a capillary-based reference electrode (3 M KCl).[153] A slope of –17.3 ± 0.8 mV/decade was obtained, confirming that the potential at the Au/sample interface depended on the concentration of the KCl even when a setup without textile was used. It may be that the potential of the redox buffer depends on the ionic strength of the solution, which is related to the concentration of KCl. In considering the final design of textile-based electrodes (Fig. 4-5), however, the only solution in contact with the Au wire is the reference solution, which contains a constant composition of 100 mM KCl. Therefore, although the potential at the Au/sample interface depends upon the concentration of KCl in the reference solution, that does not preclude the use of the redox buffer in a device with both a reference and a sensing membrane.

To evaluate the use of a [$C_{12}mim^+$][$C_1C_1N^-$] ionic liquid-based reference membrane,

we performed analogous experiments as for the initial type of tests that evaluated membrane-free textile-based devices. Briefly, 20 µL of a reference solution containing the oxidized and reduced form of the redox buffer in a 1:1 concentration ratio was applied to the reference zone while 20 µL of a sample solution of varying ratios of c_{red}/c_{ox} was applied to the sample zone. Again, the only phase boundary potential that was expected to be sample-dependent was the one between the sample solution and the Au wire. Experimentally, the potentiometric response depended on log c_{red}/c_{ox}, with a slope of –67.8 ± 8.5 mV/decade, confirming a Nernstian dependence of the phase boundary potential at the Au/solution interface and a sample-independent potential at the reference membrane/sample interface. Next, we varied the concentration of KCl in the sample solution, maintaining a constant background of 2.5 mM each of Co(II)(terpyridine)$_2$ chloride and Co(III)(terpyridine)$_2$ chloride. In this setup, we expected the potential to remain constant as the reference membrane should not respond to changes in the sample composition and the Au/solution interface is controlled by a constant background of redox buffer. These devices gave a slope of 5.6 ± 12.9 mV/decade (E^0 of 10.7 ± 18.2 mV). While the standard deviation in this result is larger than desired, the observed slope was within error consistent with the expected outcome. Analogous textile-based devices without redox buffer added to the sample and reference solutions, and with Ag/AgCl ink as a transducer resulted in a chloride response with a slope of –61.2 ± 5.1 mV/decade (E^0 of –67.1 ± 10.5 mV), again consistent with the expected Nernstian response. The increase in standard deviation of E^0 upon use of an ionic liquid-based reference membrane is a concern. Future work will explore how to optimize the composition of the ionic liquid

membrane to improve reproducibility.

Chapter 5. Textile-Based Potentiometric Devices with Ionophore Containing Sensing Membranes

Eliza Herrero and Philippe Bühlmann

PREFACE

The incorporation of ionophores into polymeric membranes gives ion-selective electrodes (ISEs) their characteristic high selectivity even in samples with complex matrices. While the Bühlmann group has shown that ionophore-free sensing membranes maintain Nernstian slopes when embedded in both paper- and textile-based devices, the incorporation of ionophores into sensing membranes in the same style of devices results in poor linearity, reproducibility, and non-theoretical response slopes. In this chapter we describe the testing of several hypotheses on the source of the sub-optimal performance, particularly, interactions between ion-selective membrane (ISM) components and the underlying textile material. To understand the scope of such interferences, we also report on textile-based ISEs with membranes doped with various ionophores targeting both monovalent and divalent cations.

INTRODUCTION

The selectivity of an ISE is achieved through the inclusion of ionophores and ionic sites in the polymeric membrane.[7] An ionophore, often an organic molecule, selectively interacts with the target ion and thereby facilitates the phase transfer of the ion from the sample solution to the membrane (Fig. 5-1). These target ion–ionophore interactions can

vary; the K^+ ionophore valinomycin is a cyclic oligopeptide which forms a pocket just the size of K^+ and binds through carbonyl groups, another K^+ ionophore 2-dodecyl-2-methyl-1,3-propanediyl bis[*N*-[5′-nitro(benzo-15-crown-5)-4′-yl]carbamate] (BME-44) forms a pocket with 2 crown ethers groups, the long chain proton ionophore tridodecylamine (TDA) binds H^+, and the Ca^{2+} ionophore *N*,*N*-dicyclohexyl-*N*′,*N*′-dioctadecyl-3-oxapentanediamide (ETH 5234) binds Ca^{2+} in a 2:1 ratio through the carbonyl units in a noncyclic backbone.[100] Ionic sites, highly hydrophobic ions of charge opposite of the target ion, must also be present in an ISM when using a neutral ionophore to maintain a constant concentration of the target ion in the membrane. In contrast, when using charged ionophores, ionic sites are not necessary but can improve the selectivity; if included, the optimum concentration depends on the charge of both the ionophore and the target ion.[7] However, the use of ionic sites may improve the selectivity of the membrane and is still encouraged.[7,174] Finally, a membrane phase that dissolves both components is used, commonly poly(vinyl chloride) (PVC) with a plasticizer such as *ortho*-nitrophenyl octyl

ether (*o*-NPOE) or bis(2-ethylhexyl) sebacate (DOS).

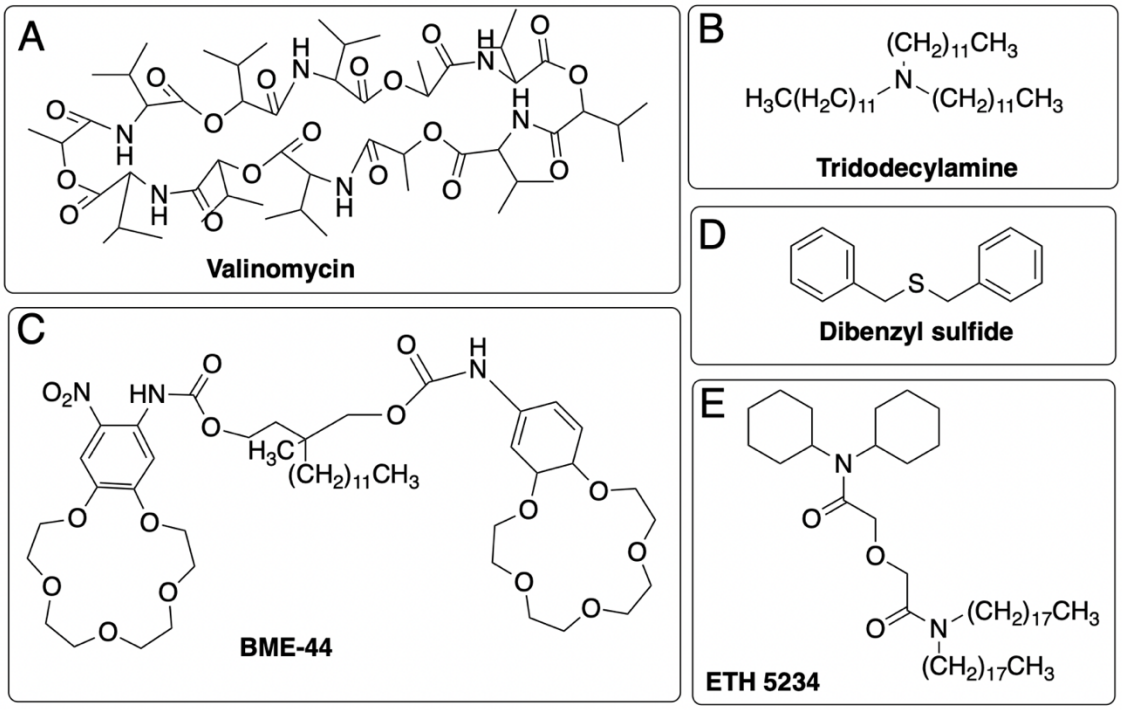

Figure 5-1. Common ionophores used in ISEs: (A) valinomycin for K^+, (B) TDA for pH, (C) BME-44 for K^+, and (D) ETH 5234 for Ca^{2+}.

To optimize selectivity, ideal ratios of the concentration of ionic site to ionophore in the membrane must be used. The proper ratio for the systems used in this section will ideally leave free ionophore in the presence of target ions but no free ionophore in the presence of interfering ions.[7] This ratio is determined by three factors: the charge of the interfering and target ions, the charge of the ionophore, and the stoichiometry of the complex formed with each ion.[174]

The incorporation of ionophores into planar ISEs often results in non-ideal performance, including poor linearity, sub-Nernstian slopes, and poor reproducibility. With

a sandwich-type ISE setup in which a free-standing ionophore-containing ISM was placed between two pieces of filter paper, sub-Nernstian slopes were observed for both mono- and di-valent cations (54.9 ± 0.6, 54.8 ± 1, and 22.9 ± 0.8 mV/decade for K^+, Na^+, and Ca^{2+}, respectively. In contrast, a Nernstian response (–61.8 ± 1.0 mV/decade) was obtained with a membrane-free Cl^- sensing system on the same kind of filter paper.[22] However, comparing these two sets of devices, one cannot confirm if the sub-Nernstian response was due to either the ISM/filter paper interface or the charge sign of the analyte, especially given previous work confirming cation adsorption onto filter paper.[27,30,81,110]

For another miniaturized ISE, filter paper was coated with polystyrene sulfonate doped poly(3,4-ethylenedioxythiophene), followed by graphene and finally an ionophore-containing ISM. The reference electrode (RE) consisted of a AgCl/Ag contact, reference membrane (RM), and dried KCl, which, upon contact with sample solution, dissolves to form a salt bridge. While Nernstian response slopes of 62.5 and 62.9 mV/decade were observed for Na^+ and K^+, respectively,[61] it is unclear if the liquid junction potential at the interface of the sample and salt bridge was accounted for, which would affect the response slope.

In a paper-based K^+ ISE with both reference and ion-selective membranes integrated into the filter paper, a poorly linear and sub-Nernstian response of 48.8 mV/decade was observed and improved to 53.3 mV/decade by the addition of 20 wt.% tetradodecylammonium tetrakis(4-chlorophenyl)borate (ETH 500), an inert hydrophobic electrolyte.[54] While ETH 500 is occasionally used to lower the resistance of ISE membranes, it is often used in less than 5 wt. % amounts.[175] Nevertheless, the resistance

of these filter paper based sensors decreased by less than an order of magnitude (from 10.9 ± 1.2 MΩ to 4.4 ± 0.8 MΩ).[54] Why ETH 500 had a favorable effect on the response slope for these paper based devices remained somewhat unclear. Another miniaturized K^+ ISE with a valinomycin-containing ISM was reported in which conductive strips of carbon ink were screen printed onto a polyethylene terephthalate (PET) substrate, followed by a solid contact of single-wall carbon nanotubes functionalized with octadecylamine groups, and finally coated by drop casting with ion-selective and reference membranes. In this device both membranes were made of photo-cured poly(*n*-butyl acrylate), and the K^+ ISM contained 1 wt % ETH 500 in addition to the ionophore and ionic site. When dipped into a beaker of sample solution, the device gave a Nernstian slope of 57.2 ± 1.2 mV/decade versus a conventional RE and a slope of 57.4 ± 1.3 mV/decade versus the integrated solid-contact RE.[25] The disparity in response slopes for the valinomycin-based K^+ ISEs with different designs highlights the effect device design has on the performance of miniaturized ISEs with ionophore-containing ISMs.

The following section describes a thorough study of the effects of incorporation of ionophores into textile-based ISEs and various efforts to improve performance. In particular, we studied the ionophores valinomycin and BME-44 for K^+ sensing, TDA for pH sensing, ETH 5234 for Ca^{2+} sensing, dibenzyl sulfide for Ag^+ sensing, and heptyl 4-trifluoroacetylbenzoate (ETH 6010) for CO_3^{2-} sensing.

EXPERIMENTAL METHODS

Materials

Reagents were purchased from the following sources: inhibitor-free anhydrous tetrahydrofuran (THF), methanol, valinomycin, BME-44, ETH 6010, DOS, potassium tetrakis(4-chlorophenyl)borate (KTpClPB), ETH 500, ammonium tetrakis(3-chlorophenyl)borate (NH_4T3ClPB), potassium chloride, sodium chloride, calcium chloride, sodium hydroxide, silver nitrate, 1,3,5-tribromobenzene, trifluoroacetic acid, and tridodecylmethylammonium chloride (TDDMACl) from Sigma-Aldrich (St. Louis, MO, USA); TDA from TCI chemical; lithium tetrakis(pentafluorophenyl)borate ethyl etherate (LiTPFPB) from Gelest; benzylsulfide from Acros Organics; 1-methyl-3-octylimidazolium bis(trifluoromethylsulfonyl)imide ($[C_8min^+][C_1C_1N^-]$) from IoLiTec (Tuscaloosa, AL, USA); high molecular weight poly(vinyl chloride) (PVC), *o*-NPOE, and ETH-5234 from Fluka (Buchs, Switzerland); Ag/AgCl ink (AGCL-675; consisting according to the material data safety sheet of 40–60% silver, 10–25% silver chloride, 25–50% γ-butyrolactone, and 5–15% urethane acrylate oligomer) from Nayaku Advanced Materials (Westborough, MA, USA); and Polx1200 polyester continuous knit filament cleanroom wipes from Berkshire Corporation (Great Barrington, MA, USA). Deionized water was purified to a resistivity of 18.2 MΩ cm with a Milli-Q PLUS reagent-grade water system (Millipore, Bedford, MA, USA).

Precursor Solutions for the Preparation of Sensor and Reference Membranes

Cl^- sensing membranes were prepared by dissolving PVC (90.0 mg), *o*-NPOE (180.0 mg), and TDDMACl (15.0 mg) in 1.5 mL THF, unless otherwise stated. K^+ selective

membranes with the ionophore valinomycin were prepared by dissolving PVC (66.0 mg), *o*-NPOE (132.0 mg), valinomycin (5.0 mg), KTpClPB (1.8 mg), and ETH 500 (50.0 mg) in THF (1 mL). K^+ selective membrane cocktails with the ionophore BME-44 were prepared by dissolving PVC (78.0 mg), DOS (158.0 mg), BME-44 (2.4 mg), and NH_4T3ClPB (0.8 mg) in THF (1 mL). H^+ selective membrane cocktails were prepared by dissolving PVC (66.0 mg), DOS (132.0 mg), TDA (2.0 mg), and KTpClPB (1.2 mg) in THF (1 mL). Ca^{2+} selective membrane cocktails were prepared by dissolving PVC (66.0 mg), *o*-NPOE (132.0 mg), ETH5234 (2.6 mg), and LiTPFPB (1.2 mg) in THF (1 mL). Ag^+ selective membrane cocktails were prepared by dissolving PVC (66 mg), DOS (132 mg), dibenzyl sulfide (2.2 mg), and KTpClPB (0.7 mg) in THF (1mL). CO_3^{2-} selective membrane cocktails were prepared by dissolving PVC (66 mg), DOS (132 mg), ETH6010 (2.7 mg), and TDDMACl (4.9 mg) in THF (1 mL). RM cocktails were prepared by dissolving PVC (60.0 mg), *o*-NPOE (60.0 mg), and the ionic liquid $[C_8min^+][C_1C_1N^-]$ (30.0 mg) in THF (1 mL), as previously reported.[54]

For pH-sensing devices, the pH-selective membrane cocktail was drop cast into a glass petri dish on Day 1, removed from the dish and placed, intact, in a 10 mM pH 7 phosphate buffer on Day 2, and removed from this conditioning solution, rinsed with H_2O, and re-dissolved in 1 mL THF on Day 3 for spotting onto textile. The same method was used for conditioning of the K^+ ISM with BME-44 in a 10 mM KCl solution and the Ca^{2+} ISM in 10 mM $CaCl_2$.

Fabrication of Textile-Based Sensors

Microfluidic zone barriers were hand drawn in matching patterns on both sides of

the textile using a Sharpie Peel-Off China Marker in either extended dog bone or rectangular shapes (Fig. 5-2). For each of the two electrical connections, Ag/AgCl ink was applied to one side of the textile using a rubber tipped paintbrush (Royal Sovereign Ltd, UK) to achieve uniform coverage. This was followed by curing for 10 min at 100 °C.

Membranes were deposited onto Polx1200 in 3 cycles of 7 µL of the cocktail solution, deposited on each side, with 10 min between cycles, for a total of 3 cycles, as previously reported.[55] For initial experiments with ISM infused Polx1200, a circle was drawn with the Sharpie Peel-Off China Marker on the Polx1200 to define the infused region and the deposition volume was increased to 30 µL for the above method of 3 cycles with 10 min between cycles. This coated Polx1200 was allowed to dry overnight and then incorporated into a an in-house ISE body.[135]

For all beaker-based experiments, a double-junction type external reference electrode (DX200, Mettler Toledo, Switzerland; 3.0 M KCl saturated with AgCl as inner filling solution and 1.0 M LiOAc as bridge electrolyte) was used.

Selectivity

Selectivity was measured using the fixed interference method and calculated according to the equation $log\ K^{pot}_{K^+,Na^+} = \frac{\log\ a_{Na^+}}{\log a_{K^+}}$, where a_{Na^+} and a_{K^+} represent the activity of the interfering ion Na^+ and the activity of the primary ion K^+ at the lower limit of detection (LOD) in the presence of the interfering ion, respectively.[176] A constant background of 100 mM NaCl as interfering electrolyte was used and the electrode was stored in 10 mM KCl between measurements.

Optimization of Infusion of Polx1200 with Membrane

Several different methods were attempted to optimize infusion of Polx1200 with membrane components and completely fill all gaps in the textile. For initial experiments in optimizing membrane coatings of Polx1200, a Tygon tube based electrode was used. The first set of membrane cocktails were prepared by dissolving 15 mg (5 wt.%) TDDMACl, 90 mg (32 wt. %) PVC, and 180 mg (63 wt. %) *o*-NPOE in 1.5 mL THF. Given a measured textile thickness of 0.047 cm, the total void volume of a 3 × 3 cm^2 square of Polx1200 was calculated as 0.309 cm^3. To ensure full coverage, more than twice the volume of the membrane cocktail solution, 846 µL, was deposited in one step on the square of Polx1200. While, this volume only corresponds to 101 µL *o*-NPOE after evaporation of THF, additional deposition of solution only resulted in leaking of cocktail solution below the Polx1200, or a buildup of a layer on top of the material. After allowing THF to evaporate overnight, 7 circles (0.24 cm Ø) were cut out of the infused Polx1200 and mounted to the end of a Tygon tube, using THF to glue membranes onto the tube. The tube was then filled with 1 mM KCl inner filling solution (IFS), and a AgCl/Ag electrode as inner reference element. All electrodes leaked immediately; therefore, the infused Polx1200 was removed from the Tygon tubes, an additional 30 µL of membrane cocktail was deposited onto each Polx1200 membrane to better contain the IFS, and the membranes were left to dry overnight before re-assembling the Tygon tube electrodes.

The ionic site was not included in the membrane cocktails in the following experiments that only tested the physical properties of infused textiles. The membranes therefore contained only the stated wt.% *o*-NPOE and PVC dissolved in a minimal amount

of THF. For the next fabrication method, we used a thermal press (Carver Model 4386, Bench Top Heat Press) to attempt to force a free-standing membrane into the porous textile material. Two membrane cocktails of either 20 wt.% PVC and 80 wt.% *o*-NPOE or 34 wt. % PVC and 66 wt.% *o*-NPOE were dissolved in a minimal amount of THF, drop cast into glass petri dishes, left to dry overnight, and then each placed on top of a piece of Polx1200 and placed into the thermal press at 34 bar for 24 h at 50 °C and then 24 h at 60 °C. The temperature was not increased further as it was suspected that the ionophore would not be stable at higher temperatures. Both membranes were still easily peeled away from the textile and attempts to infuse membranes into the textile with the thermal press were not pursued further.

The final method attempted to infuse membrane into Polx1200 was to deposit membrane cocktails with less PVC on top of Polx1200. Membrane cocktails with 1 wt.% PVC and 99 wt.% *o*-NPOE or 10 wt.% PVC and 90 wt.% *o*-NPOE were dissolved in a minimal amount of THF, drop cast into glass petri dishes and left to dry overnight. Neither of these membranes contained enough PVC to allow the membrane to be “glued” onto the Tygon tube. We did not attempt to use a PVC solution in THF, as is often used in making Tygon tube based electrodes, as the solution could have added PVC to the membrane-coated textile so that it would no longer be a 1 wt.% PVC membrane. Therefore, we switched back to using house-made electrode bodies that hold the membrane in place through pressure between individual pieces of the body. However, due to the low level PVC content, the *o*-NPOE was pushed out of the textile with the pressure from screwing electrode body into place. We then decided to gradually increase

the wt.% of PVC in the membrane to form a robust enough membrane that still improved textile coverage. Membranes with 15 and 20 wt.% PVC successfully coated Polx1200 even after being assembled into in-house ISE bodies,[135] and no leakage of IFS was observed, even after 2 days.

Potentiometric Titration

For this experiment, 2.99 ± 0.03 g (n=3) Polx1200 was weighed, placed into 100 mL H_2O with 1.5 mL of 1.0 N HCl, and then titrated with 0.096 M NaOH. A control experiment in which no Polx1200 added to the sample was also performed. The pH was monitored with a pH probe, and the equivalence point recorded. The concentration of acidic groups on Polx1200 in mol/g, $C_{acid,polx}$, was calculated as follows. The difference in the volume of NaOH needed to reach the equivalence point in the presence and absence of Polx1200 ($V_{NaOH,polx}$ and $V_{NaOH,control}$) was divided by the exact molarity of NaOH, C_{NaOH}, and the exact weight of Polx1200 used, m_{polx}:

$$C_{acid,polx} = \frac{V_{NaOH,polx} - V_{NaOH,control}}{C_{NaOH} \times m_{polx}} \quad (5\text{-}1)$$

Differential Scanning Calorimetry (DSC) and Thermogravimetric Analysis (TGA) Experiments

For this series of experiments, 15 mg Polx1200, 2 mL THF and the appropriate ISM components (in wt % corresponding to a pH ISM) were placed in a vial and stirred overnight at 20 °C (see Table 5-3 for exact amounts). The next day, the Polx1200 was removed from solution, rinsed with 3 mL THF, placed under vacuum for 1 h and analyzed with DSC (TA Instruments Discovery DSC 1 T4P) and TGA (TA Instruments TGA Q500).

A 2-cycle DSC analysis was performed on both treated and neat Polx1200 polyester wipes. In cycle 1, the sample was heated from 40-300 °C then cooled to 40 °C. In cycle 2 the sample was heated to 200.0 °C and then cooled to -50 °C. All cycles used a ramp speed of 10.0 °C/m.

Table 5-1. Composition of samples for DSC analysis.

Sample	Polx1200 (mg)	THF (mL)	Component (mg)
Polx1200, THF	16.56	2.0	---
Polx1200, THF, *o*-NPOE	15.88	2.0	256.31
Polx1200, THF, KTpClPB	16.51	2.0	1.86
Polx1200, THF, TDA	15.82	2.0	5.62

Estimation of the Polx1200 Surface Area

The surface area in a piece of Polx1200, SA_{polx}, was estimated by estimation of the total length of fibers in a given unit area, L_{fibers}, and then calculating the lateral surface area of those fibers. To determine L_{fibers}, the density of Polx1200, ρ_{Polx}, was multiplied by the weight per length of the yarn units, ρ_{yarn}, and the number of fibers per each larger yarn unit, N.

$$\rho_{Polx} \times \rho_{yarn} \times N = L_{fibers} \quad (5\text{-}2)$$

The manufacturer reported the following values of 107 g/cm^2 fabric, 9000 m yarn/ 70 g, and 36 fibers/yarn for ρ_{Polx}, ρ_{yarn}, and N for Polx1200, respectively. Insertion of these values into Equation 5-2 gives L_{fibers}as 4950 cm fibers/cm^2 fabric. This value was then multiplied by the radius of a fiber, r_{fiber}, and 2 π to give SA_{polx}.

$$(L_{fibers} \times r_{fiber} \times 2\pi) = SA_{polx} \quad (5\text{-}3)$$

We determined r_{fiber} to be 9 ± 2 μm (n=8) by examining a cross-section of fabric imaged by scanning electron microscopy (SEM, S-4700, Hitachi, Tokyo, Japan) with an accelerating voltage of 1.0 kV (Fig. 5-2). Insertion of this value and the previously calculated L_{fibers} into equation 5-2 gives SA_{polx} of 30 ± 6 cm^2 SA /cm^2 fabric.

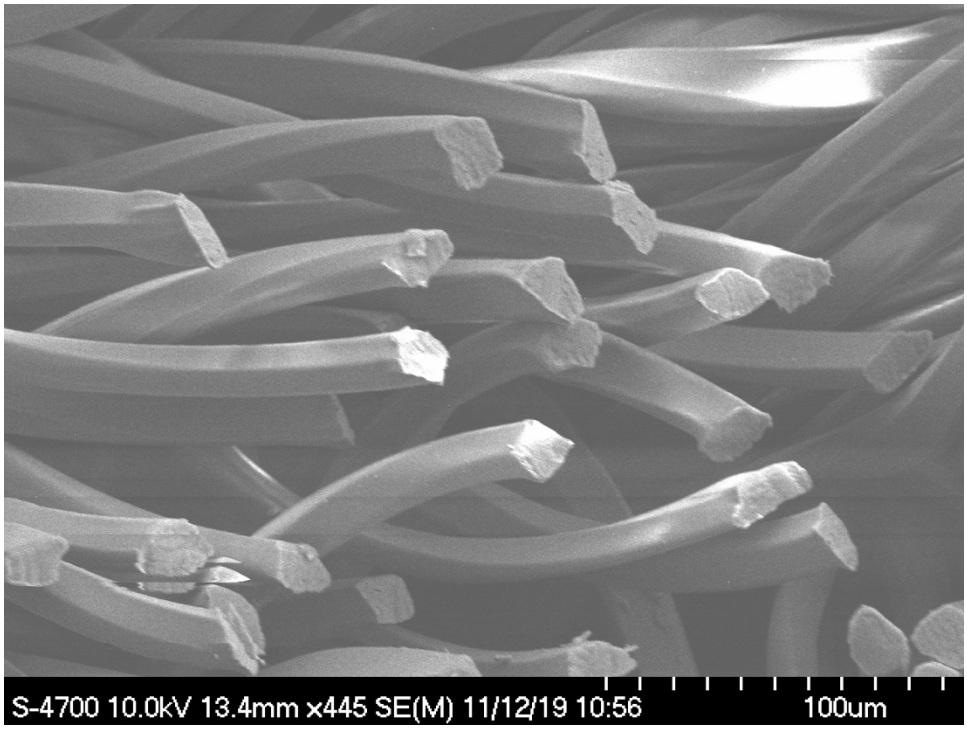

Figure 5-2. Cross-sectional SEM image of bare Polx1200 showing radius of fibers.

To calculate the adsorption capacity of Polx1200, AC, of a typical device used in this work, the previously calculated surface area of a piece of Polx1200, SA_{polx}, was multiplied by the area of Polx1200 in contact with the sensing membrane in a standard device, A_{device}, and divided by the cross-sectional area of a representative molecule, A_M:

$$SA_{polx} \times A_{device} \times A_M^{-1} = AC \quad (5\text{-}4)$$

In our experiments, $A_{device}$was 0.225 cm^2 fabric/device and SA_{polx} was 30 $\pm$ 6 cm^2 /cm^2 fabric. We used the known cross-section (2 $\times$ 10^{-15} cm^2/molecule) of a long chain carboxylic acid, $CH_3(CH_2)_{20}COOH$ for A_M.[177] Insertion of these values into Equation 5-4 gives the value of 3 $\pm$ 0.7 x 10^{15} molecules/device, as used in the results section.

^{1}H NMR Experiments

First a stock of 496.02 mg TDA and 289.64 mg 1,3,5-tribromobenzene dissolved in 5.54778 g DOS was made. A portion of this initial stock was then diluted by a factor of 10 with DOS. To examine the effect of Polx1200 on TDA concentration, 72 mg of Polx1200 and 250 mg of the solution were added to the barrel of a glass syringe, sealed at the top with Parafilm, and left to soak for either 2 h or overnight (see Table 5-1). The solution was then pushed into an NMR tube for analysis using the plunger of the syringe. Controlled experiments were also performed using the same procedure, without adding Polx1200. All experiments were performed in triplicate. A few drops of trifluoroacetic acid were added to each ^{1}H NMR sample before measurements to ensure full protonation of TDA. ^{1}H NMR were recorded with a Bruker Avance III (500 MHz).

Table 5-2. Material used for Polx1200 TDA exposure studies.

Condition	Sample solution (mg)	Polx1200 (mg)
Undiluted Stock: 2 h soak	220.34 $\pm$ 7.52	69.88 $\pm$ 2.62
Undiluted Stock: Overnight soak	229.34 $\pm$ 10.02	75.76 $\pm$ 7.63
Diluted Stock: overnight soak	232.64 $\pm$ 4.65	70.07 $\pm$ 0.69

RESULTS AND DISCUSSION

Ionophore Doped Membranes for K^+ Sensing

Textile-based devices were tested for compatibility with the K^+ ionophore valinomycin, both with and without 20 wt.% ETH 500, an inert electrolyte previously used to improve the response of analogous paper-based devices.[54] Initial device designs, referred to as extended dog bone, consisted of an ISM embedded within the textile, and a reference electrode consisting of AgCl/Ag ink in contact with a reference solution of 0.1 M KCl (see Fig. 5-3A). In this design, the only sample dependent phase boundary potential is that between the sample solution and the ISM. Devices tested for sample concentrations of 6.25–100 mM KCl responded with slopes of 56.4 ± 3.4 and 56.6 ± 1.5 mV/decade for membranes with and without the 20 wt.% ETH 500 additive, respectively. While in one experiment the extended dog bone design did show that incorporation of a valinomycin-containing K^+ ISM resulted in a Nernstian response slope, efforts to reproduce the results with the same design resulted in non-linear and unstable responses, indicating a lack of reproducibility. Therefore, in subsequent designs a reference electrode with an ionic-liquid-based RM previously shown to be compatible with textile based ISEs was incorporated into the device design.[55]

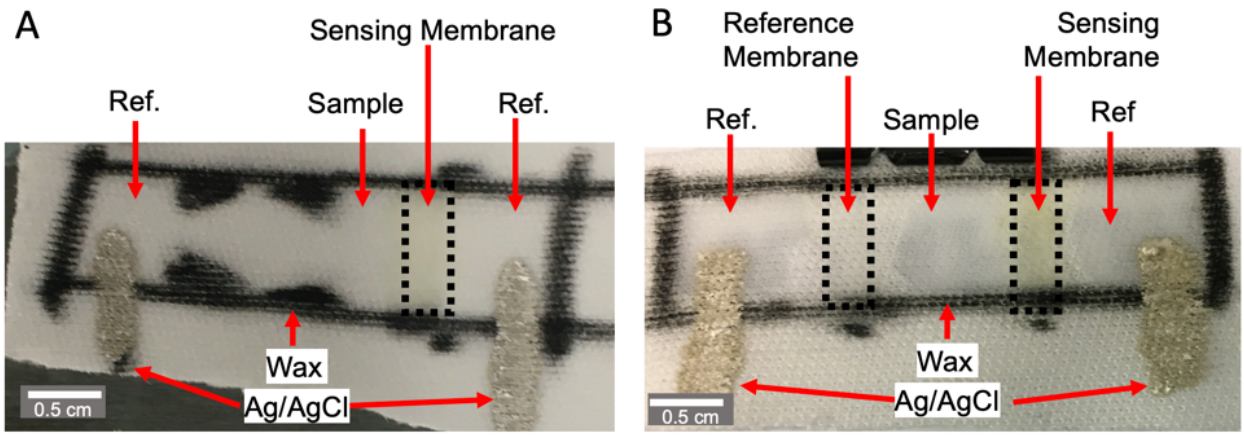

Figure 5-3. A textile-based potentiometric device (A) with an integrated sensing membrane and (B) with integrated sensing and reference membranes (Ref., reference solution).

The next set of experiments were performed with a design consisting of both sensing and reference membranes integrated into the textile (see Fig. 5-3B). Devices without ETH 500 in the ISM exhibited a response slope of 65.4 ± 17.5 mV/decade and an E^0 value of 91.0 ± 40.2 mV while devices with 20 wt. % ETH 500 exhibited a response slope of 50.4 ± 5.8 mV/decade and an E^0 value of 59.9 ± 11.9 mV (Figs. 5-4A and B). As expected, the addition of the electrolyte ETH 500 to the ISM decreased the resistance of devices, from 530 ± 200 MΩ (n=2) to 120 ± 40 MΩ (n=9). While incorporation of the ETH 500 into the ISM significantly improved performance in terms of reproducibility, the performance is still far from ideal and therefore requires further study.

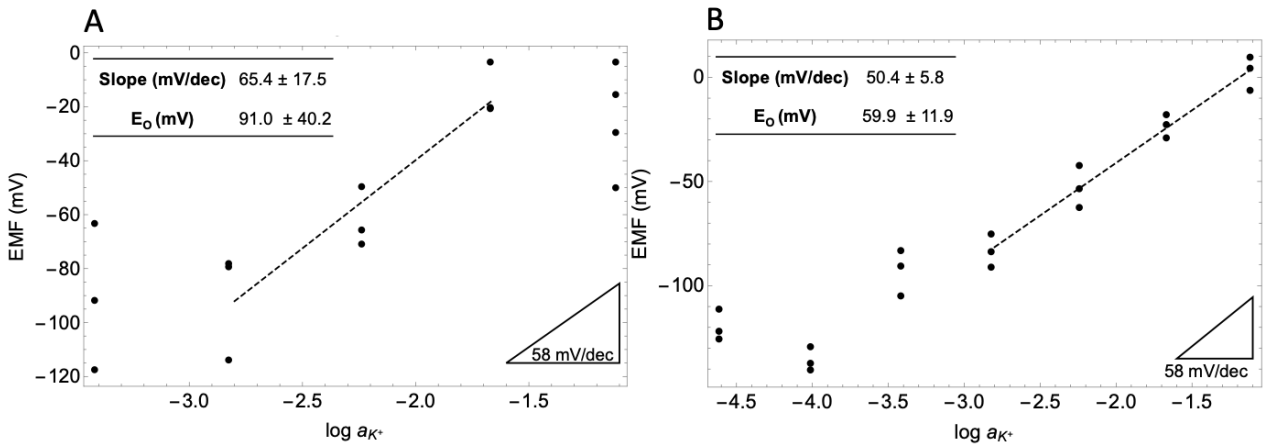

Figure 5-4. Potentiometric response of textile-based K^+ ISEs with embedded RM and ISM without (A) and with (B) ETH 500 additive in the ISM.

BME-44, a bis(crown ether) also used as a potassium ionophore,[178] was also tested for compatibility in textile-based ion-selective electrodes. As an initial design to test compatibility of the ionophore-containing ISM with textile, a piece of Polx1200 was infused with a BME-44 containing K^+ ISM and assembled into an in-house ISE body,[135] with a 1 mM KCl IFS, as shown in Figure 5-5A. After conditioning overnight in 10 mM KCl, potentiometric responses were measured in 100 mL of starting sample volume. Two identically prepared electrodes gave a linear response from $10^{-1.0}$ to $10^{-4.8}$ M KCl, with a lower LOD of $10^{-5.2 \pm 0.1}$ M KCl, slightly sub-Nernstian slopes of 56.5 and 56.7 mV/decade, and an E^0 of 373.5 and 380.8 mV (see Fig. 5-5B). The electrodes had resistances of 25.2 and 3.27 M Ω and a resistivities of 350 and 58 MΩ cm.

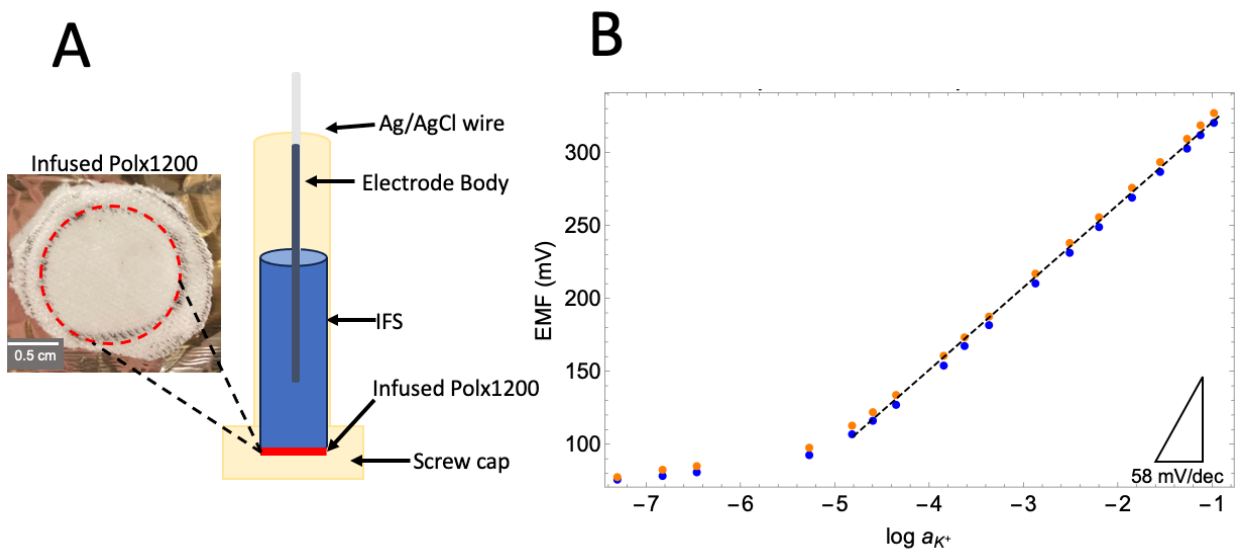

Figure 5-5. (A) Schematic representation of the conventional setup with Polx1200 infused with ISM and (B) potentiometric response for 2 electrodes shown in (A) with a commercial double junction RE.

To further study the interaction of ionophores and textiles, the selectivity of devices over time was also measured using the fixed interference method. An electrode was fabricated as previously mentioned, with a piece of textile infused with BME-44 containing K^+ ISM. The electrode gave a linear response from $10^{-1.1}$ to $10^{-3.5}$ M KCl, with a lower LOD of $10^{-3.7}$, a sub-Nernstian slope of 52.5 mV/decade, and an E^0 of 349.7 mV. This slight worsening of performance deviates from the response above for two other electrodes of the same construction and underlines fundamental problems in reproducibility of these electrodes with ionophore-doped ISMs integrated into textile. While $\log K^{\mathrm{pot}}_{\mathrm{K^+,Na^+}}$ decreased slightly from Day 6 to Day 8, from –2.5 ± 0.3 to –2.2 ± 0.3,

the change was within error and therefore not significant. The selectivity was, however, worse than the literature reported value of –3.2 for electrodes of conventional design with membranes containing the same plasticizer, polymer, and ionophore as measured using the separate solutions method.[178] In fact, the $\log K^{\mathrm{pot}}_{\mathrm{K^+,Na^+}}$ of ionophore-free ion exchange membranes based on the same *o*-NPOE plasticized PVC matrix, in which selectivity is determined by differences of the free energy of ion transfer alone, was reported as –1.8.[179] The similarity suggests that the electrode performs as an ionophore-free system in this setup.

Efforts to Improve Permeation of Polx1200 with Sensing Membrane

When using the above electrode setup for ISM-infused Polx1200 membranes mounted into an electrode body, we noticed that leakage of IFS into the sample was common. When using an analogous fabrication method for textile-based devices and imaging those membrane-coated Polx1200 with SEM, we saw larger interyarn gaps between distinct yarns and smaller interfiber gaps between the individual fibers comprising each yarn.[55] We therefore hypothesized here that the unfilled interyarn gaps allowed IFS to flow across the textile.

We tried several approaches to better fill the gaps in the textile. First, we increased the volume of membrane cocktail deposited per surface area of Polx1200 to match the volume of the textile. However, electrodes of this kind leaked and, upon additional deposition of membrane cocktail, only 2 out of 7 electrodes sealed to fully hold IFS (see Fig. 5-6A). These gave Nernstian responses from 10-1.0 to $10^{-4.4}$ M KCl, with a lower LOD

of $10^{-4.7\pm 0.1}$ M KCl, slopes of –58.7 and –57.3 mV/decade, and an E^0 of 8.84 and 8.97 mV (see Figs. 5-6A and B). The electrodes had resistances of 5172 and 419 kΩ and resistivities of 2150 and 320 kΩ cm. However, this method resulted in very low rate of successful electrode fabrication (2 out of 7), and alternative deposition methods were pursued.

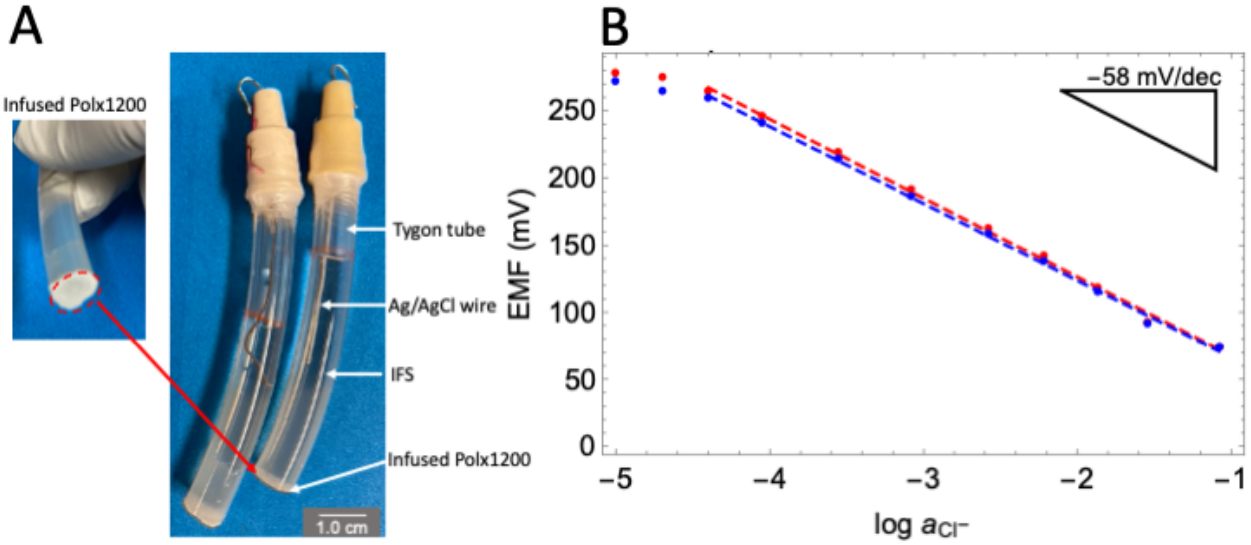

Figure 5-6. (A) Picture of Tygon tube based electrodes with Polx1200 infused with ISM and (B) potentiometric response of the two electrodes shown in (A) with respect to a commercial double-junction RE.

After attempting several variations of coating the textile with membrane, including the use of a thermal press, the final method of depositing 120 µL of an 80 wt.% *o*-NPOE, 20 wt. % PVC membrane cocktail onto a Polx1200 circle (∅ 2cm) was found to be successful. Now that an optimized fabrication method has been identified, we recommend

testing the performance of electrodes with this infused membrane, imaging coated textile with SEM to determine if interyarn gaps are filled, and adapting this method for use in planar textile-based devices.

Ionophore Doped Membranes for pH Sensing

To determine if the textile interference was dependent upon the target analyte or consistent for any ionophore-containing ISM, other target ions, including H^+ were also tested. The ISMs for these sensors used the H^+ ionophore TDA and a membrane composition as reported in the literature (see Experimental Section).[180] Textile-based devices fabricated using the ionic-liquid-based RM and pH ISM did not give stable responses upon testing in phosphate buffer solutions of various pH and thus a calibration curve could not be obtained. At this point 2 hypotheses were developed to explain the failure of pH textile-based devices.

The first hypothesis stated that the PET-based textile used in this work contained carboxylic acid impurity sites that interfere with pH sensing. To test this hypothesis, a potentiometric back titration of a solution in which textile was suspended was performed. The volume of base needed to reach an equivalence point for a solution containing Polx1200, 7.8 ± 0.3 mL, did not differ from the volume for a solution containing no additional acidic sites, 7.5 mL, indicating the absence of acidic groups on the textile. It is therefore confirmed that there are not more than 10 µmol acidic groups/g Polx1200, the lower LOD for this experimental protocol.

The second hypothesis to explain non-ideal performance of textile-based sensors with embedded ionophore-containing ISMs considers possible interactions of individual

membrane components with the textile, particularly adsorption of components onto the surface of the textile due to intermolecular interactions. Removal of membrane components from the sensing membrane would disrupt the sensing mechanism and thereby cause non-ideal performance. It has been previously shown that cations, particularly divalent heavy metal cations, adsorb onto the negatively charged cellulose backbone of filter paper, leading to their depletion from sample solutions.[143] It was therefore hypothesized that adsorption or absorption of ionophores or ionic sites from the ISM onto or into the Polx1200 might be occurring when the membrane cocktail is deposited on a textile-based platform.

Absorption of organic molecules into the voids in polymer chains leads to a swelling of the polymer, and it also results in a decrease in both glass transition temperature (T_g) and crystallinity.[181] Therefore, DSC was used to track the physical properties of the Polx1200 after exposure to ISM components and detect possible alterations due to leaching of membrane components into the textile. After exposing the textile to a solution containing THF and each of the individual membrane components (KTpClPB as ionic site, TDA as ionophore, and *o*-NPOE as plasticizer) overnight, the textile was removed from the solution, rinsed with THF, dried under vacuum, and analyzed with DSC (see Experimental section for full details).

Using modulated DSC the T_g of PET fibers was reported to range from 112-114 ºC, depending on fiber structure.[182] In our work, a clear T_g was not observed for neat Polx1200, as is common when performing conventional DSC for materials with a high degree of crystallinity. The lack of emergence of a T_g or any additional thermal event

below 114 ºC in any of the treated Polx1200 samples suggests that none of the membrane components were absorbed to a significant extent into the polymeric structure. However, an exothermic event at 275 ºC was visible for TDA-treated and, to a lesser extent, for *o*-NPOE-treated material. This suggests possible decomposition of surface adsorbed small molecules, and TGA provided further exploration of this (see Appendix for full DSC).

Examination with TGA provides information about degradation events by tracking weight change as a function of heating temperature. We examined T_{99} and T_{95}, the temperature at 1 and 5 % mass loss, respectively (see Table 5-3). While T_{95} decreases slightly from neat Polx1200 to Polx1200 exposed to THF, there is no significant change upon exposure to additional membrane components. However, T_{99} does decrease significantly from Polx1200 treated with THF to Polx1200 treated with each of the additional membrane components. The onset of degradation at a lower temperature for each of the samples exposed to membrane components implies either absorption into or adsorption onto the material that was not removed by the rinsing step after overnight soaking. Overall, analysis by DSC and TGA suggests that while components from the ISM cocktail do not absorb into the polymer structure, some surface adsorption of TDA, *o*-NPOE and KTpClPB onto Polx1200 may occur upon room temperature exposure.

Table 5-3. Comparison of T_{99} and T_{95} for Polx1200 soaked in various ISM components.

Sample	T_{99} (ºC)	T_{95} (ºC)
Polx1200	380.85	399.25
Polx1200, THF	321.12	371.49
Polx1200, THF, *o*-NPOE	139.90	373.25
Polx1200, THF, KTpClPB	141.95	377.19
Polx1200, THF, tridodecylamine	263.29	367.45

While data from DSC analysis show that ISM components do not alter the physical properties of the textile, ^{1}H NMR allowed for a more direct study of a possible depletion of membrane components in the ISM after exposure to the textile. In particular, there are three possible mechanisms by which the ionophore TDA could be removed from the ISM due to interactions with Polx1200: the formation of a monolayer on top of PET fibers, multilayer adsorption on top of PET fibers, and absorption of molecules into the PET fibers themselves.

This first possible method of substrate/membrane component interaction was evaluated considering the full surface area of the textile material. Due to the structure of the fabric consisting of discrete fibers bundled into larger yarn units that are knit into a highly ordered pattern, the total surface area of a piece of Polx1200 is 30 ± 6 cm^2 surface area/cm^2 fabric (see Experimental section for detailed calculations). Assuming a molecular cross-section for TDA similar to that of a long chain carboxylic acid $CH_3(CH_2)_{20}COOH$, the adsorption capacity of Polx1200 is $2 \pm 0.3 \times 10^{16}$ molecules/cm^2 fabric. From this, the specific adsorption capacity of a strip of Polx1200 with the dimensions used for membrane deposition is calculated as $3 \pm 0.7 \times 10^{15}$

molecules/device. Finally, we calculate the number of molecules of TDA deposited onto that strip of Polx1200 using the known composition and volume of ISM deposited. For TDA this results in 5.4×10^{16} molecules TDA deposited/device. This is an order of magnitude larger than the calculated adsorption capacity ($3 \pm 0.7 \times 10^{15}$ molecules/device). While results from TGA suggest possible surface adsorption of membrane components onto the material, even if a complete monolayer of molecules were adsorbed onto the entire available surface area of Polx1200, there would only be a 10% decrease in the ionophore concentration of the ISM. Given that 100% monolayer coverage is extremely unlikely, and a 10% change is not enough to explain the poor performance of the potentiometric devices, formation of an adsorbed monolayer on Polx1200 does not appear likely as a sufficient explanation for poor sensor performance.

In addition to the possibility of the formation of a surface monolayer, there is also the possibility of multilayer adsorption as well as absorption into the fibers themselves, both of which would result in an increase of the adsorption capacity from that calculated above. As the adsorption capacity resulting from neither of these additional mechanisms could be estimated from the available data, an experiment was designed to test for depletion of TDA in the ISM (cocktail) upon exposure to Polx1200.

We used ^{1}H NMR to track the relative response of protons in the target of interest, TDA, compared to those of the internal standard, 1,3,5-tribromobenzene, which was added to the ISM cocktail at the same time as the TDA. 1,3,5-Tribromobenzene was chosen as a standard as the peaks from the 3 identical aromatic protons appear at 10.7 ppm and do not overlap with the aliphatic protons of TDA in the region 3.6-1.3 ppm. 1,3,5-

tribromobenzene 4 was also thought to be inert towards the membrane components and Polx1200. The plasticizer DOS was used as a solvent for all samples to mimic the environment in which Polx1200 interacts with TDA on devices with ISM comprising PVC, DOS, TDA, and ionic sites. The relative response factor, R_f, is given by the following equation:

$$R_{f=}\frac{I_{TDA}/m_{TDA}}{I_{std}/m_{std}} \quad (5\text{-}5)$$

where I_{TDA}, m_{TDA}, I_{std}, and m_{std} represent the signal from the peaks of the TDA, the moles of TDA in the sample, the signal from the peaks of the 1,3,5-tribromobenzene standard, and the moles of 1,3,5-tribromobenzene in the sample, respectively.

In samples that were exposed to Polx1200, we would expect to see a decrease in the R_f if TDA adsorbs onto the textile. In preliminary experiments, samples with $2.6 \pm 0.1 \times 10^{18}$ molecules TDA/cm^2 fabric were exposed to the textile for either 2 h or overnight. There was no significant change in R_f between the initial, 2 h, and overnight soaks, as seen in Table 5-2. This ratio of molecules to surface area of Polx1200 is, however, an order of magnitude greater than that in the device so an additional sample was prepared with $2.8 \pm 0.3 \times 10^{17}$ molecules TDA/cm^2 fabric and soaked overnight. Again, there was no significant change in R_f from the non-exposed samples. It follows that a decrease in the concentration of TDA molecules could not be observed with this method.

Table 5-4. R_f Values from ^1H NMR Study of TDA Depletion.

Condition	Molecules TDA/cm^2 fabric	R_F
Available in device fabrication	2.4×10^{17}	---
Undiluted Stock	NA	2.1 ± 0.1
Undiluted Stock: 2 h soak	$2.6 \pm 0.1 \times 10^{18}$	2.0 ± 0.1
Undiluted Stock: Overnight soak	$2.6 \pm 0.3 \times 10^{18}$	2.1 ± 0.3
Diluted stock	NA	1.8 ± 0.2
Diluted Stock: overnight soak	$2.8 \pm 0.3 \times 10^{17}$	1.8 ± 0.2

While 1,3,5-tribromobenzene was initially chosen due to the suspected lack of interaction with either Polx1200 of TDA, there is a possibility of interaction through π-π stacking interactions of the PET backbone of Polx1200 and the aromatic ring of 1,3,5-tribromobenzene. If 1,3,5-tribromobenzene does in fact interact with Polx1200 and is depleted from the sample, then it is no longer an inert internal standard, and the R_f value loses meaning. However, an internal standard that is soluble in DOS but will for certain not interact with Polx1200 may be difficult to find.

Ionophore Doped Membranes for Sensing of Other Analytes

Efforts were also made to test additional targets with different ion valences, to see if the interferences when using ionophore were related to either ion valency or the structure of the ionophore. An ISM was prepared for the divalent cation, Ca^{2+}, with the ionophore ETH 5234 (Fig. 5-1) and incorporated into textile-based devices with an ionic liquid-based RM (Fig. 5-2A). In this design a 0.1 M $CaCl_2$ reference solution was used. Devices gave a linear response from $10^{-1.0}$ to $10^{-3.4}$ M $CaCl_2$, with a lower LOD of $10^{-4.0 \pm 0.6}$ M $CaCl_2$, a Nernstian slope of 28.0 ± 3.2 mV/decade, and an E^0 36.2 ± 7.9 mV.

Electrodes of the same ISM composition incorporated into a conventional electrode body with a 1 mM $CaCl_2$ IFS gave a linear response from $10^{-1.0}$ to $10^{-5.8}$ M, with a lower LOD of $10^{-6.4}$ M $CaCl_2$, a Nernstian slope of 28.1 ± 0.1 mV/decade, and an E^0 of 271.6 ± 0.5 mV. While the textile-based devices did exhibit a theoretically predicted response slope, they also showed worse reproducibility and a worsened lower LOD compared to analogous electrodes with conventional bodies.

Attempts were also made to test the performance of textile-based ISEs for the monovalent cation Ag^+, using the ionophore dibenzyl sulfide. However, the textile-based Ag^+ ISEs did not respond to changes in the concentration of Ag^+ in the range tested (1-100 mM Ag^+). When testing the performance of conventional electrodes with analogous Ag^+ ISMs, the upper LOD as caused by Donnan failure was found to be 1 mM $AgNO_3$. In addition, when testing other textile-based devices a lower LOD of 1 mM was found ($10^{-3.7}$ M KCl for Cl^- sensing and $10^{-4.0 \pm 0.6}$ M $CaCl_2$ for Ca^{2+} sensing). Therefore, with an upper limit of 1 mM as caused by Donnan failure of the Ag^+ ISM, and a possible lower LOD of 1 mM consistent in our textile-based platform, the Ag^+ textile-based ISE likely does not have a working range. Once the origin of the worsening of the lower LOD due to Polx1200 is resolved, we recommend fabricating and testing Ag^+ textile-based ISEs again.

Additionally, the divalent anion, CO_3^{2-}, was tested as a target ion with a negative charge, and one of important clinical interest. The ionophore ETH 6010 (Fig. 5-5) was incorporated in the ISM. Here, a 0.5 M K_2CO_3 solution in a background of 100 mM phosphate buffer, pH 8.8 was diluted for calibration of CO_3^{2-}. However, textile-based

CO_3^{2-} ISEs did not respond to changes in concentration of CO_3^{2-}. As the highest concentration tested was 2.5 mM and textile-based devices for both Cl^- and Ca^{2+} had lower LODs in the millimolar range, it was hypothesized that the textile-based CO_3^{2-} ISEs also had a lower LOD of approximately 1 mM. Therefore, efforts were undertaken to achieve at carbonate concentration over 1 mM for testing device responses. To reach a carbonate concentration over 1 mM, the pH had to be increased to 10.6, significantly above the buffered region of the phosphate buffer. Therefore, the phosphate buffer was not an ideal buffer and no longer used.

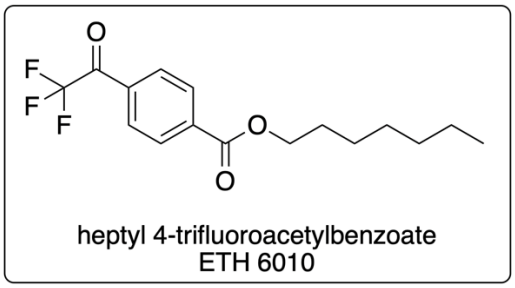

Figure 5-7. Structure of the carbonate ionophore ETH 6010

A 100 mM glycine buffer, pH 8.8, was then used to control the pH of the sample solutions. However, it appeared to interfere with the sensing mechanism. To test for interference from glycine, a controlled experiment was performed in a beaker type of experiment, with a Ag/AgCl wire in a 100 mM KCl solution and a background of pH 8.8 100 mM glycine buffer. The lower LOD of detection for Cl^- was found to be $10^{-2.7 \pm 0.1}$ M, with a response slope of –61.6 ± 2.3 mV/decade and an E^0 of 34.2 ± 3.6 mV (n=3). This is significantly higher than the expected lower LOD of Cl^- when using a AgCl coated wire

of $10^{-4.9}$ M Cl^-, as calculated from the square root of the solubility product of AgCl (1.6 x 10^{-10} M^2)[87]. This appears to result from interaction of the amine group with aqueous silver ions, which is not compatible with the Ag/AgCl based ink we use in the textile-based devices. Unfortunately, all other buffers considered either contained Cl^- or would complex with these ions and the Ag^+. We therefore decided to abandon at this time the attempt to prepare textile-based carbonate selective ISEs. Given the physiological relevance of carbonate, this topic should be revisited once the factors that determine detection limits of Polx1200 based devices are better understood.

CONCLUSIONS

The work described in this chapter shows that when incorporated into textile-based planar setups, K^+ and pH selective membranes using plasticized PVC do not perform as theoretically predicted, in terms of slope, reproducibility, and linearity. Several hypotheses on the source of interference were sequentially disproved. These include: the existence of acidic groups on Polx1200 as tested with potentiometric titration, absorption of membrane components into the polymeric structure as tested by tracking T_g, and absorption of a representative ionophore (TDA) onto Polx1200 as monitored by ^{1}H NMR spectroscopy. While TGA suggests possible surface adsorption of membrane components, accounting for the surface area of Polx1200 and the sensing membrane composition, it was shown that even complete adsorption would minimally affect the amount of available ionophores. Future work will focus on alternative hypotheses for the interference of Polx1200 in ionophore sensing membranes on planar devices.

Additionally, the optimized spotting of membrane onto Polx1200 in conventional electrodes will be adapted to the fabrication of planar devices. It is hypothesized that the filling of interyarn gaps may improve electrode performance by creating a more complete barrier between sample and reference solutions. Finally, the observed worsened lower LOD found in Polx1200 devices with embedded plasticized PVC membranes without ionophores, as described in previous sections, is also apparent in these ionophore-based membranes. When the source of that lower LOD is better understood, we recommend returning to the target ions silver and carbonate.

Chapter 6. Conclusions and Outlook

As discussed in Chapter 2, the use of a textile, instead of filter paper, as a supporting substrate for miniaturized ISEs comprised of hydrophobic wax barriers and AgCl/Ag conductive inks improved the lower limit of detection (LOD) by an order of magnitude, from $10^{-3.1}$ to $10^{-4.1}$ M Cl^-, for membrane-free systems. The successful integration of polymeric ion-sensing and reference membranes was also achieved. A structural analysis of pore coverage was achieved with the use of scanning electron microscopy (SEM) and contributed to the understanding of material porosity as correlated to sensor performance. These textiles with fully integrated membranes were then used in both aqueous samples and blood serum to detect the levels of the clinically relevant chloride ion.

In Chapter 3, a systematic study of the sources of sub-optimal performance in paper-based potentiometric sensors for chloride detection revealed contamination from filter paper and AgCl/Ag conductive inks. The use of alternate ion-to-electron transducers, such as coated plates and wires were proposed as an alternative to conductive inks and shown to improve performance. Additionally, by monitoring the concentration of Ag^+ in aliquots of $AgNO_3$ exposed to filter paper, the hypothesis that adsorption of Ag^+ onto filter paper negatively impacts performance was disproved. This work underlines the importance of careful selection and characterization of materials to be used in miniaturized sensors in which sample volumes are on the order of microliters and therefore more susceptible to significant concentration changes due to leaching of impurities.

The importance of a highly reproducible ISE for point-of-care use is highlighted in Chapter 4. Despite significant efforts in recent years to develop a variety of redox buffers to buffer redox-active impurities in ISEs, until now there has been no hydrophilic redox buffer compatible with anion sensing. After a thorough review of the literature and consideration of several species, cobalt(II/III)bis(terpyridine) chloride was presented as a viable complex to meet this need. Upon incorporation into the inner filling solution of a conventional chloride sensing electrode, the redox buffer improved the standard deviation of E^0 from 2.7 to 0.3 mV. The redox buffer is also compatible with ionic-liquid-based reference membranes and textile-based sampling platforms. The complex may additionally find uses outside of the field of ISEs, such as in geochemistry or chemical biology.

In the short term, this can be achieved through optimization of the ionic-liquid-based reference membrane. Previous work in the Bühlmann group has shown the importance of washing ionic-liquids to remove ionic impurities that may enter in the manufacturing process.[183] Additionally, a C8 based ionic liquid was used in initial textile-based devices while a C12 based ionic liquid was used in the textile-based devices with redox buffer. Considering the possible effects of salt containing contaminants and ionic liquid hydrophobicity, additional reference membranes will be tested using cleaned ionic liquids of different chain lengths. Once this source of irreproducibility is addressed, the chloride-sensing devices will also be used in serum samples to test performance in more complex sample matrices. Additionally, the stability of the complex and inner-filling solution with the redox buffer over time will be studied.

The need for detection of additional ions with ionophore-doped ion-sensing membranes is addressed in Ch. 5. While ionophore-containing ion-selective membranes work well in conventional systems, their use in textile- and paper-based ISEs results in sub-optimal performance. Several hypotheses are presented to explain the performance limitations and sequentially disproved, using ^{1}H NMR and potentiometric techniques. These included absorption and/or adsorption of sensing components onto textile and interactions of functional groups on the textile to alter the pH of sample solutions. Further understanding of the coating of fibers and yarns with polymeric membranes may lead to an understanding of the source of issues in ionophore-doped membranes. Study of the optimized fabrication of coated-textiles with SEM will provide information on the degree of coverage of interyarn gaps. It is hypothesized that full coverage of interyarn gaps by polymeric membranes will improve performance. If the current textile material does not allow for this coverage, then alternative materials with a single sized pore structure must be proposed. In the current state, the unfilled interyarn gaps may allow for contact between sample and reference solutions and thereby cause issues in the lower limit of detection with chloride-sensing membranes and poor performance in ionophore-doped sensing membranes.

Chapter 7. Bibliography

(1) Mabey, D.; Peeling, R. W.; Ustianowski, A.; Perkins, M. D. Diagnostics for the Developing World. *Nat. Rev. Microbiol.* **2004**, *2*, 231–240.

(2) Pai, N. P.; Vadnais, C.; Denkinger, C.; Engel, N.; Pai, M. Point-of-Care Testing for Infectious Diseases: Diversity, Complexity, and Barriers in Low-And Middle-Income Countries. *PLoS Med.* **2012**, *9*.

(3) ElSaboni, Y.; Hunt, J. A.; Stanley, J.; Moffatt, C.; Wei, Y. Development of a Textile Based Protein Sensor for Monitoring the Healing Progress of a Wound. *Sci. Rep.* **2022**, *12*.

(4) Rousseau, C. R.; Bühlmann, P. Calibration-Free Potentiometric Sensing with Solid-Contact Ion-Selective Electrodes. *TrAC Trends Anal. Chem.* **2021**, *140*.

(5) Bakker, E. Can Calibration-Free Sensors Be Realized? *ACS Sens.* **2016**, *1*, 838–841.

(6) Kumar, A. A.; Hennek, J. W.; Smith, B. S.; Kumar, S.; Beattie, P.; Jain, S.; Rolland, J. P.; Stossel, T. P.; Chunda-liyoka, C.; Whitesides, G. M. From the Bench to the Field in Low-Cost Diagnostics : Two Case Studies. *Angew. Chem., Int. Ed.* **2015**, *54*, 5836–5853.

(7) Bühlmann, P.; Chen, L. D. Ion-Selective Electrodes With Ionophore-Doped Sensing Membranes. In *Supramolecular Chemistry: From Molecules to Nanomaterials; Volume 5: Self-Assembly and Supramolecular Devices*; Steed, J. W., Gale, P. A., Eds.; John Wiley & Sons, Chichester, UK, 2012; pp 2539–2579.

(8) Borchardt, M.; Diekmann, C.; Dumschat, C.; Cammann, K.; Knoll, M. Disposable Sodium Electrodes. *Talanta* **1994**, *41*, 1025–1028.

(9) Diekmann, C.; Dumschat, C.; Cammann, K.; Knoll, M. Disposable Reference Electrode. *Sensors Actuators B. Chem.* **1995**, *24–25*, 276–278.

(10) Walsh, S.; Diamond, D.; McLaughlin, J.; McAdams, E.; Woolfson, D.; Jones, D.; Bonner, M. Solid-State Sodium-Selective Sensors Based on Screen-Printed Ag/AgCl Reference Electrodes. *Electroanalysis* **1997**, *9*, 1318–1324.

(11) Deroco, P. B.; Wachholz Junior, D.; Kubota, L. T. Paper-Based Wearable Electrochemical Sensors: A New Generation of Analytical Devices. *Electroanalysis* **2022**, *2200177*, 1–11.

(12) Parrilla, M.; Cuartero, M.; Crespo, G. A. Wearable Potentiometric Ion Sensors. *TrAC Trends Anal. Chem.* **2019**, *110*, 303–320.

(13) Krikstolaityte, V.; Ding, R.; Hui Xia, E. C.; Lisak, G. Paper as Sampling Substrates and All-Integrating Platforms in Potentiometric Ion Determination. *Trends Anal. Chem.* **2020**, *133*, 116070.

(14) Sinha, A.; Dhanjai; Stavrakis, A. K.; Stojanović, G. M. Textile-Based Electrochemical Sensors and Their Applications. *Talanta* **2022**, *244*, 123425.

(15) Curme, H.; Rand, R. N. Early History of Eastman Kodak Ektachem Slides and Instrumentation. *Clin. Chem.* **1997**, *43*, 1647–1652.

(16) Calem, R. E. Moving the Common Blood Test Closer to the Patient. *New York Times*. June 21, 1992, p 12.

(17) Szűcs, J.; Gyurcsányi, R. E. Towards Protein Assays on Paper Platforms with Potentiometric Detection. *Electroanalysis* **2012**, *24*, 146–152.
(18) Cui, J.; Lisak, G.; Strzalkowska, S.; Bobacka, J. Potentiometric Sensing Utilizing Paper-Based Microfluidic Sampling. *Analyst* **2014**, *139*, 2133–2136.
(19) Lisak, G.; Cui, J.; Bobacka, J. Paper-Based Microfluidic Sampling for Potentiometric Determination of Ions. *Sens. Actuators, B* **2015**, *207*, 933–939.
(20) Kelani, K. M.; Badran, O. M.; Rezk, M. R.; Elghobashy, M. R.; Eid, S. M. Widening the Applications of the Just-Dip-It Approach: A Solid Contact Screen-Printed Ion-Selective Electrode for the Real-Time Assessment of Pharmaceutical Dissolution Testing in Comparison to off-Line HPLC Analysis. *RSC Adv.* **2021**, *11*, 13366.
(21) Novell, M.; Parrilla, M.; Crespo, G. A.; Rius, F. X.; Andrade, F. J. Paper-Based Ion-Selective Potentiometric Sensors. *Anal. Chem.* **2012**, *84*, 4695–4702.
(22) Lan, W. J.; Zou, X. U.; Hamedi, M. M.; Hu, J.; Parolo, C.; Maxwell, E. J.; Bühlmann, P.; Whitesides, G. M. Paper-Based Potentiometric Ion Sensing. *Anal. Chem.* **2014**, *86*, 9548–9553.
(23) Bouhoun, M. L.; Blondeau, P.; Louafi, Y.; Andrade, F. J. A Paper-Based Potentiometric Platform for Determination of Water Hardness. *chemosensors* **2021**, *9*.
(24) Rostampour, M.; Lawrence Jr, D.; Hamid, Z.; Darensbourg, J.; Calvo-Marzal, P.; Chumbimuni-Torres, K. Y. Highly Reproducible Flexible Ion-Selective Electrodes for the Detection of Sodium and Potassium in Artificial Sweat. *Electroanalysis* **2022**, *34*, 1–7.
(25) Rius-Ruiz, F. X.; Crespo, G. A.; Bejarano-Nosas, D.; Blondeau, P.; Riu, J.; Rius, F. X. Potentiometric Strip Cell Based on Carbon Nanotubes as Transducer Layer: Toward Low-Cost Decentralized Measurements. *Anal. Chem.* **2011**, *83*, 8810–8815.
(26) Ding, R.; Kumar Joon, N.; Ahamed, A.; Shafaat, A.; Guzinski, M.; Wagner, M.; Ruzgas, T.; Bobacka, J.; Lisak, G. Gold-Modified Paper as Microfluidic Substrates with Reduced Biofouling in Potentiometric Ion Sensing. *Sens. Actuators, B* **2021**, *344*.
(27) Ding, R.; Krikstolaityte, V.; Lisak, G. Inorganic Salt Modified Paper Substrates Utilized in Paper Based Microfluidic Sampling for Potentiometric Determination of Heavy Metals. *Sens. Actuators, B* **2019**, *290*, 347–356.
(28) Silva, R.; Zhao, K.; Ding, R.; Chan, W. P.; Yang, M.; Yip, J. S. Q.; Lisak, G. Ion-Selective Membrane Modified Microfluidic Paper-Based Solution Sampling Substrates for Potentiometric Heavy Metal Detection. *R. Soc. Chem.* **2022**, *147*, 4500–4509.
(29) Ding, R.; Lisak, G. Sponge-Based Microfluidic Sampling for Potentiometric Ion Sensing. *Anal. Chim. Acta* **2019**, *1091*, 103–111.
(30) Ding, R.; Cheong, Y. H.; Zhao, K.; Lisak, G. Acidified Paper Substrates for Microfluidic Solution Sampling Integrated with Potentiometric Sensors for Determination of Heavy Metals. *Sens. Actuators, B* **2021**, *347*, 130567.
(31) Lisak, G.; Arnebrant, T.; Ruzgas, T.; Bobacka, J. Textile-Based Sampling for

Potentiometric Determination of Ions. *Anal. Chim. Acta* **2015**, *877*, 71–79.
(32) Silva, R.; Ahamed, A.; Cheong, Y. H.; Zhao, K.; Ding, R.; Lisak, G. Non-Equilibrium Potentiometric Sensors Integrated with Metal Modified Paper-Based Microfluidic Solution Sampling Substrates for Determination of Heavy Metals in Complex Environmental Samples. *Anal. Chim. Acta* **2022**, *1197*, 339495.
(33) Soda, Y.; Bakker, E. Ionic Strength-Independent Potentiometric Cation Concentration Sensing on Paper Using a Tetrabutylammonium-Based Reference Electrode. *Sensors Actuators B. Chem.* **2021**, *346*, 130527.
(34) Ding, R.; Fiedoruk-Pogrebniak, M.; Pokrzywnicka, M.; Koncki, R.; Bobacka, J.; Lisak, G. Solid Reference Electrode Integrated with Paper-Based Microfluidics for Potentiometric Ion Sensing. *Sens. Actuators, B* **2020**, *323*, 128680.
(35) Michalska, A.; Maksymiuk, K. All-Plastic, Disposable, Low Detection Limit Ion-Selective Electrodes. *Anal. Chim. Acta* **2004**, *523*, 97–105.
(36) Mensah, S. T.; Gonzalez, Y.; Calvo-Marzal, P.; Chumbimuni-Torres, K. Y. Nanomolar Detection Limits of Cd2+, Ag+, and K+ Using Paper-Strip Ion-Selective Electrodes. *Anal. Chem.* **2014**, *86*, 7269–7273.
(37) Rostampour, M.; Bailey, B.; Autrey, C.; Ferrer, K.; Vantoorenburg, B.; Patel, P. K.; Calvo-Marzal, P.; Chumbimuni-Torres, K. Y. Single-Step Integration of Poly(3-Octylthiophene) and Single-Walled Carbon Nanotubes for Highly Reproducible Paper-Based Ion-Selective Electrodes. *Anal. Chem.* **2021**, *93*, 1271–1276.
(38) Kalisz, J.; Węgrzyn, K.; Maksymiuk, K.; Michalska, A. 3D-Drawn Supports for Ion-Selective Electrodes. *Anal. Chem.* **2022**, *95*, 3436–3440.
(39) Anastasova, S.; Radu, A.; Matzeu, G.; Zuliani, C.; Mattinen, U.; Bobacka, J.; Diamond, D. Disposable Solid-Contact Ion-Selective Electrodes for Environmental Monitoring of Lead with Ppb Limit-of-Detection. *Electrochim. Acta* **2012**, *73*, 93–97.
(40) Jendrlin, M.; Khumngern, S.; Numnuam, A.; Thavarungkul, P.; Kanatharana, P.; Kirsanov, D.; Zholobenko, V. L.; Mendecki, L.; Radu, A. Ion Sensing Pencil: Draw Your Own Sensor. *Sensors Actuators B. Chem.* **2021**, *337*, 129751.
(41) Novell, M.; Guinovart, T.; Blondeau, P.; Rius, F. X.; Andrade, F. J. A Paper-Based Potentiometric Cell for Decentralized Monitoring of Li Levels in Whole Blood. *Lab Chip* **2014**, *14*, 1308–1314.
(42) Armas, S. M.; Manhan, A. J.; Younce, O.; Calvo-Marzal, P.; Chumbimuni-Torres, K. Y. Ready-to-Use Single-Strip Paper Based Sensor for Multiplex Ion Detection. *Sens. Actuators, B* **2018**, *255*, 1781–1787.
(43) Wang, F.; Liu, Y.; Zhang, M.; Zhang, F.; He, P. Home Detection Technique for Na + and K + in Urine Using a Self-Calibrated All-Solid-State Ion-Selective Electrode Array Based on Polystyrene−Au Ion-Sensing Nanocomposites. *Anal. Chem.* **2021**, *93*, 8318–8325.
(44) An, Q.; Gan, S.; Xu, J.; Bao, Y.; Wu, T.; Kong, H.; Zhong, L.; Ma, Y.; Song, Z.; Niu, L. A Multichannel Electrochemical All-Solid-State Wearable Potentiometric Sensor for Real-Time Sweat Ion Monitoring. *Electrochem. commun.* **2019**, *107*, 106553.
(45) Jiang, C.; Li, X.; Yao, Y.; Ying, Y.; Ping, J. Fully Written Flexible Potentiometric Sensor Using Two-Dimensional Nanomaterial-Based Conductive Ink. *Anal. Chem.*

2018, *90*, 13088–13095.
(46) Kamel, A. H.; Amr, A. E.-G.; Almehizia, A. A.; Elsayed, E. A.; Moustafa, G. O. Low-Cost Potentiometric Paper-Based Analytical Device Based on Newly Synthesized Macrocyclic Pyrido-Pentapeptide Derivatives as Novel Ionophores for Point-of-Care Copper(II) Determination. *RSC Adv.* **2021**, *11*, 27174–27182.
(47) Wei, J.; Zhang, X.; Mugo, S. M.; Zhang, Q. A Portable Sweat Sensor Based on Carbon Quantum Dots for Multiplex Detection of Cardiovascular Health Biomarkers. *Anal. Chem.* **2022**, *94*, 12772–12780.
(48) Mou, L.; Xia, Y.; Jiang, X. Epidermal Sensor for Potentiometric Analysis of Metabolite and Electrolyte. *Anal. Chem.* **2022**, *93*, 11525–11531.
(49) Lan, W. J.; Maxwell, E. J.; Parolo, C.; Bwambok, D. K.; Subramaniam, A. B.; Whitesides, G. M. Paper-Based Electroanalytical Devices with an Integrated, Stable Reference Electrode. *Lab Chip* **2013**, *13*, 4103–4108.
(50) Carrilho, E.; Martinez, A. W.; Whitesides, G. M. Understanding Wax Printing: A Simple Micropatterning Process for Paper-Based Microfluidic. *Anal. Chem.* **2009**, *81*, 7091–7095.
(51) Lu, Y.; Shi, W.; Jiang, L.; Qin, J.; Lin, B. Rapid Prototyping of Paper-Based Microfluidics with Wax for Low-Cost, Portable Bioassay. *Electrophoresis* **2009**, *30*, 1497–1500.
(52) Bell, J. G.; Mousavi, M. P. S.; Abd El-Rahman, M. K.; Tan, E. K. W.; Homer-Vanniasinkam, S.; Whitesides, G. M. Paper-Based Potentiometric Sensing of Free Bilirubin in Blood Serum. *Biosens. Bioelectron.* **2019**, *126*, 115–121.
(53) Glasco, D. L.; Ho, N. H. B.; Mamaril, A. M.; Bell, J. G. 3D Printed Ion-Selective Membranes and Their Translation into Point-of-Care Sensors. *Anal. Chem.* **2021**, *93*, 15826–15831.
(54) Hu, J.; Stein, A.; Bühlmann, P. A Disposable Planar Paper-Based Potentiometric Ion-Sensing Platform. *Angew. Chem., Int. Ed.* **2016**, *55*, 7544–7547.
(55) Herrero, E. J.; Bühlmann, P. Potentiometric Sensors with Polymeric Sensing and Reference Membranes Fully Integrated into a Sample-Wicking Polyester Textile. *Anal. Sens.* **2021**, *1*, 188–195.
(56) Xu, G.; Cheng, C.; Yuan, W.; Liu, Z.; Zhu, L.; Li, X.; Lu, Y.; Chen, Z.; Liu, J.; Cui, Z.; Liu, J.; Men, H.; Liu, Q. Smartphone-Based Battery-Free and Flexible Electrochemical Patch for Calcium and Chloride Ions Detections in Biofluids. *Sens. Actuators, B* **2019**, *297*, 126743.
(57) Mousavi, M. P. S.; Ainla, A.; Tan, E. K. W.; Abd El-Rahman, M. K.; Yoshida, Y.; Yuan, L.; Sigurslid, H. H.; Arkan, N.; Yip, M. C.; Abrahamsson, C. K.; Homer-Vanniasinkam, S.; Whitesides, G. M. Ion Sensing with Thread-Based Potentiometric Electrodes. *Lab Chip* **2018**, *18*, 2279–2290.
(58) Wang, L.; Wang, L.; Zhang, Y.; Pan, J.; Li, S.; Sun, X.; Zhang, B.; Peng, H. Weaving Sensing Fibers into Electrochemical Fabric for Real-Time Health Monitoring. *Adv. Funct. Mater.* **2018**, *28*, 1804456.
(59) Hu, J.; Ho, K. T.; Zou, X. U.; Smyrl, W. H.; Stein, A.; Bühlmann, P. All-Solid-State Reference Electrodes Based on Colloid-Imprinted Mesoporous Carbon and Their

Application in Disposable Paper-Based Potentiometric Sensing Devices. *Anal. Chem.* **2015**, *87*, 2981–2987.
(60) Hu, J.; Zhao, W.; Bühlmann, P.; Stein, A. Paper-Based All-Solid-State Ion-Sensing Platform with a Solid Contact Comprising Colloid-Imprinted Mesoporous Carbon and a Redox Buffer. *ACS Appl. Nano Mater.* **2018**, *1*, 293–301.
(61) Ruecha, N.; Chailapakul, O.; Suzuki, K.; Citterio, D. Fully Inkjet-Printed Paper-Based Potentiometric Ion-Sensing Devices. *Anal. Chem.* **2017**, *89*, 10608–10616.
(62) Zhang, T.; Ratajczak, A. M.; Chen, H.; Terrell, J. A.; Chen, C. A Step Forward for Smart Clothes-Fabric-Based Microfluidic Sensors for Wearable Health Monitoring. *ACS Sens.* **2022**, *7*, 3857–3866.
(63) Ozer, T.; Henry, C. S. Microfluidic-Based Ion-Selective Thermoplastic Electrode Array for Point-of-Care Detection of Potassium and Sodium Ions. *Michrochimica Acta* **2022**, *189*, 152.
(64) Parrilla, M.; Ortiz-Gómez, I.; Cánovas, R.; Salinas-Castillo, A.; Cuartero, M.; Crespo, G. A. Wearable Potentiometric Ion Patch for On-Body Electrolyte Monitoring in Sweat: Toward a Validation Strategy to Ensure Physiological Relevance. *Anal. Chem.* **2019**, *91*, 8644–8651.
(65) Gao, W.; Emaminejad, S.; Nyein, H. Y. Y.; Challa, S.; Chen, K.; Peck, A.; Fahad, H. M.; Ota, H.; Shiraki, H.; Kiriya, D.; Lien, D.-H.; Brooks, G. A.; Davis, R. W.; Javey, A. Fully Integrated Wearable Sensor Arrays for Multiplexed in Situ Perspiration Analysis. *Nature* **2016**, *529*, 509–514.
(66) Cao, Q.; Liang, B.; Mao, X.; Wei, J.; Tu, T.; Fang, L.; Ye, X. A Smartwatch Integrated with a Paper-Based Microfluidic Patch for Sweat Electrolytes Monitoring. *Electroanalysis* **2021**, *33*, 643–651.
(67) Sweilam, M. N.; Cordery, S. F.; Totti, S.; Velliou, E. G.; Campagnolo, P.; Varcoe, J. R.; Delgado-Charro, M. B.; Crean, C. Textile-Based Non-Invasive Lithium Drug Monitoring: A Proof-of-Concept Study for Wearable Sensing. *Biosens. Bioelectron.* **2020**, *150*, 111897.
(68) Sweilam, M. N.; Varcoe, J. R.; Crean, C. Fabrication and Optimization of Fiber-Based Lithium Sensor: A Step toward Wearable Sensors for Lithium Drug Monitoring in Interstitial Fluid. *ACS Sens.* **2018**, *3*, 1802–1810.
(69) Guinovart, T.; Valdés-Ramírez, G.; Windmiller, J. R.; Andrade, F. J.; Wang, J. Bandage-Based Wearable Potentiometric Sensor for Monitoring Wound PH. *Electroanalysis* **2014**, *26*, 1345–1353.
(70) Parrilla, M.; Ferré, J.; Guinovart, T.; Andrade, F. J. Wearable Potentiometric Sensors Based on Commercial Carbon Fibres for Monitoring Sodium in Sweat. *Electroanalysis* **2016**, *28*, 1267–1275.
(71) Wang, R.; Zhai, Q.; Zhao, Y.; An, T.; Gong, S.; Guo, Z.; Shi, Q.; Yong, Z.; Cheng, W. Stretchable Gold Fiber-Based Wearable Electrochemical Sensor toward PH Monitoring. *J. Mater. Chem. B* **2020**, *8*, 3655.
(72) Terse-Thakoor, T.; Punjiya, M.; Matharu, Z.; Lyu, B.; Ahmad, M.; Giles, G. E.; Owyeung, R.; Alaimo, F.; Shojaei Baghini, M.; Brunyé, T. T.; Sonkusale, S. Thread-Based Multiplexed Sensor Patch for Real-Time Sweat Monitoring. *Flex. Electron.*

2020, *4*, 18.
(73) Napier, B. S.; Matzeu, G.; Presti, M. Lo; Omenetto, F. G. Dry Spun, Bulk-Functionalized RGO Fibers for Textile Integrated Potentiometric Sensors. *Adv. Mater. Technol.* **2021**, *7*, 2101508.
(74) Land, K. J.; Boeras, D. I.; Chen, X. S.; Ramsay, A. R.; Peeling, R. W. REASSURED Diagnostics to Inform Disease Control Strategies, Strengthen Health Systems and Improve Patient Outcomes. *Nat. Microbiol.* **2019**, *4*, 46–54.
(75) Gong, H.; Ozgen, B. Fabric Structures: Woven, Knitted, or Nonwoven. In *Engineering of High-Performance Textiles*; Miao, M., Xin, J. H., Eds.; Woodhead Publishing, 2017; pp 107–131.
(76) Postlewaite, J.; Lyon, B.; Kalelkar, S. Cleanroom Wiper Applications for Removal of Surface Contamination. In *Developments in Surface Contamination and Cleaning: Applications of Cleaning Techniques*; Kohli, R., Mittal, K. L., Eds.; Elsevier, 2013; pp 555–564.
(77) Michalska, A.; Ocypa, M.; Maksymiuk, K. Highly Selective All-Plastic, Disposable, Cu2+-Selective Electrodes. *Electroanalysis* **2005**, *17*, 327–333.
(78) Wang, J.; Wang, L.; Li, G.; Yan, D.; Liu, C.; Xu, T.; Zhang, X. Ultra-Small Wearable Flexible Biosensor for Continuous Sweat Analysis. *ACS Sens.* **2022**, *7*, 3102–3107.
(79) Guinovart, T.; Parrilla, M.; Crespo, G. A.; Rius, F. X.; Andrade, F. J. Potentiometric Sensors Using Cotton Yarns, Carbon Nanotubes and Polymeric Membranes. *Analyst* **2013**, *138*, 5208–5215.
(80) Noviana, E.; Ozer, T.; Carrell, C. S.; Link, J. S.; McMahon, C.; Jang, I.; Henry, C. S. Microfluidic Paper-Based Analytical Devices: From Design to Applications. *Chem. Rev.* **2021**, *121*, 11835–11885.
(81) Ding, R.; Cheong, Y. H.; Ahamed, A.; Lisak, G. Heavy Metals Detection with Paper-Based Electrochemical Sensors. *Anal. Chem.* **2021**, *93*, 1880–1888.
(82) Arduini, F. Electrochemical Paper-Based Devices: When the Simple Replacement of the Support to Print Ecodesigned Electrodes Radically Improves the Features of the Electrochemical Devices. *Curr. Opin. Electrochem.* **2022**, *35*, 1–8.
(83) Cuartero, M.; Parrilla, M.; Crespo, G. A. Wearable Potentiometric Sensors for Medical Applications. *Sensors* **2019**, *19*, 1–24.
(84) Choi, M.-Y.; Lee, M.; Kim, J.-H.; Kim, S.; Choi, J.; So, J.-H.; Koo, H.-J. A Fully Textile-Based Skin PH Sensor. *J. Ind. Text.* **2022**, *51*, 441S-457S.
(85) Militky, J. The Chemistry, Manufacture and Tensile Behavior of Polyester Fabrics. In *Handbook of Tensile Properties of Textile and Technical Fibers*; Bunsell, A. R., Ed.; Woodhead Publishing: New York, 2009; pp 223–314.
(86) Xu, J.; Zhang, Z.; Gan, S.; Gao, H.; Kong, H.; Song, Z.; Ge, X.; Bao, Y.; Niu, L. Highly Stretchable Fiber-Based Potentiometric Ion Sensors for Multichannel Real-Time Analysis of Human Sweat. *ACS Sens.* **2020**, *5*, 2834–2842.
(87) Morf, W. E. *The Principles of Ion-Selective Electrodes and of Membrane Transport*; Elsevier Science: New York, 1981.
(88) Meier, P. C. Two Parameter Debye-Hückel Approximation for the Evaluation of Mean Activity Coefficients of 109 Electrolytes. *Anal. Chim. Acta* **1982**, *136*, 363–

368.
(89) Szigeti, Z.; Vigassy, T.; Bakker, E.; Pretsch, E. Approaches to Improving the Lower Detection Limit of Polymeric Membrane Ion-Selective Electrodes. *Electroanalysis* **2006**, *18*, 1254–1265.
(90) Jaworska, E.; Pomarico, G.; Berionni Berna, B.; Maksymiuk, K.; Paolesse, R.; Michalska, A. All-Solid-State Paper Based Potentiometric Potassium Sensors Containing Cobalt(II) Porphyrin/Cobalt(III) Corrole in the Transducer Layer. *Sens. Actuators, B* **2018**, *277*, 306–311.
(91) Herrero, E. J.; Troudt, B. K.; Bühlmann, P. The Effect of Paper on the Detection Limit of Paper-Based Potentiometric Chloride Sensors. *Anal. Chem.* **2022**, *94*, 14898–14905.
(92) Laboratory Requirements. In *US Code of Federal Regulations,Section 493.931*; 2003.
(93) Yehia, A. M.; Farag, M. A.; Tantawy, M. A. A Novel Trimodal System on a Paper-Based Microfluidic Device for on-Site Detection of the Date Rape Drug “Ketamine.” *Anal. Chim. Acta* **2020**, *1104*, 95–104.
(94) Vinoth, R.; Nakagawa, T.; Mathiyarasu, J.; Mohan, A. M. V. Fully Printed Wearable Microfluidic Devices for High-Throughput Sweat Sampling and Multiplexed Electrochemical Analysis. *ACS Sens.* **2021**, *6*, 1174–1186.
(95) Ping, J.; Wang, Y.; Fan, K.; Tang, W.; Wu, J.; Ying, Y. High-Performance Flexible Potentiometric Sensing Devices Using Free-Standing Graphene Paper. *J. Mater. Chem. B* **2013**, *1*, 4781.
(96) Zhen, X. V.; Rousseau, C. R.; Bühlmann, P. Redox Buffer Capacity of Ion-Selective Electrode Solid Contacts Doped with Organometallic Complexes. *Anal. Chem.* **2018**, *90*, 11000–11007.
(97) Cheong, Y. H.; Ge, L.; Zhao, N.; Kuan Teh, L.; Lisak, G. Ion Selective Electrodes Utilizing a Ferrocyanide Doped Redox Active Screen-Printed Solid Contact-Impact of Electrode Response to Conditioning. *J. Electroanal. Chem.* **2020**, *870*.
(98) Vanamo, U.; Bobacka, J. Instrument-Free Control of the Standard Potential of Potentiometric Solid-Contact Ion-Selective Electrodes by Short-Circuiting with a Conventional Reference Electrode. *Anal. Chem.* **2014**, *86*, 10540–10545.
(99) Buck, R. P.; Lindner, E. Recomendations for Nomenclature of Ion-Selective Electrodes. *Pure Appl. Chem.* **1994**, *66*, 2527–2536.
(100) Bühlmann, P.; Pretsch, E.; Bakker, E. Carrier-Based Ion-Selective Electrodes and Bulk Optodes. 2. Ionophores for Potentiometric and Optical Sensors. *Chem. Rev.* **1998**, *98*, 1593–1688.
(101) Bobacka, J.; Ivaska, A.; Lewenstam, A. Potentiometric Ion Sensors. *Chem. Rev.* **2008**, *108*, 329–351.
(102) Lewenstam, A. Routines and Challenges in Clinical Application of Electrochemical Ion-Sensors. *Electroanalysis* **2014**, *26*, 1171–1181.
(103) Macdonald, J. E.; Struthers, A. D. What Is the Optimal Serum Potassium Level in Cardiovascular Patients? *J. Am. Coll. Cardiol.* **2004**, *43*, 155–161.
(104) Bakker, E.; Bühlmann, P.; Pretsch, E. Carrier-Based Ion-Selective Electrodes and

Bulk Optodes. 1. General Characteristics. *Chem. Rev.* **1997**, *97*, 3083–3132.
(105) Luppa, P. B.; Bietenbeck, A.; Beaudoin, C.; Giannetti, A. Clinically Relevant Analytical Techniques, Organizational Concepts for Application and Future Perspectives of Point-of-Care Testing. *Biotechnol. Adv.* **2016**, *34*, 139–160.
(106) Sharma, S.; Zapatero-Rodríguez, J.; Estrela, P.; Richard, O. Point-of-Care Diagnostics in Low Resource Settings: Present Status and Future Role of Microfluidics. *Biosensors* **2015**, *5*, 577–601.
(107) Hoekstra, R.; Blondeau, P.; Andrade, F. J. Distributed Electrochemical Sensors: Recent Advances and Barriers to Market Adoption. *Anal. Bioanal. Chem.* **2018**, *410*, 4077–4089.
(108) Dumschat, C.; Borchardt, M.; Diekmann, C.; Cammann, K.; Knoll, M. Potentiometric Test Strip. *Sens. Actuators, B* **1995**, *24–25*, 279–281.
(109) Sjöberg, P.; Määttänen, A.; Vanamo, U.; Novell, M.; Ihalainen, P.; Andrade, F. J.; Bobacka, J.; Peltonen, J. Paper-Based Potentiometric Ion Sensors Constructed on Ink-Jet Printed Gold Electrodes. *Sens. Actuators, B* **2016**, *224*, 325–332.
(110) Ota, R.; Yamada, K.; Suzuki, K.; Citterio, D. Quantitative Evaluation of Analyte Transport on Microfluidic Paper-Based Analytical Devices (MPADs). *Analyst* **2018**, *143*, 643–653.
(111) McDonald, C.; Duncan, H. J. Reproducibility of Elemental Impurity Levels in Millipore Filter (EHWP). *Anal. Chim. Acta* **1978**, *102*, 241–244.
(112) Jardine, P. M.; Zelazny, L. W.; Evans, A. Solution Aluminum Anomalies Resulting from Various Filtering Materials. *Soil Sci. Soc. Am. J.* **1986**, *50*, 891–894.
(113) Spencer, D. W.; Manheim, F. T. Ash Content and Composition of Millipore HA Filters. *U.S. Geol. Surv. Prof. Pap. 650* **1969**, 288–290.
(114) Malzahn, K.; Windmiller, J. R.; Valdés-Ramírez, G.; Schöning, M. J.; Wang, J. Wearable Electrochemical Sensors for in Situ Analysis in Marine Environments. *Analyst* **2011**, *136*, 2912–2917.
(115) Mishra, R. K.; Martín, A.; Nakagawa, T.; Barfidokht, A.; Lu, X.; Sempionatto, J. R.; Mengjia Lyu, K.; Karajic, A.; Musameh, M. M.; Kyratzis, I. L.; Wang, J. Detection of Vapor-Phase Organophosphate Threats Using Wearable Conformable Integrated Epidermal and Textile Wireless Biosensor Systems. *Biosens. Bioelectron.* **2018**, *101*, 227–234.
(116) Parrilla, M.; Cánovas, R.; Jeerapan, I.; Andrade, F. J.; Wang, J. A Textile-Based Stretchable Multi-Ion Potentiometric Sensor. *Adv. Healthcare Mater.* **2016**, *5*, 996–1001.
(117) Schazmann, B.; Morris, D.; Slater, C.; Beirne, S.; Fay, C.; Reuveny, R.; Moyna, N.; Diamond, D. A Wearable Electrochemical Sensor for the Real-Time Measurement of Sweat Sodium Concentration. *Anal. Methods* **2010**, *2*, 342–348.
(118) Nilghaz, A.; Liu, X.; Ma, L.; Huang, Q.; Lu, X. Development of Fabric-Based Microfluidic Devices by Wax Printing. *Cellulose* **2019**, *26*, 3589–3599.
(119) Rajendra, V.; Sicard, C.; Brennan, J. D.; Brook, M. A. Printing Silicone-Based Hydrophobic Barriers on Paper for Microfluidic Assays Using Low-Cost Ink Jet Printers. *Analyst* **2014**, *139*, 6361–6365.

(120) Wang, J.; Monton, M. R. N.; Zhang, X.; Filipe, C. D. M.; Pelton, R.; Brennan, J. D. Hydrophobic Sol-Gel Channel Patterning Strategies for Paper-Based Microfluidics. *Lab Chip* **2014**, *14*, 691–695.
(121) Nilghaz, A.; Wicaksono, D. H. B.; Gustiono, D.; Abdul Majid, F. A.; Supriyanto, E.; Abdul Kadir, M. R. Flexible Microfluidic Cloth-Based Analytical Devices Using a Low-Cost Wax Patterning Technique. *Lab Chip* **2012**, *12*, 209–218.
(122) Nilghaz, A.; Ballerini, D. R.; Shen, W. Exploration of Microfluidic Devices Based on Multi-Filament Threads and Textiles: A Review. *Biomicofluidics* **2013**, *7*, 1–15.
(123) Hollies, N. R. S.; Kaessinger, M. M.; Bogaty, H. Water Transport Mechanisms in Textile Materials Part I: The Role of Yarn Roughness in Capillary-Type Penetration. *Text. Res. J.* **1956**, 829–835.
(124) Kettle, J. Moisture and Fluid Transport. In *Paper Physics*; Kaarlo, N., Ed.; Finnish Paper Engineers' Association, Helsinki, 2008; pp 266–288.
(125) McHale, G.; Shirtcliffe, N. J.; Newton, M. I. Contact-Angle Hysteresis on Super-Hydrophobic Surfaces. *Langmuir* **2004**, *20*, 10146–10149.
(126) Bowen, R. A. R.; Remaley, A. T. Interferences from Blood Collection Tube Components on Clinical Chemistry Assays. *Biochem. Med.* **2014**, *24*, 31–44.
(127) Ghosh, R.; Gopalakrishnan, S.; Savitha, R.; Renganathan, T.; Pushpavanam, S. Fabrication of Laser Printed Microfluidic Paper-Based Analytical Devices (LP-MPADs) for Point-of-Care Applications. *Sci. Rep.* **2019**, *7896*.
(128) Zhang, T.; Lai, C. Z.; Fierke, M. A.; Stein, A.; Bühlmann, P. Advantages and Limitations of Reference Electrodes with an Ionic Liquid Junction and Three-Dimensionally Ordered Macroporous Carbon as Solid Contact. *Anal. Chem.* **2012**, *84*, 7771–7778.
(129) Nishi, N.; Murakami, H.; Yasui, Y.; Kakiuchi, T. Use of Highly Hydrophobic Ionic Liquids for Ion-Selective Electrodes of the Liquid Membrane Type. *Anal. Sci.* **2008**, *24*, 1315–1320.
(130) Kakiuchi, T.; Yoshimatsu, T. A New Salt Bridge Based on the Hydrophobic Room-Temperature Molten Salt. *Bull. Chem. Soc. Jpn.* **2006**, *79*, 1017–1024.
(131) Tietz, N. W. *Textbook of Clinical Chemistry*; Bhagavan, N. V., Caraway, W. T., Conn, R. B., Kachmar, J. F., Pruden, E. L., Whitley, R. J., Eds.; W.B. Saunders Company: Philadelphia, 1986.
(132) Grygolowicz-Pawlak, E.; Crespo, G. A.; Ghahraman Afshar, M.; Mistlberger, G.; Bakker, E. Potentiometric Sensors with Ion-Exchange Donnan Exclusion Membranes. *Anal. Chem.* **2013**, *85*, 6208–6212.
(133) Ogawara, S.; Carey, J. L.; Zou, X. U.; Bühlmann, P. Donnan Failure of Ion-Selective Electrodes with Hydrophilic High-Capacity Ion-Exchanger Membranes. *ACS Sens.* **2016**, *1*, 95–101.
(134) Brown, G. E.; O'Brien, R. C. Method for Recovering Terephthalic Acid and Ethylene Glycol from Polyester Materials. 3,952,053, 1974.
(135) Chen, X. V.; Mousavi, M. P. S.; Bühlmann, P. Fluorous-Phase Ion-Selective PH Electrodes: Electrode Body and Ionophore Optimization for Measurements in the Physiological PH Range. *ACS Omega* **2020**, *5*, 13621–13629.

(136) Good, R. J. Contact Angle, Wetting, and Adhesion: A Critical Review. *J. Adhes. Sci. Technol.* **1992**, *6*, 1269–1302.
(137) Ataide, V. N.; Mendes, L. F.; Gama, L. I. L. M.; de Araujo, W. R.; Paixão, T. R. L. C. Electrochemical Paper-Based Analytical Devices: Ten Years of Development. *Anal. Methods* **2020**, *12*, 1030–1054.
(138) Mettakoonpitak, J.; Boehle, K.; Nantaphol, S.; Teengam, P.; Adkins, J. A.; Srisa-Art, M.; Henry, C. S. Electrochemistry on Paper-Based Analytical Devices: A Review. *Electroanalysis* **2016**, *28*, 1420–1436.
(139) Gordon, A. H.; Martin, A. J. P.; Synge, R. L. M. Partition Chromatography of Free Amino-Acids and Peptides. *Proc. Biochem. Soc.* **1943**, *37*, xiii–xiv.
(140) Oliver, G. On Albumen Tests and Peptonuria Versus Albuminuria. *Br. Med. J.* **1883**, *765*, 1164.
(141) Tswett, M. S. O Novoy Kategorii Adsorbtsionnykh Yavleny i o Primenenii Ikh k Biokkhimicheskomu Analizu (On a New Category of Adsorption Phenomena and on Its Application to Biochemical Analysis). *Proc. Warsaw Soc. Nat. Biol. Sect.* **1905**, *14*, 20–39.
(142) Yang, Y.; Noviana, E.; Nguyen, M. P.; Geiss, B. J.; Dandy, D. S.; Henry, C. S. Paper-Based Microfluidic Devices: Emerging Themes and Applications. *Anal. Chem.* **2016**, *89*, 71–91.
(143) Pickering, W. F. Inorganic Adsorption Paper Chromatography III. The Adsorption of Divalent Metal Ions by Filter Paper. *J. Chromatogr.* **1960**, *4*, 481–484.
(144) Engin, M. S.; Uyanik, A.; Cay, S.; Icbudak, H. Effect of the Adsorptive Character of Filter Papers on the Concentrations Determined in Studies Involving Heavy Metal Ions. *Adsorpt. Sci. Technol.* **2010**, *28*, 837–846.
(145) Su, P.; Granholm, K.; Pranovich, A.; Harju, L.; Holmbom, B.; Ivaska, A. Sorption of Metal Ions to Untreated, Alkali-Treated and Peroxide-Bleached TMP. *Cellulose* **2010**, *17*, 1033–1044.
(146) Liu, P.; Sehaqui, H.; Tingaut, P.; Wichser, A.; Oksman, K.; Mathew, A. P. Cellulose and Chitin Nanomaterials for Capturing Silver Ions (Ag^+) from Water via Surface Adsorption. *Cellulose* **2014**, *21*, 449–461.
(147) Liu, P.; Borrell, P. F.; Božič, M.; Kokol, V.; Oksman, K.; Mathew, A. P. Nanocelluloses and Their Phosphorylated Derivatives for Selective Adsorption of Ag^+, Cu^{2+} and Fe^{3+} from Industrial Effluents. *J. Hazard. Mater.* **2015**, *294*, 177–185.
(148) Zhu, C.; Dobryden, I.; Rydén, J.; Öberg, S.; Holmgren, A.; Mathew, A. P. Adsorption Behavior of Cellulose and Its Derivatives toward Ag(I) in Aqueous Medium: An AFM, Spectroscopic, and DFT Study. *Langmuir* **2015**, *31*, 12390–12400.
(149) Sjostrom, E. The Origin of Charge on Cellulosic Fibers. *Nord. Pulp Pap. Res. J.* **1989**, *4*, 90–93.
(150) Chai, X.-S.; Hou, Q. X.; Zhu, J. Y.; Chen, S.-L.; Wang, S. F.; Lucia, L. Carboxyl Groups in Wood Fibers. 1. Determination of Carboxyl Groups by Headspace Gas Chromatography. *Ind. Eng. Chem. Res.* **2003**, *42*, 5440–5444.
(151) Barbosa, L. C. A.; Maltha, C. R. A.; Demuner, A. J.; Cazal, C. M.; Reis, E. L.; Colodette, J. L. A Rapid Method for Quantification of Carboxyl Groups in Cellulose

Pulp. *BioResources* **2013**, *8*, 1043–1054.
(152) EPA Method 325.2: Chloride-Colorimetric, Automated, Ferricyanide, AA II. 1978.
(153) Anderson, E. L.; Troudt, B. K.; Bühlmann, P. Easy-to-Make Capillary-Based Reference Electrodes with Controlled, Pressure-Driven Electrolyte Flow. *ACS Sens.* **2021**, *6*, 2211–2217.
(154) Khan, M. A. R.; Vieira, C. A. C.; Riu, J.; Sales, M. G. F. Fabrication and Modification of Homemade Paper-Based Electrode Systems. *Talanta* **2021**, *224*, 121861.
(155) Taylor, J. K.; Smith, R. E. Effects of Maxima Suppressors on Polarographic Diffusion Currents. *J. Res. Natl. Bur. Stand.* **1952**, *48*, 172–178.
(156) Whatman Grade 1 Qualitative Filter Papers https://www.cytivalifesciences.com/en/us/shop/whatman-laboratory-filtration/cellulose-filter-papers/qualitative-standard-filter-paper/grade-1-qualitative-filter-papers-p-00070 (accessed 2021 -12 -22).
(157) Speight, J. G. *Lange's Handbook Of Chemistry, 16th Ed.*; McGraw-Hill Education: New York, 2005.
(158) Boyd, C. E. Dissolved Oxygen and Other Gases. In *Water Quality*; Springer: Cham, 2020; pp 142–162.
(159) Bickelhaupt, D. H.; Porter, J. H. Water Sample Contamination by Glass Fiber and Cellulose Filters. *Commun. Soil Sci. Plant Anal.* **1990**, *21*, 1477–1501.
(160) Sparrow, S. D.; Masiak, D. T. Errors in Analyses for Ammonium and Nitrate Caused by Contamination from Filter Papers 1. *Soil Sci. Soc. Am. J.* **1987**, *51*, 107–110.
(161) Dams, R.; Rahn, K. A.; Winchester, J. W. Evaluation of Filter Materials and Impaction Surfaces for Nondestructive Neutron Activation Analysis of Aerosols. *Environ. Sci. Technol.* **1972**, *6*, 441–448.
(162) Bajpai, P. Brief Description of the Pulp and Papermaking Process. In *Biotechnology for Pulp and Paper Processing*; Springer: Singapore, 2018.
(163) Sokalski, T.; Maj-Zurawska, M.; Hulanicki, A. Determination of True Selectivity Coefficients of Neutral Carrier Calcium Selective Electrode. *Mikrochim. Acta* **1991**, *I*, 285–291.
(164) Hu, G.; Kang, J.; Ng, L. W. T.; Zhu, X.; Howe, R. C. T.; Jones, C. G.; Hersam, M. C.; Hasan, T. Functional Inks and Printing of Two-Dimensional Materials. *Chem. Soc. Rev* **2018**, *47*, 3265.
(165) Taheri, A.; MacFarlane, D. R.; Pozo-Gonzalo, C.; Pringle, J. M. Application of a Water-Soluble Cobalt Redox Couple in Free-Standing Cellulose Films for Thermal Energy Harvesting. *Electrochim. Acta* **2019**, *297*, 669–675.
(166) Zou, X. U.; Cheong, J. H.; Taitt, B. J.; Bühlmann, P. Solid Contact Ion-Selective Electrodes with a Well-Controlled Co(II)/ Co(III) Redox Buffer Layer. *Anal. Chem.* **2013**, *85*, 9350–9355.
(167) Zou, X. U.; Chen, L. D.; Lai, C. Z.; Bühlmann, P. Ionic Liquid Reference Electrodes With a Well-Controlled Co(II)/Co(III) Redox Buffer as Solid Contact. *Electroanalysis* **2015**, *27*, 602–608.
(168) Zou, X. U.; Zhen, X. V.; Cheong, J. H.; Bühlmann, P. Calibration-Free Ionophore-Based Ion-Selective Electrodes with a Co(II)/Co(III) Redox Couple-Based Solid

Contact. *Anal. Chem.* **2014**, *86*, 8687–8692.
(169) Rousseau, C. R.; Honig, M. L.; Bühlmann, P. Hydrogels Doped with Redox Buffers as Transducers for Ion-Selective Electrodes. *Anal. Chem.* **2021**, *94*, 1143–1150.
(170) Binstead, R. A.; Beattie, J. K. Partial Molal Volumes of Spin-Equilibrium Metal Complexes. *Inorg. Chem.* **1986**, *25*, 1481–1484.
(171) Barton, J. K.; Raphael, A. L. Photoactivated Stereorspecific Cleavage of Double-Helical DNA by Cobalt (III) Complexes. *J. Am. Chem. Soc.* **1984**, *106*, 2466–2468.
(172) Chen, Y.-W. D.; Santhanam, K. S. V.; Bard, A. J. Solution Redox Couples for Electrochemical Energy Storage: II . Cobalt(III)-Cobalt(II) Complexes with O-Phenanthroline and Related Ligands. *J. Electrochem. Soc.* **1982**, *129*.
(173) Jaworska, E.; Naitana, M. L.; Stelmach, E.; Pomarico, G.; Wojciechowski, M.; Bulska, E.; Maksymiuk, K.; Paolesse, R.; Michalska, A. Introducing Cobalt(II) Porphyrin/Cobalt(III) Corrole Containing Transducers for Improved Potential Reproducibility and Performance of All-Solid-State Ion-Selective Electrodes. *Anal. Chem.* **2017**, *89*, 7107–7114.
(174) Amemiya, S.; Bühlmann, P.; Rusterholz, B.; Umezawa, Y. Cationic or Anionic Sites? Selectivity Optimization of Ion-Selective Electrodes Based on Charged Ionophores. *Anal. Chem.* **2000**, *72*, 1618–1631.
(175) Nagele, M.; Mi, Y.; Bakker, E.; Pretsch, E. Influence of Lipophilic Inert Electrolytes on the Selectivity of Polymer Membrane Electrodes. *Anal. Chem.* **1995**, *40*, 1686–1691.
(176) Bakker, E.; Pretsch, E.; Bühlmann, P. Selectivity of Potentiometric Ion Sensors. *Anal. Chem.* **2000**, *72*, 1127–1133.
(177) Clint, J. H.; Walker, T. Interaction Energies between Layers of Alkyl and Partially Fluorinated Alkyl Chains in Langmuir-Blodgett Multilayers. *J. Colloid Interface Sci.* **1974**, *47*, 172–185.
(178) Lindner, E.; Tóth, K.; Jeney, J.; Horváth, M.; Pungor, E.; Bitter, I.; Ágai, B.; Töke, L. Novel Bis(Crown Ether)-Based Potassium Sensor for Biological Applications. *Mikrochim Acta* **1990**, *I*, 157–168.
(179) Boswell, P. G.; Lugert, E. C.; Rábai, J.; Amin, E. A.; Bühlmann, P. Coordinative Properties of Highly Fluorinated Solvents with Amino and Ether Groups. *J. Am. Chem. Soc.* **2005**, *127*, 16976–16984.
(180) Bühlmann, P.; Pretsch, E.; Bakker, E. Carrier-Based Ion-Selective Electrodes and Bulk Optodes. 2. Ionophores for Potentiometric and Optical Sensors. *Chem. Rev.* **1998**, *98*, 1593–1687.
(181) Agboola, O. D.; Benson, N. U. Physisorption and Chemisorption Mechanisms Influencing Micro (Nano) Plastics-Organic Chemical Contaminants Interactions: A Review. *Front. Environ. Sci.* **2021**, *9*, 1–27.
(182) De Clerck, K.; Rahier, H.; Van Mele, B.; Kiekens, P. Thermal Properties Relevant to the Processing of PET Fibers. *J. Appl. Polym. Sci.* **2003**, *89*, 3840–3849.
(183) Dong, X. I. N.; Spindler, B. D.; Kim, M.; Stein, A.; Bühlmann, P. Spontaneous Mesoporosity-Driven Sequestration of Ionic Liquids from Silicone-Based Reference Electrode Membranes. *ACS Sens.* **2023**, *8*, 1774–1781.